UNIVERSITY OF SOUTHAMPTON

THE CHARACTERISATION OF SOME HIGH TEMPERATURE MOLECULES USING MATRIX ISOLATION

A Thesis Submitted for
the Degree of
Doctor of Philosophy
by

SIMON N JENNY

April 1981

UNIVERSITY OF SOUTHAMPTON

ABSTRACT

FACULTY OF SCIENCE

CHEMISTRY

Doctor of Philosophy

THE CHARACTERISATION OF SOME HIGH TEMPERATURE MOLECULES USING MATRIX ISOLATION

by Simon Nicholas Jenny

The molecules studied were those obtained from heating samples of sodium phosphate, arsenic oxide, antimony oxide and phosphorus oxides.

A survey is given of previous applications of matrix isolation to high temperature chemistry. The experimental apparatus used in this work is described and the method of analysing vibrational spectra is given. Isotopic substitution is shown to be a powerful aid to spectral interpretation and was extensively used. The application of isotopic substitution is discussed with reference to the molecule $FeCl_3$.

Sodium phosphate vapour was studied in order to identify the major vapour phase species and this resulted in the determination of the geometry of the molecule $NaPO_3$, which until now has remained unknown. The ^{18}O isotope pattern is shown to distinguish between mono- and bi-dentate coordination of the cation and experiments carried out on ^{18}O enriched material show that coordination of the cation is bidentate. This conclusion is confirmed by a force constant analysis.

The vapour above heated antimony trioxide was studied to determine the major species present, and matrix isolated molecular Sb_4O_6 was obtained. For the first time vibrational data was obtained for molecular Sb_4O_6 and parallel studies on As_4O_6 were carried out for comparative purposes. A method of identification of molecules of this type, via isotopic substitution was developed and an approach to the location of inactive fundamentals is discussed.

The oxides of phosphorus P_4O_6, and P_4O_{10} were studied as an extension to the studies on As_4O_6 and Sb_4O_6. The molecules P_4O_7, P_4O_8 and P_4O_9 were also prepared, and the frequencies of some of their fundamentals were measured. The results obtained represent the most complete set of vibrational data so far available for these molecules. The use of mass spectroscopy in conjunction with matrix isolation is shown to be a powerful method for studying high temperature vapours.

ACKNOWLEDGEMENTS

I would like to thank my supervisor, Dr J S Ogden, for his continuous help and encouragement throughout the course of this work. I would also like to thank Professor I R Beattie for his advice and for many helpful discussions. Thanks are also due to my immediate colleagues on the sixth floor for their wit and many pertinent comments. I am grateful to my wife for being patient during the production of this thesis and to Julia Quinn who typed the manuscript.

The financial support of the Department of Chemistry at Southampton is gratefully acknowledged.

CONTENTS

CHAPTER 1

MATRIX ISOLATION
IN
HIGH TEMPERATURE CHEMISTRY

1.1 INTRODUCTION

The identification and characterisation of high temperature gas phase species is of interest industrially as well as to the structural chemist. Corrosion problemsassociated with gas turbines are thought to arise in some cases from the deposition on the turbine blades of species from the gas phase originating from the combustion of some common fuels,[1] and the identification of the culpable species and the subsequent elimination of the problem must start with the development of capable techniques. Although this is one isolated example of the industrial importance of high temperature gas phase chemistry, for the structural inorganic chemist the vapour phase offers a rich hunting ground for novel and interesting information, in cases where little or nothing is known about vapour composition and molecular structure of gas phase species.

Although the high temperature chemist is often confronted with information concerning the condensed phases or solutions, definitive gas phase studies are often less abundant. Into this category fall the alkali metal phosphate systems studied in this work where solution and melt studies have been numerous[2] but the nature of their gas phase behaviour has until recently remained unknown. Gas phase studies of phosphorus and arsenic oxide systems have been carried out[3] and thermodynamic data has been produced for arsenic and antimony oxide,[4] but no definitive gas phase study of antimony oxide exists and moreover the composition of the vapour above heated Sb_4O_6 has remained in doubt.[5,6] In the case of phosphorus, the oxides P_4O_6 and P_4O_{10} are well known and have been subjected to gas phase studies,[3] but although P_4O_7 has been prepared[7] little is known about gas phase behaviour of this oxide and the other possible intermediate oxides P_4O_8 and P_4O_9, an area investigated in this work.

An important aspect of gas phase studies is that they enable the examination of discrete molecules, the focus of attention in this work, where in condensed phases polymers may predominate, and this approach can thus provoke some interesting comparisons between gas phase and condensed phase structures. In many cases polymeric material may persist in the vapour above the solid or liquid and a combination of both high temperat-

ures and low pressures may be necessary to generate monomeric species. This requires considerable modification of techniques suitable for room temperature, ambient pressure systems and the development of new approaches.

The ability to study species present in the vapour phase can lead to the identification of hitherto unknown molecules,[8,9,10] giving some insight into chemical behaviour not available by other means. The nature of the thermal decomposition of vapour phase species in many cases is uncertain and the ability to study such equilibria can often lead to surprising conclusions,[11] where the decomposition products present in the vapour phase at first sight seem unusual.

The term 'high temperature' in this work is used to refer to vapourisation processes carried out above ambient temperature although the actual temperatures used ranged from $\sim$ 373 K to $\sim$ 1673 K, a region where the technological problems of achieving vapourisation (container materials and temperature attainment) are not limiting.

1.2 PHYSICAL METHODS

Although vibrational spectroscopy is the technique used almost exclusively in this work, and its use for structural elucidation is well established, there are other techniques available to the high temperature inorganic chemist and it is as well to consider these at this stage, when the reasons for the choice of vibrational spectroscopy will become apparent.

At room temperature in the solid state X-ray crystallography is the predominant technique, but requires that radiation-stable single crystals can be grown. Where the compound under investigation is either low melting, or soluble without reaction (properties not always associated with inorganic species) nmr spectroscopy offers an attractive aid to structural determination by indication of the relative number of magnetically equivalent nuclei in each molecular environment. A further limitation of this technique, however, is that it requires that the atom under detection has a non zero nuclear spin. Moreover the spectra obtained may be complicated by exchange processes.

In the gas phase, mass spectrometry can yield information concerning the composition of the vapour.[12] Here though, confusion can arise owing to the occurrence of fragmentation reactions within the spectrometer, or more fundamentally, reactions arising during the vaporisation process, the latter complication being an important consideration in all gas phase studies. Microwave spectroscopy requires the presence of a permanent dipole moment and the analysis of the spectra can be difficult for molecules of low symmetry. Electron diffraction may be imprecise for high temperature species where high amplitudes of vibration lead to "shrinkage" effects for non-bonded distances with the result that linear molecules appear bent[13] and planar molecules pyramidal.[14]

Definitive quantitative information, then, can be obtained from Xray, microwave and electron diffraction studies, but where a single crystal cannot be grown, a permanent dipole moment does not exist, nmr is inapplicable, or mass spectrometry inconclusive, more qualitative methods such as vibrational spectroscopy become important. Vibrational spectroscopy has the added advantage that all species are detected simultaneously so that changes in composition may be studied. When coupled with matrix isolation, the observed bandwidths are such that impurities and decomposition products are often easily recognised and isotopic shifts can be observed for many species.

If, as in this work, we are concerned with high temperature vapours in the main, then the sensitivities of the various techniques become important;[15]

Mass Spec	10^{-11}	torr
Microwave	10^{-4}	torr
Electron diffraction	1	torr
Vibrational ir	1	torr
Vibrational Raman	100	torr (ν^4 dependent)

In the vapour phase, then, at elevated temperatures, vibrational spectroscopy coupled with mass spectroscopy where possible, presents a realistic and generally applicable approach to qualitative determination of vapour composition and structural determination of the species present.

1.3 VIBRATIONAL SPECTROSCOPY OF HIGH TEMPERATURE VAPOURS

By far the most attractive way of studying high temperature vapours is in a closed system where an equilibrium state is under investigation. Here the effect of temperature and pressure variation can be simultaneously studied. Using vibrational spectroscopy, the spectra obtained derive from transitions between vibrational levels the selection rules for which are well known.[16,17]

The major experimental problem associated with this kind of study lies with the design of suitable high temperature cells. The criteria for a suitable cell present some major technological difficulties;

(1) The cell windows must be transparent to the radiation used in the experiment.

(2) Both cell and windows must be capable of withstanding the temperatures required.

(3) The cell and windows must be unreactive, even at elevated temperatures.

(4) The windows must be attached to the cell with a gas tight seal.

(5) It should ideally be possible to evacuate the cell after introduction of the sample, and where necessary to load the sample in an inert atmosphere.

In the case of gas phase infrared spectroscopy many attempts have been made to satisfy the above requirements, but the selection of suitable window materials and their subsequent attachment to the cell have limited the ultimate working temperature of the system. Both polythene and silver chloride windows present major problems, and silicon, although it can be sealed directly to pyrex, suffers from attack by oxidising materials. Diamond, perhaps the most satisfactory window material, undergoes graphitisation in air which limits the ultimate temperature to around $600^{o}C$.[17] In addition to the technological problems of cell construction, gas phase infrared spectroscopy suffers from the fact that background radiation emitted by hot cells can seriously limit the sensitivity of the technique.

Gas phase Raman spectroscopy has a distinct advantage over its infrared counterpart in that glass or silica cells can be used, as visible radiation is used as the exciting source and the scattered light

is also in the visible region of the electromagnetic spectrum. However reactivity problems can become limiting at temperatures in the region 800°C - 1000°C. Sapphire, although useful above 1000°C, cannot be blown as is the case with glass, and plunger type cells have proved unsatisfactory for various reasons not least of which is the difficulty of dismantling after the experiment. Again background radiation from hot cells causes major 'stray light' problems at elevated temperatures, even when using a triple monochromator with its inherent enhanced stray light rejection, making it at best very difficult to observe weak signals.

More recent advances in laser technology have initiated the birth of Coherent Raman techniques of which Coherent antistokes Raman spectroscopy is the most popular.[18] This technique has the same selection rules as conventional Raman, but has the added advantages that a coherent or laser-like signal is generated, that the high powers available from modern lasers significantly increases sensitivity and that the coherent nature of the signal enables spatial resolution of background cell radiation. All sapphire equilibrium cells, with a working temperature of up to 1600°C have been developed,[19] in which the sapphire windows are sealed directly to a polycrystalline alumina body, and although results are only preliminary, this may prove to be an advance in the study of high temperature equilibrium vapours.

Matrix isolation provides a very attractive alternative to equilibrium studies when the latter are impractical and possesses many properties which, when exploited, can yield information not available from the gas phase even under the most favourable conditions. Moreover, matrix isolation, being a cumulative technique, can overcome the relatively low sensitivity of vibrational spectroscopy and this is particularly important in the case of Raman scattering. It was for these reasons that matrix isolation was used almost exclusively in this work.

1.4 MATRIX ISOLATION

Matrix isolation[20-24] was originally devised to trap reactive chemical species for spectroscopic investigations,[25,26] and its application to high temperature molecules has been extensively reviewed.[27,28]

The technique consists essentially of 'freezing out' the molecular species of interest together with a large excess of inert gas at cryogenic temperatures so that reactions between molecules of the species to be studied are effectively prevented. Thus species which under normal conditions may have only a very short lifetime can be examined over a long period of time by one or more spectroscopic techniques. The suitability of matrix materials must be subject to certain requirements. The most common matrix materials used are the noble gases, of which argon is by far the most popular. It is clearly important that, at the temperatures involved (10 K typically) the matrix gas takes the form of a rigid solid. Moreover the matrix material must also be unreactive towards the species of interest and must not absorb in the spectral region of interest. The noble gas solids fulfil these requirements adequately being transparent from below 100 cm^{-1} to the vacuum uv. They do however have phonon spectra below 100 cm^{-1} as a result of lattice defects which can be both infrared and Raman active but these are easily recognised.[29,30] Nitrogen is another commonly used matrix gas and the presence of the Raman active N≡N stretching mode at $\sim$ 2330 cm^{-1} has proved a distinct advantage as an aid to spectral alignment.

The low temperatures necessary for matrix isolation (typically 10 - 12 K), were initially achieved using complicated liquid helium transfer systems, but may now be easily and conveniently obtained utilising commercial closed cycle refrigerators. These, combined with the necessary vacuum equipment, are designed to fit the sample compartments of most commercial spectrometers. Full details of the apparatus used in this work are given later.

The technique of matrix isolation then, provides a novel approach to the study of high temperature species, by overcoming some of the major problems associated with closed system equilibrium studies. Container problems are overcome by generation of a molecular beam from the sample using one of many available techniques. Reactions between species present in the vapour can be quenched or monitored within the resulting matrix by controlled diffusion studies, in which the matrix is allowed to warm up to 20 - 30 K for a finite time before recooling. The behaviour of the matrix can be observed either before and after, or during

this process. Lastly, matrix isolation provides a means of studying species which have only short lifetimes under normal conditions.

1.5 VIBRATIONAL SPECTROSCOPY OF MATRIX ISOLATED SPECIES

Although there are obvious practical advantages of studying high temperature systems using matrix isolation it is useful to compare some of the characteristics of the spectra produced with those of conventionally produced spectra.

At the low temperatures involved in matrix isolation population of excited vibrational states is negligible, and consequently 'hot bands' are absent. Moreover for all but the smallest molecules (e.g. H_2O, CO_2) there is a complete loss of rotational structure. At first sight this may appear to be more of a disadvantage than an advantage, but although there is a loss of potential information, the resulting narrowness of the bands (1 - 2 cm^{-1}) not only enables resolution of transitions with similar energy but also small isotopic shifts of as little as 2 - 3 cm^{-1}. This means that one is in the position to resolve isotope fine structure for a significant number of main group and transition metals (e.g., Mg, Ca, Sr, Ga, Sn, Fe, Cr) as well as the much larger isotopic shifts associated with ^{18}O, ^{34}S or ^{37}Cl. Provided it is possible to carry out the necessary isotopic substitution for a particular molecule, it is sometimes possible to identify the stoichiometry unequivocably, simply by examining the consequent isotope patterns.[31,32] The importance of this type of isotopic information will become evident later in this work.

The shape of the molecules SO_2,[33,34] SiF_2,[35] GeF_2[36,37] and SeO_2[38,39] have been shown to be the same in the matrix as in the gas phase, although small frequency shifts (around 5 - 10 cm^{-1}) have been observed for the fundamental vibrations of these molecules, and many others, on changing the environment. As well as these differences between gas phase vibrational frequencies and those of the matrix isolated species, multiplet absorptions can also arise where there should be only a singlet absorption. These shifts in frequency and the occurrence of multiplets may be caused by several factors. Under the broad heading 'Matrix Effects' we may distinguish three different types of perturbation, matrix induced

frequency shifts, matrix site effects, and molecular distortions.

When considering the vibrational shift from the gas phase to the matrix ($\Delta\nu = \nu_{gas} - \nu_{matrix}$) the problem presents itself as a complex interaction of many contributing inductive, repulsive and dispersive forces. This complexity has rendered quantitative evaluation of matrix frequency shifts impractical. However we may consider these shifts to be the result of what may be regarded as a solvent effect of the matrix and this approach has been discussed in some detail.[40,41] Matrix site effects, which can result in the appearance of multiplet absorptions where single bands are expected arise from the trapping of molecules in different sites within the matrix cage (each site having a characteristic frequency shift) or in different orientations within the same sites. Alternatively actual molecular distortions may occur appearing in the spectrum as the splitting of certain bands whose degeneracy has been partly or completely removed. With respect to genuine molecular distortions, one of the mechanisms by which this can occur is as a result of coordination of the matrix gas with the species of interest. Monomeric $AlCl_3$ was reported to be pyramidal in a nitrogen matrix[42] but this was later shown to be caused by production of species of the type $AlCl_3.N_2$, and $AlCl_3$ has since been shown to be planar in argon matrices.[32] Finally it is possible that a trapped molecule has as its nearest neighbour another guest molecule, resulting in considerable intermolecular forces being exerted. These potentially confusing complications can however very often be eliminated, or at least recognised for what they are, by simply changing the matrix gas, carrying out diffusion experiments, or varying the concentration of the matrix (matrix ratio). The effect of changing the matrix gas can often be dramatic, as is shown by Figure 1.1 which shows the infrared spectrum of ν_3 of matrix isolated PCl_3 under high resolution in argon and nitrogen matrices. Whereas in argon a complex multi-line pattern is observed, in nitrogen the spectrum appears as the expected four line pattern[32] (see Chapter 2) and the complication in argon can confidently be assigned as being caused by matrix site effects.

Provided then, that care is taken in assigning spectra when these perturbations are present, the matrix isolation technique possesses some fundamental advantages over more conventional methods, which can result in

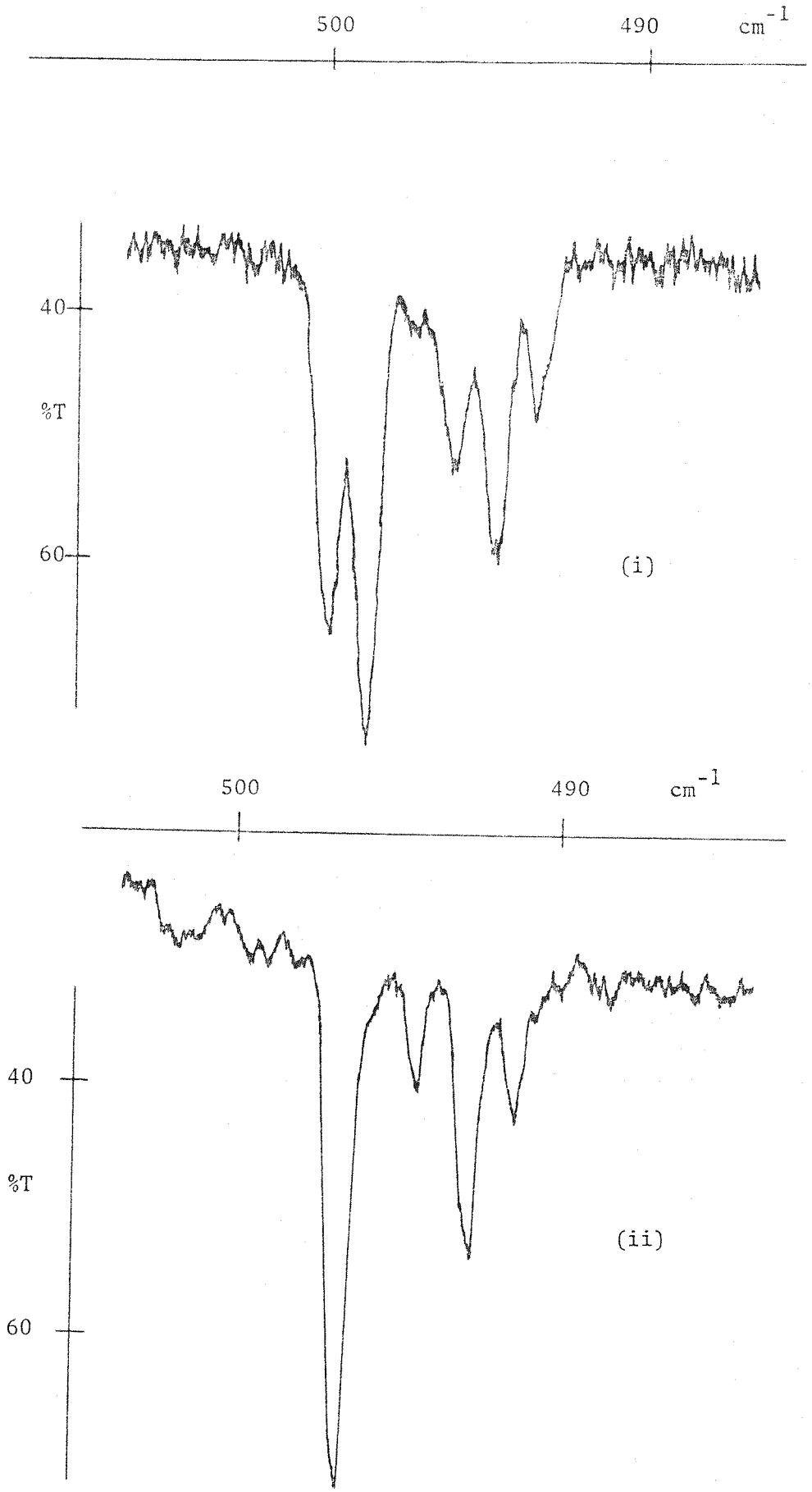

Figure 1.1 High resolution spectra of ν_3 PCl_3

(i) argon matrix

(ii) nitrogen matrix

characterisation of high temperature vapours for which other techniques have proved unsuccessful. An adequate characterisation of vapour phase species using matrix isolation and vibrational spectroscopy can be thought of as consisting essentially of two stages, qualitative and quantitative. The first stage results, in favourable cases, in the assignment of the observed spectrum to the most likely molecular model, the second stage in the calculation of a realistic force field for the molecule which reproduces the observed spectrum and thus gives further weight to the preferred structural model. In more fortunate cases this approach might give some indication as to the nature of the bonding within the molecule or may provide a means to test bonding theories. This is not always the case and very often one has to be content with a tentative proposal of molecular shape particularly for more complex molecules. Here other techniques apart from vibrational spectroscopy and matrix isolation may have to be applied for further clarification of the problems.

REFERENCES

1. "Deposition and Corrosion in Gas Turbines", Ed A B Hart, A J B Cutler, Appl Science Publishers, London, (1973).

2. J R Van Wazer, "Phosphorus and it's Compounds", Interscience, New York, (1958).
D E C Carbridge, "The Structural Chemistry of Phosphorus", Elsevier, London, (1974).

3. I R Beattie, R M S Livingstone, G A Ozin, D J Reynolds, J Chem Soc (A), (1970), 449.

4. R G Behrens, G M Rosenblatt, J Chem Thermodynamics, (1972), 4, 175.
R G Behrens, G M Rosenblatt, J Chem Thermodynamics, (1973), 5, 173.

5. J H Norman, H G Staley, J Chem Phys, (1964), 41, 5, 1503.

6. A J H Boerboom, H W Reyn, M F Vogts, J Kistemaker, J Adv Mass Spec, (1966), 3, 945.

7. M L Walker, J L Mills, Syn React Inorg Metal-Org Chem, (1975), 5, 29.

8. J S Ogden, M J Ricks, J Chem Phys, (1970), 53, 3, 896.

9. J S Anderson, J S Ogden, J Chem Phys, (1969), 51, 10, 4189.

10. L Andrews, J Phys Chem, (1969), 73, 3922.
L Andrews, J Phys Chem, (1971), 54, 4935.
L Andrews, J T Hwang, C Trindle, J Phys Chem, (1973), 77, 1065.

11. P J Ficalora, O M Uy, D W Muenow, J L Margrave, J Amer Chem Soc, (1968), 51, 574.

12. See e.g. M J Vasile, F A Stevie, W E Falconer, Int J Mass Spec Ion Phys, (1975), 17, 195.

13. K Kashiwabara, S Konaka, M Kimura, Bull Chem Soc Japan, (1973), 4, 410.

14. E Z Zasorin, N G Rambidi, Zh Strukt Khim, (1967), 8, 391.

15. I R Beattie, Chem Soc Rev, (1975), 4, 107.

16. E B Wilson, J C Decius, P C Cross, "Molecular Vibrations", McGraw-Hill, New York, (1955).

17. C Barraclough, I R Beattie, D Everett, "Vibrational Spectra and Structure", Vol 5, Ed J R Durig, Elsevier, Amsterdam, (1976).

18. J D Black, T R Gilson, "Advances in Infrared and Raman Spectroscopy", Vol 5, Ed R J H Clark, R E Hester, Heyden, London, (1977).

19. S N Jenny, unpublished work.

20. A J Downs, S C Peake, "Molecular Spectroscopy", Vol 1, Specialist Periodical Report, The Chemical Society, London, (1973).

21. B M Chadwick, "Molecular Spectroscopy", Vol III, Specialist Periodical Report, The Chemical Society, London, (1975).

22. B M Chadwick, "Molecular Spectroscopy", Vol VI, Specialist Periodical Report, The Chemical Society, London (1979).

23. J S Ogden, J J Turner, Chem in Britain, (1971), 7, 186.

24. J W Hastie, R H Hauge, J L Margrave, "Spectroscopy in Inorganic Chemistry, Vol 1, Eds C N R Nao, J R Ferraro, (Academic Press), (1970), 58.

25. I Norman, G Porter, Nature, (1954), 174, 508.

26. E Whittle, D A Dows, G C Pimentel, J Chem Phys, (1954), 22, 1943.

27. W Weltner Jr, Adv High Temp Chem, (1969), 2, 85.

28. A Snelson. Infrared Studies of Vaporising Molecules Trapped in Low Temperature Matrices in "Vibrational Spectroscoy of Trapped Species", H E Hallam, Ed, (Wiley and Sons), London, (1973).

29. G O Jones, J M Woodfine, Proc Phys Soc, (1965), 86, 101.

30. H E Hallam, G F Scrimshaw, "Vibrational Spectroscopy of Trapped Species", Ed H E Hallam, Wiley, London, (1973).

31. J H Darling, J S Ogden, JCS Dalton, (1973), 1079.

32. I R Beattie, H E Blayden, S M Hall, S N Jenny, J S Ogden, JCS Dalton, (1976), 666.

33. M Allavena, R Rysnik, D White, V Calder, D Mann, J Chem Phys, (1969), 50, 3399.

34. J W Hastie, R Hauge, J Margrave, J Inorg Nucl Chem, (1969), 31, 281.

35. J W Hastie, R Hauge, J Margrave, J Amer Chem Soc, (1969), 91, 2536.

36. H Takeo, R F Curl, P W Wilson, J Mol Spec, (1971), 38, 464.

37. J W Hastie, R Hauge, J Margrave, J Phys Chem, (1968), 72, 4492.

38. A J Hinchcliffe, D.Phil. Thesis, Oxford University, (1971).

39. H Takeo, E Hirota, Y Morino, J Mol Spec, (1970), 34, 370.

40. A Barnes, "Vibrational Spectroscopy of Trapped Species", Ed H E Hallam, Wiley, London, (1973).

41. M Moskovits, G A Ozin, "Cryochemistry" Ed M Moskovits, G A Ozin, Wiley Interscience, New York, (1976).

42. M L Lesiecki, J S Shirk, J Chem Phys, (1972), 56, 4171.

CHAPTER 2

EXPERIMENTAL DETAILS AND VIBRATIONAL ANALYSIS

The first part of this chapter is concerned with methods of generating high temperature species and with the experimental details of the apparatus used in this work; the second part deals with the analysis of the vibrational spectra obtained.

2.1 THE GENERATION OF HIGH TEMPERATURE SPECIES

There are many methods which have been employed for the production of matrix isolated species.[1] These range from methods suitable for species volatile at room temperature to those used for the production of high temperature species and as the bulk of this work was concerned with generation of species above ambient temperatures attention will be focussed on high temperature methods. In all but a few experiments Knudsen cell techniques were employed for the production of species studied in this work.

The use of Knudsen cells in high temperature chemistry is as extensive as the cell designs are varied, and the characteristics of this type of cell are well documented.[2]

Knudsen cells can be used not only for the production of pure vapours but also for the study of Knudsen cell reactions where one or more substances are reacted together within the cell and the products allowed to effuse out. The species AlO, AlO_2 and Al_2O_2 have been thus produced by reacting alumina with Al[3] and similarly SiO, Si_2O_2, Si_3O_3 have been produced by reacting silica with silicon.[4] Moreover double oven Knudsen cells have been employed for production of monomeric species from predominantly polymeric vapours. A double oven Knudsen cell consists essentially of two separate cells each of which can be held at different temperatures, so that in the lower temperature part a vapour can be produced which can then be subsequently superheated in the second part of the cell before deposition. This approach has been successfully applied to the halides of group IIB[5] and to the group IIIB trichlorides.[6] It is important of course, when Knudsen cells are employed, to consider possible reaction between the sample and the cell material, and the reduction of YF_3 to YF_2 has been observed in a tantalum cell.[7]

The designs of the Knudsen cells used are shown in Figure 2.1. When

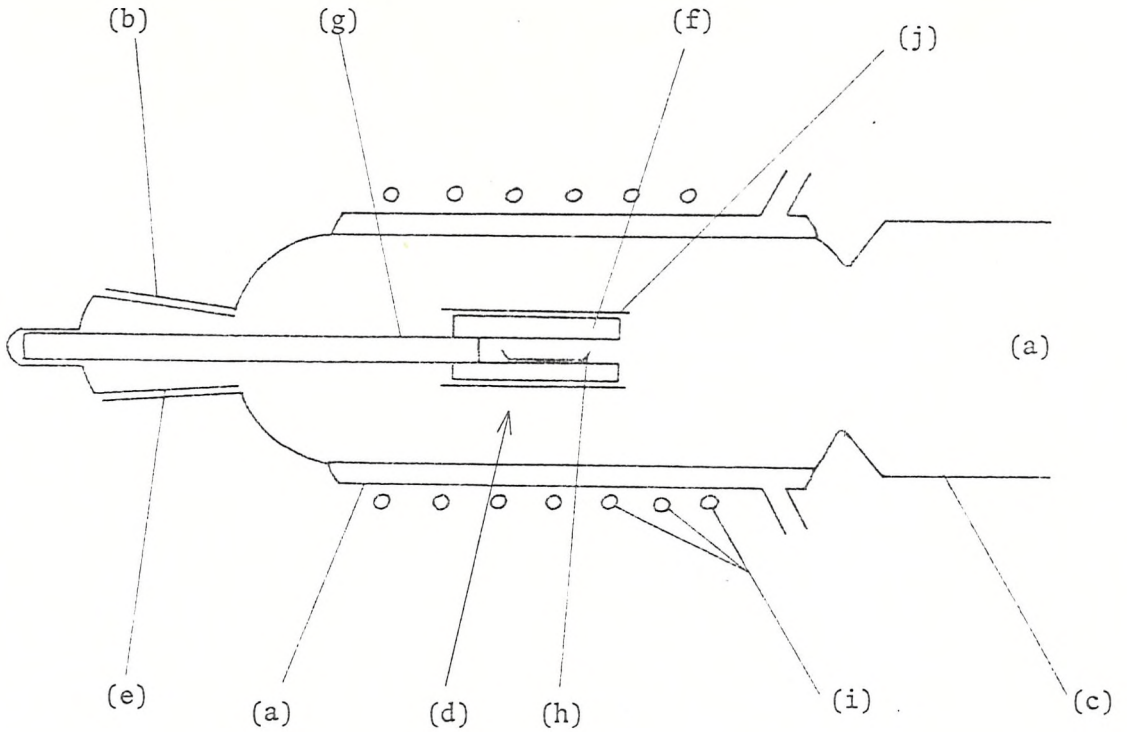

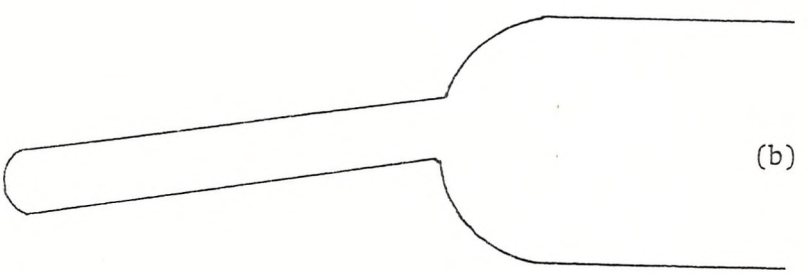

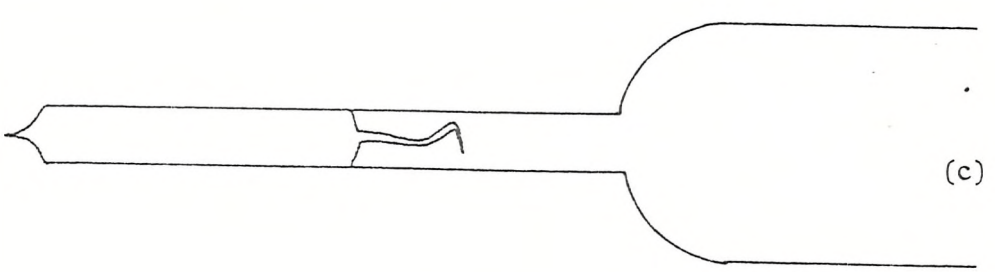

Figure 2.1

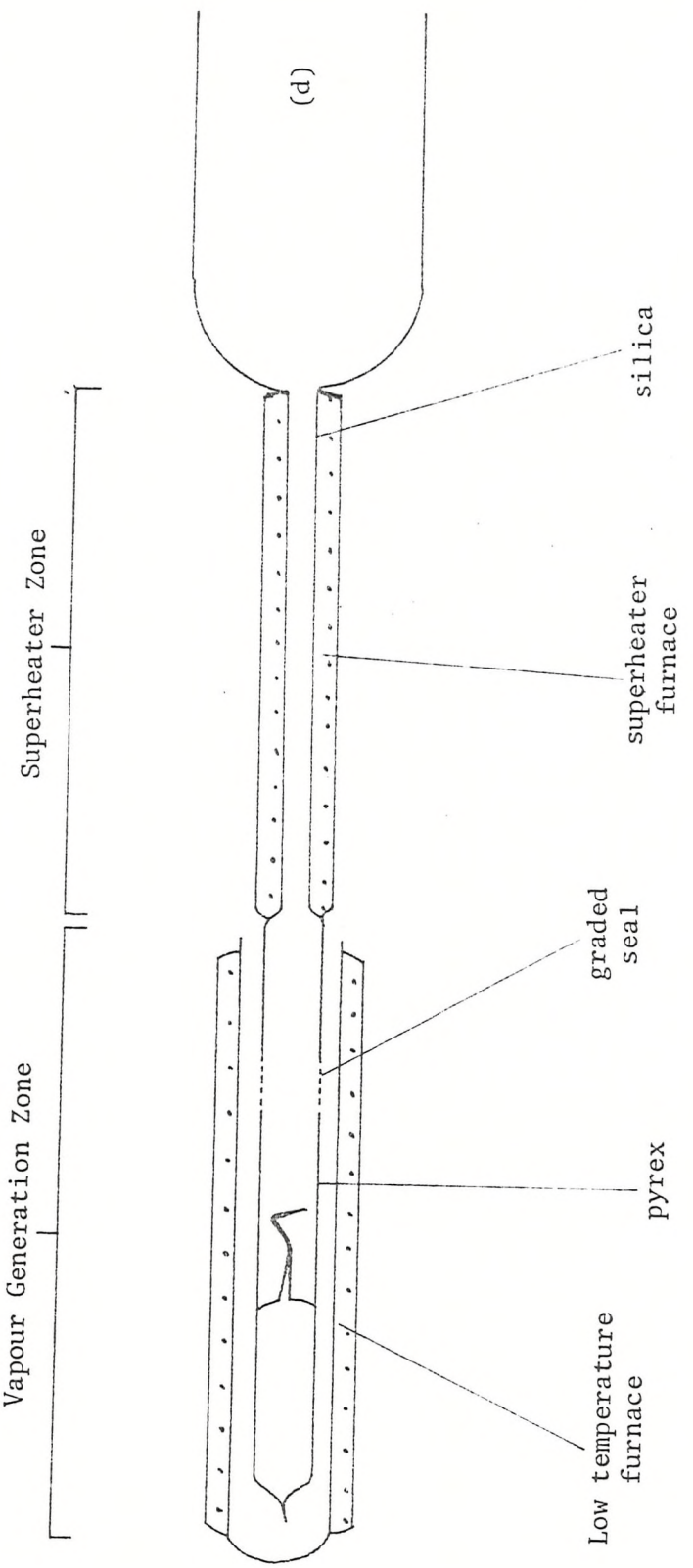

Figure 2.1 (cont)

high temperatures (> 1000°C) were required, or where glass was found not to be sufficiently unreactive, the cell used was of the type shown in Figure 2.1(a). This consists of a pyrex water cooled vacuum jacket (a) with a greaseless socket (b) and bell (c) designed to fit the matrix isolation apparatus. The sample holder (d) was supported inside the outer jacket by the greaseless cone (e). The sample holder was fabricated from recrystallised alumina and consisted of a short length of open tube (f) attached by means of high temperature alumina cement to an alumina rod (g). The sample was placed inside the open tube either directly in contact with the alumina or supported in a platinum boat (h). The cell was heated inductively by radio-frequency coupling between an external coil (i) and a cylindrical tantalum susceptor (j) placed around the sample holder. This apparatus was used successfully at temperatures up to 1400°C. Below 1000°C silica or pyrex cells were used, depending on the ultimate temperature required to achieve vapourisation. Figure 2.1(b) shows a simple open cell used for samples which were air stable. Samples which were air sensitive were vacuum sublimed into 'break seal' ampoules which were subsequently attached either directly or via greaseless taps (for low temperature vapourisation only) to the mounting 'bell', Figure 2.1(c). These cells were heated by means of resistive electrical furnaces wound either directly onto the glass or on to a separate pyrex or silica former which could be removed from the cell if necessary. Finally, Figure 2.1(d) shows a typical 'double oven' arrangement, used to produce monomeric $FeCl_3$ (see later in this Chapter) where two separate resistive furnaces were used and a graded seal was employed to allow superheating up to temperatures of 800°C-900°C.

2.2 THE DISPLEX UNIT AND VACUUM EQUIPMENT

The Displex units used exclusively in this work were Air Products CSW 202 units.[8] These are closed cycle low temperature refrigerators which utilise helium as the working fluid and the ultimate temperature attainable at the cold tip is ∿ 12 K. The compressor and expander stages of the refrigerator are housed in separate units interconnected by flexible high pressure gas lines. The expander module contains the

target window and is supported in the sample compartment of the spectrometer within its vacuum shroud. The essential features of the combined 'Displex'/vacuum jacket arrangement is shown in Figure 2.2. The vacuum jacket consists essentially of a brass cylinder (a) with a rotatable vacuum 'O' ring seal (b), and a pumping port (c). The lower section of the shroud, containing the outer windows (d), was demountable to allow for easy access to the target window (e) which was attached to the expander module using a suitable copper holder (f) and an indium gasket. The lower part of the expander module was surrounded by a copper radiation shield (g) with holes which allowed the passage of radiation. The matrix gas was introduced via the gas inlet (h) using a suitable needle valve to regulate the spray on rate. The sample cell was supported in the mounting collar (i) and the whole unit could be evacuated by a silicone oil diffusion pump backed by a rotary pump, the ultimate vacuum attainable being $\sim 10^{-7}$ Torr.

The choice of target and outer windows depends on whether infrared or Raman studies are being carried out. These windows must be transparent in the spectral region of interest and the target window must also have suitable thermal properties. For infrared work CsI windows were used for both target and outers, and for Raman work a Pt mirror soldered to a copper block was used as the target with glass as the outers. Apart from optics the essential difference between the Raman and infrared apparatus was that for Raman work the 'Displex' unit was mounted horizontally. The incident laser light entered the vacuum shroud from the underside and impinged on the Pt mirror at an angle of ca 30^{o}, the scattered light being collected at 90^{o} to the incident light. The sample holders could then still be mounted horizontally so that the same holders could be used for both infrared and Raman studies, without modification.

2.3 SPECTROMETERS

For infrared work the spectrometer used was a Perkin Elmer 225, which is a double beam instrument covering the range 5000 cm^{-1} to 200 cm^{-1}. A closed cycle dry air purger was used to remove water vapour and significantly improve the performance of the spectrometer in the region

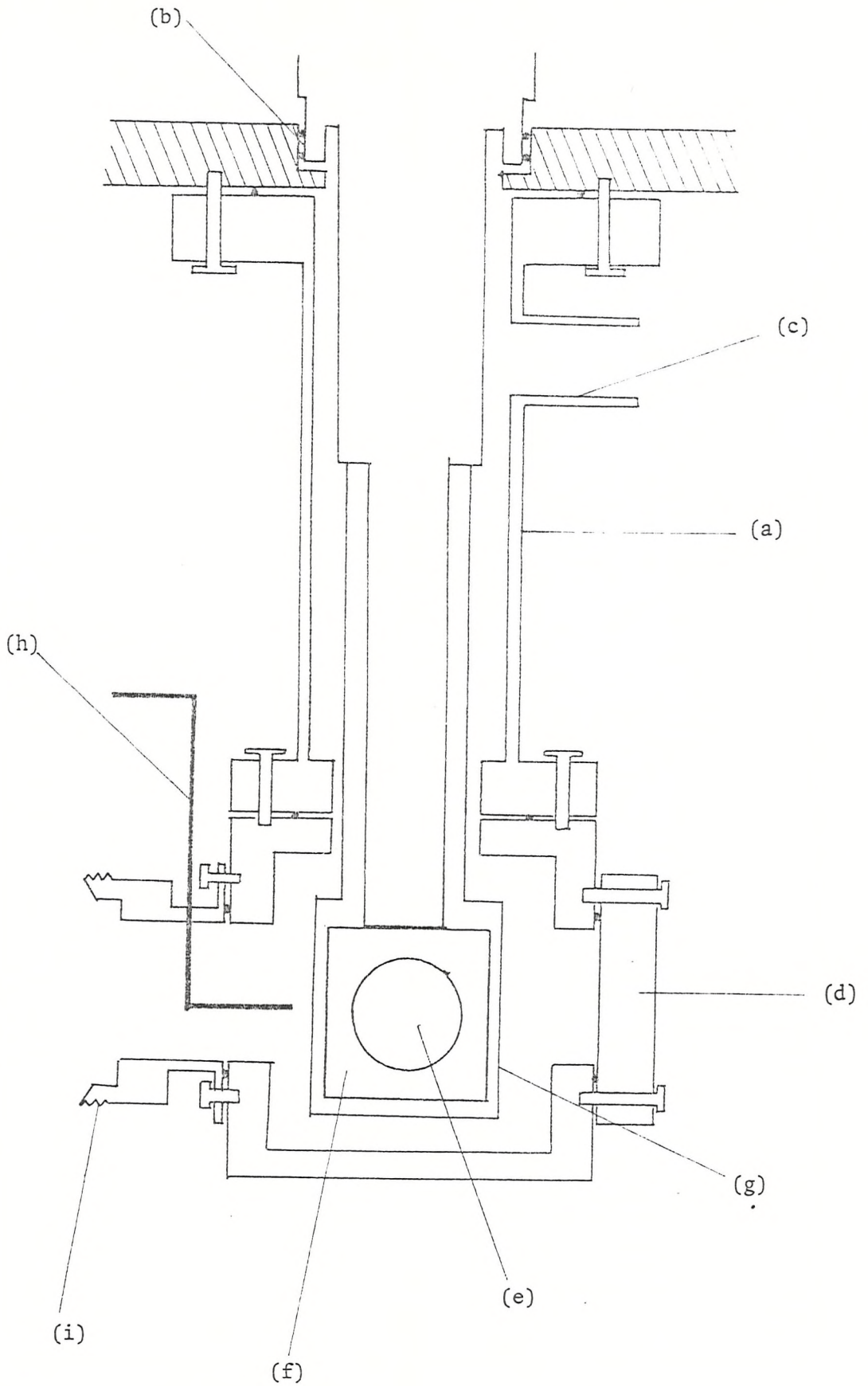

Figure 2.2 The 'displex'/vacuum shroud assembly

450 cm^{-1} to 200 cm^{-1}. The instrument was calibrated by recording the vibration/rotation bands of atmospheric water and carbon dioxide, and cells of ammonia, were also used. The frequencies of these bands are accurately known.[9]

The Raman spectrometer used was a standard Cary 82 fitted with a triple monochromator. The exciting source was an argon ion laser (Spectra Physics 170) of which the 514.5 nm line only was used and power levels at the sample were in the region of 500 mW.

2.4 EXPERIMENTAL TECHNIQUES

Since infrared absorption is a relatively sensitive technique, dilute matrices can be employed with a resulting gain in spectral quality. Because of this high sensitivity, great advantage can be taken of the narrow slitwidths possible to resolve isotopic fine structure, and more generally, matrix infrared spectroscopy presents no major experimental problems.

In contrast, matrix Raman spectroscopy is a far more difficult technique. The experimental difficulties arise primarily because the Raman effect is weak and because it is a scattering, rather than an absorption process. The weakness of the effect usually requires the use of more concentrated matrices, larger spectral slitwidths (2-5 cm^{-1} as opposed to 0.5-2 cm^{-1} for IR) and high incident laser power. The use of concentrated matrices can compound the problems of aggregation, resulting in deterioration of ultimate resolution, while local heating of the matrix can cause evaporation of the matrix gas, matrix annealing and in severe cases destruction of the matrix. Since the technique relies on the collection of scattered light, accurate alignment and stability of optics is important as also is the quality of the matrix. Glassy or transparent matrices are desirable, as this allows penetration of the matrix by the incident beam, and collection of scattered light from a depth of matrix, whereas if frosty matrices are used, one is reliant on a surface effect, and greater scattering of the incident light will occur leading to a higher optical noise level. Finally, fluorescence effects are a problem as with any application of the Raman effect, although in this work they were not found to be serious.

For an experiment to be performed, it was generally found to be advantageous to clean both the deposition surface and the outer windows. This was achieved by removing the lower part of the vacuum shroud and cleaning the surfaces with ethanol. The sample was then loaded and after reassembly, the whole system was evacuated. When the pressure was sufficiently low (usually after 1-2 hours pumping) the Displex unit was switched on, and after 'cool down' (when the pressure had reached ca 10^{-7} Torr) the sample and sample holder were degassed by gentle heating. During this process the expander head was orientated so that the radiation shield faced the sample. A background spectrum was then recorded before deposition. After rotating the expander head so that the target faced the sample, the sample furnace was brought up to vaporisation temperature, and the matrix gas flow rate adjusted by means of a needle valve, the flow rate being monitored on a Penning gage. Reproducible matrix gas flow rates could thus be achieved. After a few minutes deposition, it was generally found to be helpful to record a spectrum to check the deposition rates, any necessary adjustments being made at this stage. Deposition was then continued until a suitable spectrum was obtained. For Raman experiments, optimum alignment of the system was achieved by back projection of the entrance slit of the spectrometer on to the matrix, and adjustment of the incident light to coincide with the slit image. When nitrogen was the matrix gas, the N≡N stretching mode at $\sim$ 2330 cm^{-1} was utilised for fine adjustment. It was often found to be advantageous to perform diffusion experiments. Here, the temperature of the matrix is allowed to rise and the trapped species to diffuse within the matrix before recooling. The temperature of the cold surface during diffusion was monitored using a hydrogen vapour bulb thermometer for infrared studies, and a chromel vs gold (iron doped) thermocouple for Raman work. The spectrum could be monitored during this process and any changes noted.

2.5 SPECTRAL ANALYSIS - SYMMETRY SELECTION RULES

The work described in the following chapters was carried out with the aim of deducing the molecular symmetry of some vapour phase molecules, trapped in inert gas matrices, using vibrational spectroscopy. The

deduction of molecular symmetry from vibrational data relies on the application of the symmetry selection rules governing the appearance of infrared absorption and Raman scattering.

A vibration will be infrared active if one or more of the transition moment integrals;[10]

$$\int \psi_{v'} \mu_x \psi_{v''} d\tau, \quad \int \psi_{v'} \mu_y \psi_{v''} d\tau \quad \text{or} \quad \int \psi_{v'} \mu_z \psi_{v''} d\tau \qquad (1)$$

is non-zero. Here $\psi_{v'}$ and $\psi_{v''}$ are the vibrational wave functions of the lower and upper vibrational levels, $\mu_{x,y,z}$ are components of the electric moment of the molecule along the x, y and z directions. v is the vibrational quantum number, changes in which are governed by the simple harmonic oscillator selection rule which states that $\Delta v = \pm 1$. It has been shown[11] that the wave functions for states with $v = 0$ (the ground vibrational state) belong to the totally symmetric representation and for $v = 1$, the wave functions belong to the same symmetry species as the vibrational mode. At low temperatures the transition $v = 0 \rightarrow 1$ is the only transition considered as only the ground state, $v = 0$, will be significantly populated. For the above integral to be non-zero the integrand must be invariant to all the symmetry operations of the molecular point group. That is, the direct product $\mu_{x,y,z} \cdot \psi_{v'}$ must contain the totally symmetric representation. Thus a vibrational fundamental is active in the infrared if its symmetry species is the same as that of at least one of the components of the electric moment of the molecule.

In the case of Raman scattering it is necessary that at least one of the integrals of the type,[10]

$$\int \psi_{v'} P \psi_{v''} d\tau \qquad (2)$$

be non-zero, where P is a component of the derivative of the polarisability tensor. The physical meaning of the above non-zero requirement is that there must be a change in the polarisability of the molecule when the transition occurs and by similar reasoning to that used regarding infrared absorption, a vibrational fundamental will be Raman active if the normal mode involved belongs to the same representation as one or more of the components of the derivative of the polarisability tensor of the molecule.

Before the above symmetry selection rules can be applied, the number and symmetry of the normal modes of vibration of the molecule under investigation must be determined. This process is best illustrated by means of an example and the molecule chosen is of the type MX_3. The first step is the choice of a suitable model for the molecule and here two will be considered, a planar model (a) and a pyramidal model (b):

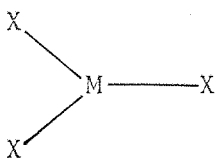

D_{3h}
(a)

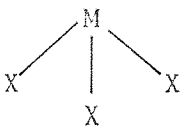

C_{3v}
(b)

Considering first the planar geometry, this molecule belongs to the point group D_{3h}. Applying the symmetry operations of this group to the set of cartesian displacement vectors on each atom results in a reducible representation, the characters of which are;

	E	$2C_3$	$3C_2$	σ_n	$2S_3$	$3\sigma_v$
Γ_{red}	12	0	-2	4	-2	2

If a_i is the number of times the ith irreducible representation occurs in the reducible representation then;

$$a_i = \frac{1}{h} \sum_r \chi(R)\chi_i(R) \qquad (3)$$

where h is the order of the group, $\chi(R)$ is the character of the reducible representation under operation R and $\chi_i(R)$ is the character of the irreducible representation under operation R (for derivation of Equation (3) see Reference 11). Applying this formula to the above example gives:

$$\Gamma_{cartesian} = A_1' + A_2' + 3E' + 2A_2'' + E''$$

This expression contains contributions from rotational and translational modes as well as from genuine internal vibrations. Consulation of the D_{3h} Character Table enables identification of the translational and roational contributions and these are:

translational components $A_2'' + E'$

rotational components $A_2' + E''$

giving:

$$\Gamma_{vib} = A_1' + A_2'' + 2E'$$

for the genuine internal vibrations of a planar MX_3 molecule. The nature of the vibrations in terms of changes in the internal coordinates may be found using the three bond lengths (ℓ) and three interbond angles (α) as internal coordinates. However this gives rise to:

$$\Gamma_{vib} = 2A_1' + 2E'$$

and it is evident firstly that a redundancy exists in the A_1' representation and secondly that this choice of internal coordinates does not generate an A_2'' mode. The redundancy arises from the fact that it is impossible to simultaneously increase all three interbond angles. The choice of a further set of internal coordinates overcomes this problem and it is found to be convenient to consider the angles between the bonds and the three fold axis (β). This gives rise to:

$$\Gamma_{\beta} = A_1' + E' + A_2'' + E''$$

where the A_2'' mode is taken to represent the out of plane bending vibration of the molecule.

Applying an exactly similar treatment to the pyramidal model (b) which belongs to the point group C_{3v} gives:

$$\Gamma_{cartesian} = 3A_1 + A_2 + 4E$$

which may be reduced by removing rotational and translational components to:

$$\Gamma_{vib} = 2A_1 + 2E$$

Applying the set of internal coordinates consisting of the three bond lengths (ℓ) and three interbond angles (θ) for the C_{3v} model does not result in redundancy as is the case for the D_{3h} model, since all interbond angles can increase simultaneously and this gives:

$$\Gamma_{\ell} = A_1 + E$$

$$\Gamma_{\alpha} = A_1 + E$$

Now, the symmetry selection rules can be easily applied to the vibrations arising from each model by consulting the character tables for each point group. In Equation (2) P transforms in the same way as the quadratic functions of the cartesian coordinates, i.e. x^2, y^2, z^2, xy, yz, zx or linear combinations such as $x^2 - y^2$,[12] and these are listed opposite their associated representations in the character tables. Hence for the planar D_{3h} model it is found that the A_1' vibration is Raman active only, the A_2'' infrared active only and the E' modes both infrared and Raman active. For pyramidal C_{3v} MX_3, $A_1 + E$ vibrations are found to be both infrared and Raman active. The activities and coincidences expected for each model are summarised in Table 2.1 below.

MX_3	No of IR active bands	No of R active bands	No of Coincidences
D_{3h} Planar	3	3	2
C_{3v} Pyramidal	4	4	4

Table 2.1. The number and activity of vibrations for D_{3h} and C_{3v} MX_3.

If we consider only the stretching modes of these two possible models ($A_1' + E'$, D_{3h} and $A_1 + E$, C_{3v}) the appearance of an absorption due to the totally symmetric stretching mode of the molecule in the infrared spectrum is clearly evidence for a pyramidal structure and hence for an interbond angle of $< 120^{\circ}$. This distinction is illustrated by a comparison of the infrared spectrum of $InCl_3$, $AlCl_3$ and $GaCl_3$ [13] with that of PCl_3, a molecule with known pyramidal geometry and interbond angle of $100^{\circ}6'$. The non-appearance in the infrared of the totally symmetric stretch of $InCl_3$, $AlCl_3$ and $GaCl_3$ would imply a bond angle of 120°. The application of symmetry selection rules and simple 'band counting' can then distinguish between two possible molecular geometries. The limitations of this approach lie with the possibility of the breakdown of the selection rules and with the sensitivity of detection of very low intensity

absorptions. In a matrix environment, molecular distortions due to coordination of the matrix gas or impurities can result in observation of formally 'inactive' bands, (see Chapter 1). The calculation of the exact 'degree of planarity' can be seriously affected by the sensitivity of determining relative intensities for very weak absorptions. In cases where these problems are apparent, or where further evidence is required for a particular preferred geometry, isotopic substitution (see Section 2.7) may provide an invaluable aid to structural determination.

2.6 THE CALCULATION OF FORCE CONSTANTS. THE FG MATRIX METHOD[11]

In addition to the qualitative methods for determining the symmetry and number of normal modes for a molecule, there is also the quantitative aspect of relating the frequencies of these vibrations to the masses of the atoms, bond lengths, bond angles and force constants of the bonds.

The starting point for this process is the equation due to Wilson,[10]

$$|FG - E\lambda| = 0 \qquad (4)$$

where E is the unit matrix and $\lambda = 4\pi^2c^2\omega^2$ (ω here refers to the vibrational frequency in cm^{-1} in contrast to ν which will be used to represent observed transitions). F in equation (4) is a matrix containing the force constants, describing the potential energy of the molecule, and G is a matrix involving the kinetic energy of the molecule. Once the elements of the F and G matrices are known for the molecule, then Equation (4) can be written out explicitly. Using known vibrational frequencies a force field can be proposed and some of the principal force constants can be calculated. Alternatively, force constants can be used to calculate the frequencies of normal modes of vibration. The elements of the G matrix can be constructed using the relationship:

$$g_{tt'} = \sum_{i=1}^{3N} \mu_i B_{ti} B_{t'i} \qquad (5)$$

$$(tt' = 1 \rightarrow 3N - 6)$$

in which μ_i is the reciprocal mass of the atom i and the coefficients B_{ti} relate to the internal coordinates s_t with the cartesian displacement coordinates P by:

$$s_t = \sum_{i=1}^{3N} B_{ti} P_i \qquad (6)$$

$(t = 1 \rightarrow 3N - 6)$

Linear combinations of the internal coordinates which transform according to each of the irreducible representations of the 3N - 6 normal modes, known as symmetry coordinates, can be obtained from the expression:

$$S = Us \qquad (7)$$

where U is a matrix of the coefficients of the internal coordinates contained in the linear combinations. Now, if f is a matrix of force constants, the matrix F contained in Equation (4) is given by:

$$F = UfU' \qquad (8)$$

where U' is the transpose of U. Similarly the matrix G is obtained from the elements g defined by Equation (5):

$$G = UgU' \qquad (9)$$

The potential energy of the molecule can be obtained from:

$$V = \sum_{tt'} f_{tt'} S_t S_{t'} \qquad (10)$$

where an element such as $f_{tt} S_t^2$ represents the potential energy of stretching a bond or bending an angle, and elements such as $f_{tt'} S_t S_{t'}$ represent energies of interaction.

The above process results in the F and G matrices being factored into blocks corresponding to each of the symmetry species of the normal vibrations. For example, the matrices for a pyramidal MX_3 molecule would contain a 2 x 2 block for the $2A_1$ modes, and two identical 2 x 2 blocks for the two components of the doubly degenerate E modes. Thus, using the basic FG relationship, Equation (4), two quadratic equations are obtained where the values of λ are the roots, each root corresponding to a normal mode. The normal procedure used in subsequent chapters begins with the interpretation of an observed spectrum in terms of a preferred molecular geometry. This involves the choice of a suitable model and the subsequent calculation of some of the principal force constants, using the observed values of λ. This is most conveniently achieved using a computer, where

an iterative procedure can be incorporated which refines an initial set of force constants until calculated values of λ agree with those observed.

In this work the program SOTONVIBP, which has been fully described[14] was used. This program operates on a modified FG method and the input consists a set of approximate cartesian coordinates together with the masses of the atoms, a set of internal coordinates (which may be redundant) and an initial set of force constants, which may be related to one another if appropriate. The output of the program includes a set of principal cartesian coordinates (with the origin at the centre of mass) the principal moments of inertia, calculated frequencies and refined force constants. Isotopic substitution provides further information as an aid to band assignment and determination of molecular geometry, and using this program the frequencies of isotopic variants are readily calculated simply by altering the masses of the atoms in the program input.

2.7 THE IMPORTANCE OF ISOTOPES

When an atom of a molecule is replaced by an isotopic atom of the same element two basic assumptions are made (see Reference 10, p182). The first concerns the potential energy function of the molecule which is assumed to remain invariant (i.e. the force constants remain the same) and the second assumes an unchanged geometry. However, owing to the mass change, vibrational frequencies may be appreciably altered. The observation of these 'isotope shifts' can provide further information about the molecule, both qualitative and quantitative.

The introduction of the isotopes Y' and Y'' into a molecule of the type XY_n in a random manner will result in the production of at least $n + 1$ different molecular species.[15] The relative proportions of the resultant isotopomers will be determined by the relative abundances of Y' and Y'' (in the case of naturally occurring isotopes, e.g. ^{37}Cl, ^{35}Cl) or by the extent of isotopic enrichment used in the preparation of an isotopically substituted sample (e.g. ^{18}O, ^{16}O). The relative proportions of the isotopomers follows a distribution given by the binomial theorem. In general partial isotopic enrichment of a molecular species results in the appearance, in the vibrational spectrum, of multiplets where singlets

occurred for the isotopically pure species. These patterns, however, vary according to molecular geometry, number of atoms and type of vibrations, and in order to appreciate the problems involved the next section deals with the determination of the molecular shape of $FeCl_3$.

2.8 THE SHAPE OF MOLECULAR $FeCl_3$

The molecule $FeCl_3$ has been the subject of recent investigations concerned with the determination of its molecular shape. Up to 600 K the vapour exists mainly as Fe_2Cl_6 dimer and high temperatures are needed to ensure monomer production. From electron diffraction studies[16] planar D_{3h} and bridged D_{2h} structures were suggested for the monomer and dimer respectively. Infrared matrix isolation studies[17] of $FeCl_2$, $FeCl_3$ and their dimers have been interpreted in the case of $FeCl_3$ in terms of a planar geometry. These spectra however were of mixtures of Fe_2Cl_6, $FeCl_3$, Fe_2Cl_4 and $FeCl_2$ and their consequent complexity rendered interpretation difficult. Moreover a weak absorption noted at similar frequency to that of the Raman active (D_{3h}) A_1 totally symmetric stretch could be evidence for a pyramidal geometry. More recent matrix Raman studies[18] have been interpreted in terms of a pyramidal (C_{3v}) geometry for $FeCl_3$ monomer with a bond angle of 115.66^{o}. Doubt as to the molecular shape of $FeCl_3$ monomer clearly exists and a series of experiments was carried out, exploiting the existence of naturally occurring chlorine isotopes, in an attempt to resolve this problem.

For a planar or pyramidal $FeCl_3$ molecule, with three equivalent chlorine atoms, four isotopomers are possible resulting from the occurrence of ^{35}Cl and ^{37}Cl. The relative proportions of each isotopomer will be as follows:

$Fe(^{35}Cl)_3$		$Fe(^{35}Cl)_2(^{37}Cl)$		$Fe(^{35}Cl)(^{37}Cl)_2$		$Fe(^{37}Cl)_3$
1	:	3	:	3	:	1

Incorporation of the natural abundance of ^{37}Cl ($^{35}Cl:^{37}Cl$ = 3:1) gives each isotopomer the following statistical weights:

27 : 27 : 9 : 1

Now, if we are concerned with the non-degenerate A_1 mode (pyramidal) or A_1' mode (planar) then we would expect four lines in the high resolution spectrum with intensity ratios 27:27:9:1. This pattern was observed in the Raman spectrum of $FeCl_3$ monomer, Figure 2.3(a) and in those of the trichlorides of group IIIB.[19] For degenerate vibrations (E, pyramidal, E', planar) isotopic substitution in general results in a pattern which shows a clear departure from a binomial intensity distribution, Figure 2.3 (b). This is because the degeneracy is invariably lifted in the partially substituted species and the spectrum contains either more than n + 1 distinct lines, or an anomalous intensity distribution due to band overlap.[20] The infrared spectrum of $FeCl_3$ shown in Figure 2.3(b) is again similar to those observed for the group IIIB trichlorides.[19] This four line pattern arises from the virtual coincidence of the A_1 and B_2 components of the partially substituted $(Fe(^{35}Cl)_2(^{37}Cl)$, $Fe(^{35}Cl)(^{37}Cl)_2)$ molecules, which now have C_{2v} symmetry, with the parent E' mode and equal intensity distribution between resulting A_1 and B_2 modes. These conditions arise only if the A_1 symmetric stretch and the in-plane bending mode are well removed in frequency from the parent E' antisymmetric mode. In cases where this is not so, a six line pattern may be expected.[20] Using isotope patterns then, bands observed can be unambiguously assigned to a particular species and to a particular vibration and in the case of $FeCl_3$, both the symmetric and antisymmetric stretches of the monomer can be identified.

The quantitative information which can be obtained using isotopic substitution is concerned with the estimation of bond angles and the refinement of force constants. Before proceeding with the example of $FeCl_3$, it is as well here to mention the limitations of a quantitative approach to isotopic substitution. In general, the frequencies, ω, used in equations to calculate bond angles are based on the assumption that vibrations are simple harmonic. This is not the case and it has been shown that[21] if observed frequencies are not corrected for anharmonicity central atom (M) substitution gives rise to a lower limit for the bond angle (α_ℓ) and outer atom (X) substitution gives rise to an upper limit (α_n). In this case, a reasonable estimate for θ is $\frac{1}{2}(\alpha_\ell + \alpha_n)$. Furthermore, uncertainty in the experimentally obtained isotopic shifts can result in large errors in α. This has been shown to be particularly true for a

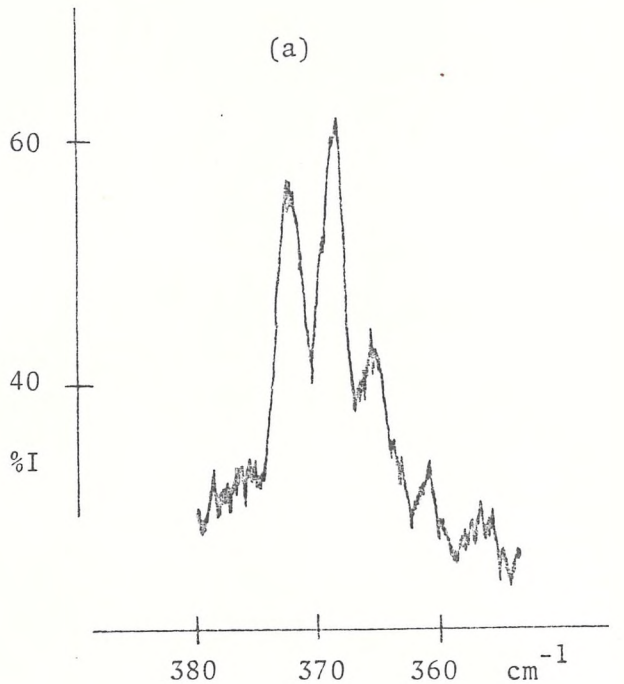

Figure 2.3 (a) High resolution Raman spectrum of ν_1 $FeCl_3$

(b) High resolution Infrared spectrum of ν_3 $FeCl_3$

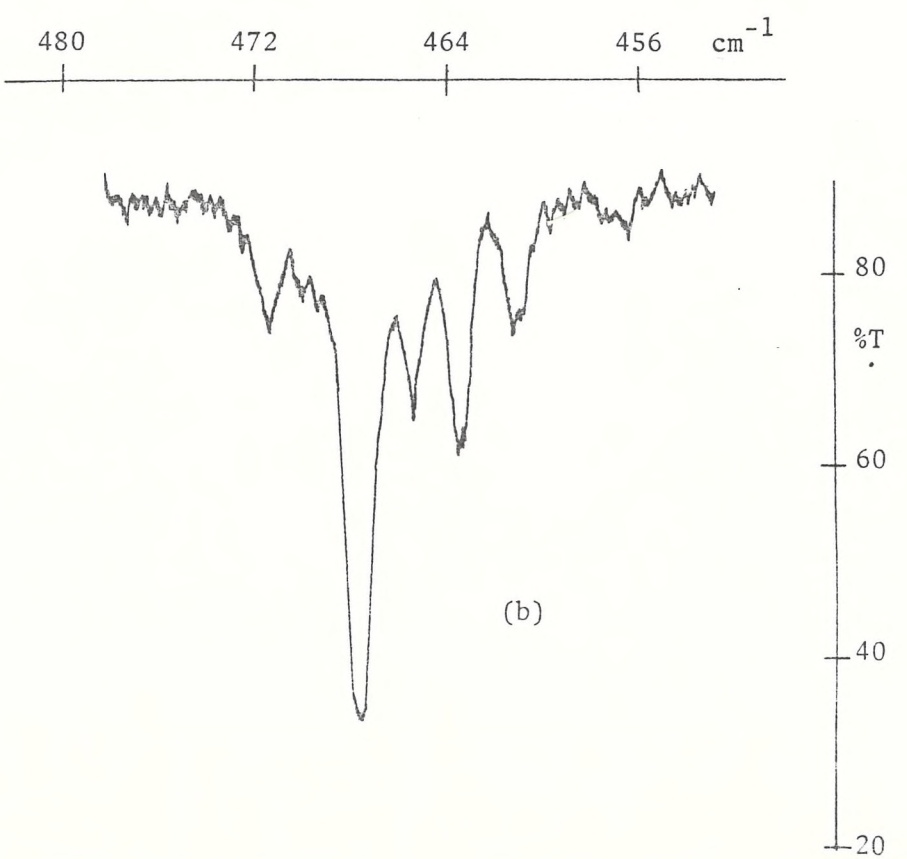

triatomic molecule of the type XY_2 where, as the YXY angle approaches 180^o, increasingly large errors in α are noted for a given isotopic shift uncertainty.[22] These limitations must be considered when any quantitative information is sought from observed isotopic shifts.

The spectra of $FeCl_3$ obtained in this work would appear to point to a planar D_{3h} geometry on the basis of symmetry selection rules (i.e. the non-observance in the infrared spectrum of the symmetric stretch). However on one spectrum a small band was observed in the infrared spectrum at 370 cm^{-1} (Raman observed,$\Delta\nu$, 371 cm^{-1}) when the antisymmetric stretch (ν_3) was off scale, (Figure 2.4(a)). The high resolution spectrum of this band is shown in Figure 2.4(b), and the absolute frequency, and isotope pattern observed would suggest that this is in fact ν_1. The appearance of ν_1 in the infrared spectrum could be due to the fact that $FeCl_3$ monomer is in fact pyramidal (bond angle < 120^o) or that a breakdown of the selection rules has occurred. This could be caused by the presence of impurities in the matrix (not unlikely after extended deposition) or as a result of matrix induced molecular distortion.

The estimation of bond angles for an MX_3 molecule from relative infrared intensities can be made if certain assumptions concerning the dipole moment of the molecule are made. If it is assumed that the stretching modes of the molecule are uncoupled from the bending modes then it can be shown that[10,12,23]

$$I_{A_1} = \left(\frac{\delta\mu}{\delta S_{A_1}}\right)^2 G_{A_1}$$

and

$$I_E = \left(\frac{\delta\mu}{\delta S_E}\right)^2 G_E$$

Where I_{A_1} and I_E represent the intensities of the A_1 and E vibrational modes respectively. $\frac{\delta\mu}{\delta S_k}$ represents the change in dipole moment with symmetry coordinate S_k, and μ represents the dipole moment of the molecule. G_k are G matrix elements for the irreducible representations k. If β is the semi-vertical angle between a bond and the C_3 axis (90^o for planar) then the changes in dipole moment with respect to each symmetry coordinate can be expressed as:

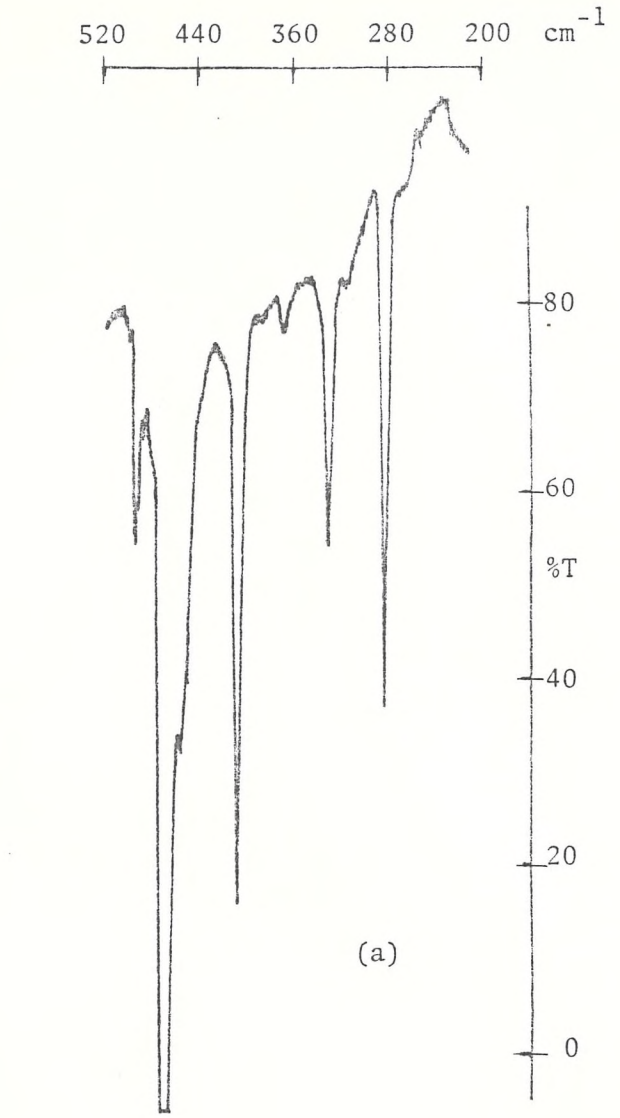

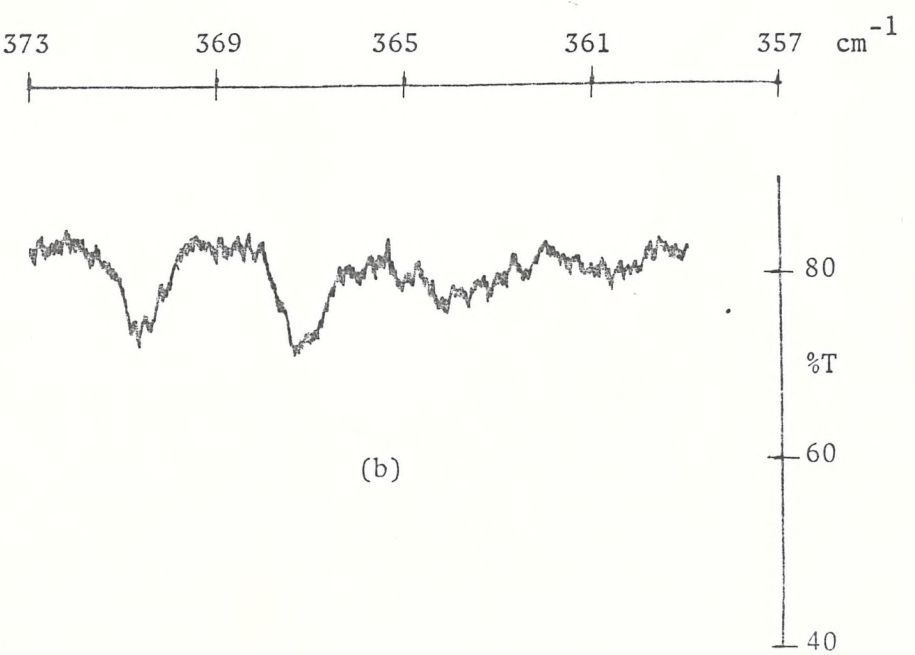

Figure 2.4(a) Infrared spectrum of matrix isolated $FeCl_3$/Fe_2Cl_6 after extended deposition

(b) High resolution spectrum of part of (a).

$$d\mu_{A_1} = \sqrt{3}\cos\beta \left(\frac{\delta\mu_r}{\delta r}\right) dr$$

and $$d\mu_E = \sqrt{2}\sqrt{3}\sin\beta \left(\frac{\delta\mu_r}{\delta r}\right) dr$$

where $\frac{\delta\mu_r}{\delta r}$ represents the change in dipole moment with respect to internal displacement coordinate.

It is assumed here that all elements μ_r can be vectorially summed over the whole molecule. Now,

$$G_{A_1} = \mu_X + \mu_M(1 + 2\cos\beta) \text{ and } G_E = \mu_X + \mu_M(1 - \cos\beta)$$

where μ_X and μ_M are the reciprocal masses of atoms X and M respectively. Therefore,

$$\frac{I_{A_1}}{I_E} = \frac{1}{2}\cot^2\beta \ \frac{(\mu_X + \mu_M(1 + 2\cos\beta))}{(\mu_X + \mu_M(1 - \cos\beta))}$$

If $\mu_X >> \mu_M$ (i.e. M is much more massive than X)

$$G_{A_1} \approx G_E$$

and $$\frac{I_{A_1}}{I_E} = \frac{1}{2}\cot^2\beta \qquad (11)$$

Although this final assumption is not strictly valid if atoms X and M are Cl and Fe the necessary correction will be small and Equation (11) can be used to give an estimate of the bond angle α which is related to the semi-vertical angle β by:

$$\sin\frac{\alpha}{2} = \frac{\sqrt{3}}{2}\sin\beta$$

The estimation of β, and hence α, for $FeCl_3$ from the spectrum shown in Figure 2.4(a) is further complicated by the fact that dimer bands present in the spectrum affect the observed relative intensities. This is because of the coincidence of $\nu_3(FeCl_3)$ and $\nu_8(Fe_2Cl_6)$. If however, $\nu_3(FeCl_3)$ is assumed to exhibit 80% transmittance, and ν_1 1% transmittance, then

estimation of the bond angle using Equation (11) yields a value of β of 84.8^{o} and a bond angle of 119.2^{o}. As this would appear from the spectrum to be a conservative estimate for the intensity of ν_3 then this approach would seem to add weight to the argument for a planar D_{3h} structure for monomeric $FeCl_3$.

A definitive estimation of the bond angle can be obtained in principle by exploiting central atom isotopic substitution. It is well known that the totally symmetric stretching mode of BCl_3 shows characteristic chlorine isotope splitting,[24] but a boron isotope effect has never been observed for this molecule. This is because during this vibration, for a truly D_{3h} species such as BCl_3, the central atom does not move at all, and the same may be expected for any D_{3h} planar MX_3 species. Using the procedures outlined in Section 2.6 and employing again the assumption that bending modes can be treated independently of stretching modes the following expressions can be obtained for the frequency of the totally symmetric stretching mode of a molecule of the type MX_3 where β is defined as before.

$$\lambda_1 = (Fr + 2Frr)(3\cos^2\beta\mu_M + \mu_X)$$

where $\lambda = 4\pi^2c^2\omega^2$ and Fr is the principal stretching force constant and Frr is the interaction constant. On substituting the central metal atom, a similar procedure yields a similar expression in terms of M' where M' is an isotopic variant of M and the assumption that the force field remains unchanged is made:

$$\lambda_1' = (Fr + 2Frr)(3\cos^2\beta\mu_{M'} + \mu_X)$$

This leads to an expression for the totally symmetric stretching frequency on central atom substitution of:

$$\omega_1^2(M') = \frac{M}{M'}\left(\frac{3M_X\cos^2\beta + M'}{3M_X\cos^2\beta + M}\ \omega_1^2(M)\right) .$$

where M_X is the mass of chlorine in the case of $FeCl_3$. It can be shown for a planar geometry ($\beta = 90^{o}$, $\cos 90^{o} = 0$) that this expression reduces to:

$$\omega_1^2(M') = \omega_1^2(M)$$

That is, no isotopic shift would be expected. Simple calculations based upon the above expression allow estimation of the bond angle for a given isotopic shift. In the case of the molecule $FeCl_3$, the expected shifts on central atom substitution ($^{58}Fe/^{54}Fe$) for some given bond angles are shown below.

β^o	Bond angle^o	$\nu_1(54)cm^{-1}$	$\nu_1(58)cm^{-1}$	$\nu_1(54)-\nu_1(58)cm^{-1}$
90	120.00	370	370	0
85	119.25	370	369.81	0.19
80	117.05	370	369.29	0.71
75	113.55	370	368.53	1.47
70	108.94	370	367.63	2.37

Table 2.2. The expected isotopic shifts for $FeCl_3$, on central atom substitution, for varying bond angles.

Clearly the shifts concerned are small and the accurate determination of the bond angle must be dependent upon the accuracy of the shift measurement. At this time, no conclusive experiments involving central atom substitution have been carried out for $FeCl_3$ and until this is achieved the shape of $FeCl_3$ monomer must remain in doubt. However all the evidence obtained from this work would point to a D_{3h} planar geometry.

In general therefore, isotopic substitution can yield information on a qualitative level concerning the identification of molecular species and individual vibrational bands, and on a quantitative level concerning the calculation of bond angles and refinement of force constants. The change in isotopic mass on substitution is usually of the order of 1 or 2 amu, and this means that the isotopic shift will be dependent upon the atomic mass of M or X. Therefore, although useful information can be readily obtained for $^{18}O/^{16}O$ and $^{35}Cl/^{37}Cl$, shifts due to $^{54}Fe/^{58}Fe$ substitution will be more difficult to observe and $^{81}Br/^{79}Br$ for example is of little use.

In this work isotopic substitution is used to confirm assignments of observed spectra to particular vibrations and to identify the species present. In addition, comparison of calculated and observed isotopic

splitting patterns is used to check the validity of proposed force fields and to refine force constant as well as to differentiate between possible molecular structures.

REFERENCES

1. M Moskovits, G A Ozin, Chapter 2 in 'Cryochemistry', Ed M Moskovits, G A Ozin, Wiley Interscience, NY, (1976).

2. R C Paule, J L Margrave, Chapter 6 in 'The Characterisation of High Temperature Vapours, Ed J L Margrave, Wiley NY, (1967).

3. L B Knight, W Weltner, J Chem Phys, (1971), 55, 5066.

4. J S Anderson, J S Ogden, J Chem Phys, (1969), 51, 10, 4189.

5. A Lowenschus, A Ron, O Schnepp, J Chem Phys, (1968), 49, 272.

6. I R Beattie, H E Blayden, S M Hall, S N Jenny, J S Ogden, J Chem Soc Dalton Trans, (1976), 666.

7. R D Wesley, C W DeKock, J Chem Phys, (1973), 77, 466.

8. Air Products and Chemicals Inc, Advanced Products Department, Allentown, Penn, USA.

9. Tables of Wavenumbers. International Union of Pure and Applied Chemistry, Butterworth, London, (1961).

10. 'Molecular Vibrations', E B Wilson, J C Decius, P C Cross, McGraw-Hill, NY, (1955).

11. 'Chemical Applications of Group Theory', F A Cotton, Wiley-Interscience, NY, 1971.

12. 'Infrared and Raman Spectroscopy', G Herzberg, Van Nostrand, Princeton, (1904).

13. I R Beattie, H E Blayden, S M Hall, S N Jenny, J S Ogden, J Chem Soc Dalton Trans, (1976), 666.

14. I R Beattie, N Cheetham, M S Gardner, D E Rogers, J Chem Soc (A), (1971), 2240.
M S Gardner, Ph.D. Thesis, Southampton University.

15. J S Ogden, Nat Bur Standards, Special Publication, 561, (1979), 511.

16. E Z Zasorin, N G Rambidi, Izv Akad Nauk SSSR, (1964), 2.
E Z Zasorin, N G Rambidi, J Struct Chem, (1963), 4, 836.

17. R A Frey, R D Werner, H H Gunthard, J Mol Spec, (1970), 35, 260.

18. L Lowenschus, A Givan, Ber Bunsen Phys Chem, (1978), 82, 75.

19. See Reference 6.

20. J S Ogden, Ber Bunsen Phys Chem, (1978), 82, 76.

21. M Allavena, R Rysnik, D White, V Calder, D E Mann, J Chem Phys, (1969), 50, 3399.

22. A J Downs, S C Peak, 'Molecular Spectroscopy', Ed R F Barrow, D A Long, D J Millen, Spec Per Reports, The Chem Soc, (1973), Vol 1, 523.

23. R A Crocombe, Ph.D. Thesis, Southampton University, (1978).

24. R J H Clark, P D Mitchell, J Chem Phys, (1972), 56, 2225.

CHAPTER 3

MATRIX ISOLATION STUDIES ON ALKALI-METAL PHOSPHATE VAPOURS

3.1 INTRODUCTION

Alkali-metal phosphates constitute a major area of inorganic chemistry, but until recently structural determinations of these systems have been concerned with the solid state and with solution species. In the solid state X-ray crystallography has been the major technique employed and a large collection of results has been assessed.[1-3] Vibrational spectroscopy has been used to a lesser extent in the study of solutions,[4] glasses[5] and powders.[6] The last decade has also seen growing interest in molten phosphates as potential solvents,[7] but it is only quite recently that alkali-metal phosphate molecules have been identified in the vapour phase. Here high temperature mass spectrometry in particular[8-14] has shown that the monomeric species MPO_3 (M = Li, Na, K, Rb, Cs) are prominent species in the vapour above heated metaphosphates, but no structural data have yet been reported for these molecules.

In general gaseous group Vb oxides have been examined to a far greater extent than the vapours above the corresponding oxo-anions, but a recent investigation using matrix isolation coupled with isotopic substitution has resolved the structure of KNO_3 in favour of bidentate coordination of the metal ion[15] where doubt previously existed. The spectrum of NO_2^- has also been reported.[16]

The aim of the work described in this chapter was to identify some of the species present in the vapour above heated alkali-metal phosphates and to use isotopic substitution to obtain a structural characterisation of the molecule $NaPO_3$ which has been identified in the vapour phase by mass spectrometry.[9,10]

3.2 THE INFRARED SPECTRA OF MATRIX ISOLATED ALKALI METAL PHOSPHATES

The starting point of this investigation was the vaporisation of some commonly occurring alkali metal phosphate salts. Those used were the metaphosphates of both sodium and potassium and the orthophosphate of sodium. The metaphosphates were obtained as anhydrous salts (BDH) and anhydrous sodium orthophosphate was obtained in quantitative yield from the hydrated salt ($Na_3PO_4.12H_2O$) by heating in vacuo to $\sim 250^{\circ}C$.[17] These phosphates were all vaporised from inductively heated alumina holders at

temperatures of 1550-1650 K, and the products of vaporisation were condensed in an argon matrix at 12 K. The infrared spectra of these deposits were typically as those in Figure 3.1.

Figure 3.1(a) shows the infrared spectrum obtained from a deposit of sodium orthophosphate after a deposition time of ca 40 minutes, and sharp absorptions were observed at 1341.7 cm^{-1} and 1211.2 cm^{-1}. Weaker features were also noted at 1004.0 cm^{-1}, 586.6 cm^{-1}, 474.0 cm^{-1} and 287.0 cm^{-1}. The metaphosphate of sodium also exhibited bands at 1341.7 cm^{-1}, 1211.2 cm^{-1}, 1004.0 cm^{-1}, 536.6 cm^{-1} and 474.0 cm^{-1}, but in addition bands at 1144.0/1137.5 cm^{-1} (doublet) and 1058.0/1052.2 cm^{-1} (doublet) were also observed, Figure 3.1(b). The spectrum of potassium metaphosphate consisted of bands at 1333.75 cm^{-1}, 1221.0 cm^{-1}, 1085.0 cm^{-1}, 521.5 cm^{-1} and 476 cm^{-1}, Figure 3.1(c). All observed frequencies are summarised in Table 3.1. Minor variations in deposition conditions (e.g. matrix gas flow rate, sample temperature) produced no detectable changes in the relative intensities of the bands observed for the sodium orthophosphate and potassium metaphosphate systems. However, the 1144.0/1137.5 cm^{-1} and 1058.0/1052.2 cm^{-1} doublets observed in the sodium metaphosphate system, although always present, did vary in intensity relative to the other bands observed in the spectrum. Controlled diffusion studies performed on the two metaphosphate systems also showed no significant relative intensity variations. The two highest frequency bands in both cases decreased in intensity with the growth of broad polymer features, Figure 3.2. The 1144.0/1137.5 cm^{-1} doublet observed in the sodium metaphosphate spectrum behaved in a similar manner, while the 1058.0/1052.2 cm^{-1} doublet was not observed after diffusion, possibly as a result of its relatively low intensity in the original spectrum.

It would appear therefore, that in each case, (apart from the 1144.0/1137.5 cm^{-1} and 1058.0/1052.2 cm^{-1} doublets in the sodium metaphosphate spectrum) all bands are associated with a single molecular species. At this stage, the spectra observed were assigned to the species $NaPO_3$ and KPO_3 and subsequent work has shown that the 1144.0/1137.5 cm^{-1} and 1058.0/1052.2 cm^{-1} doublets are fundamentals of the species $NaPO_2$.[18] The interpretation of these spectra in terms of the molecules $NaPO_3$ and KPO_3 is suggested by three observations. First, the considerable qualitative

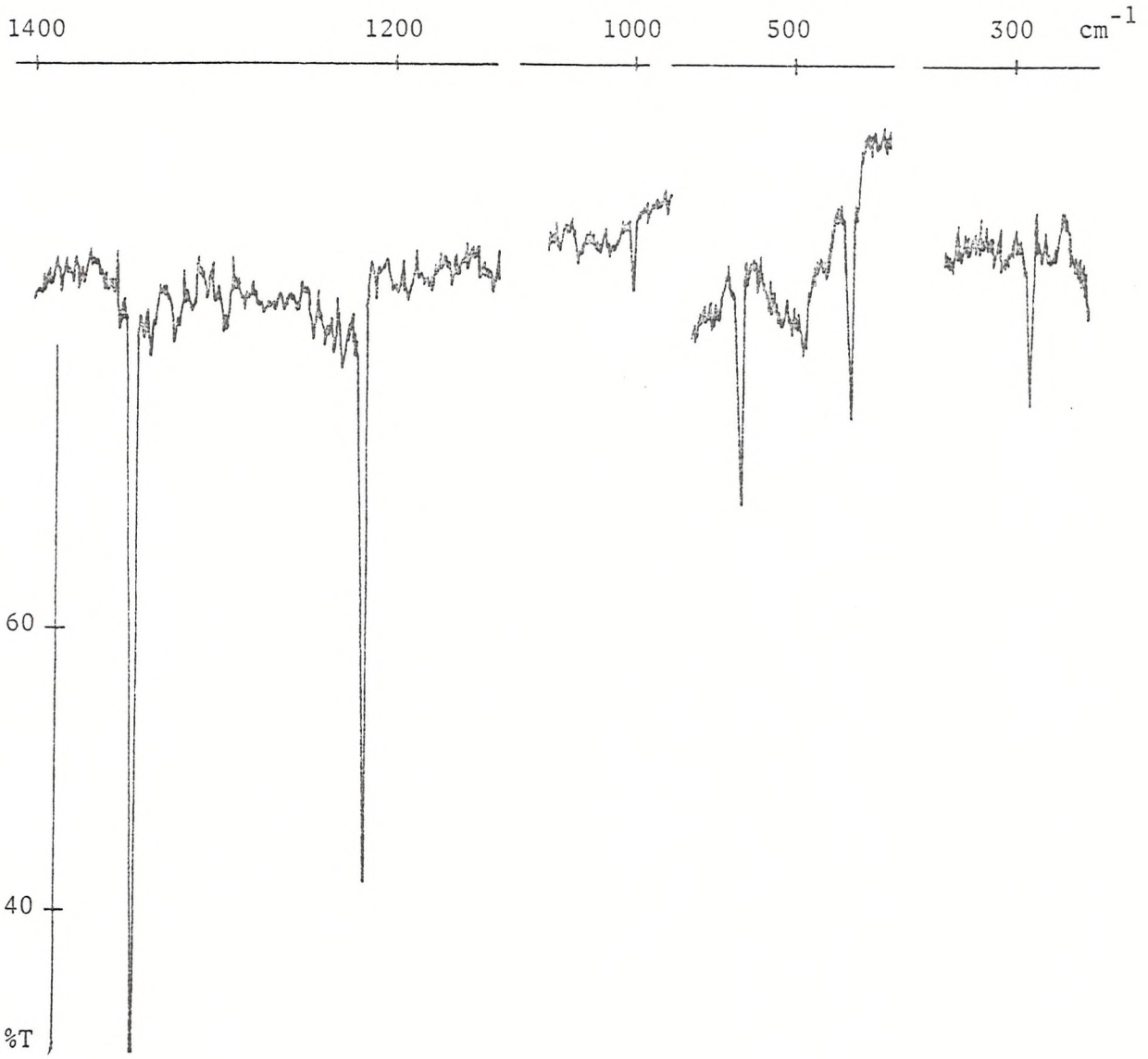

Figure 3.1(a) Infrared spectrum of matrix isolated sodium orthophosphate vapour (argon matrix).

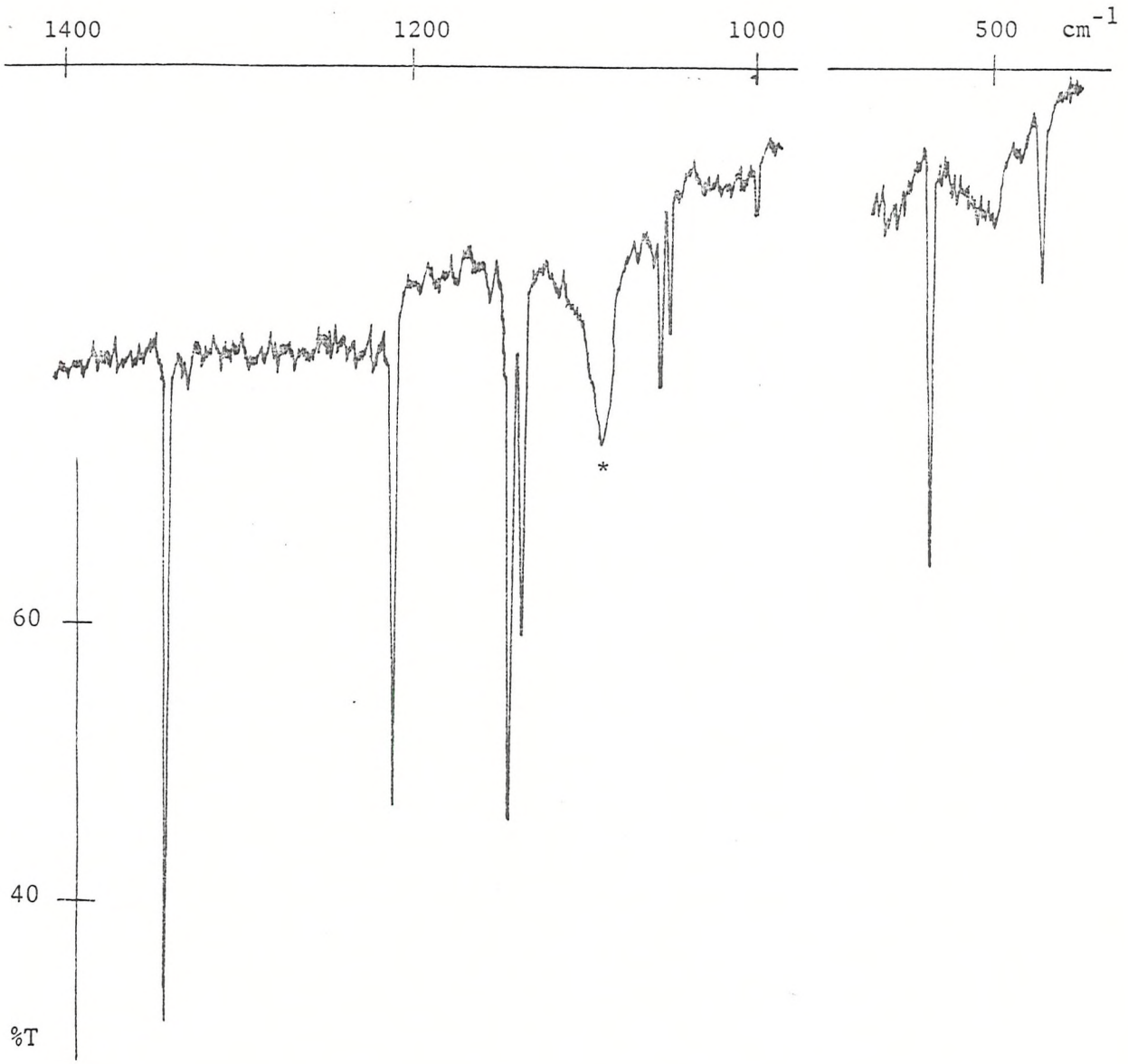

Figure 3.1(b) Infrared spectrum of matrix isolated sodium metaphosphate vapour (argon matrix). (* present on background spectrum).

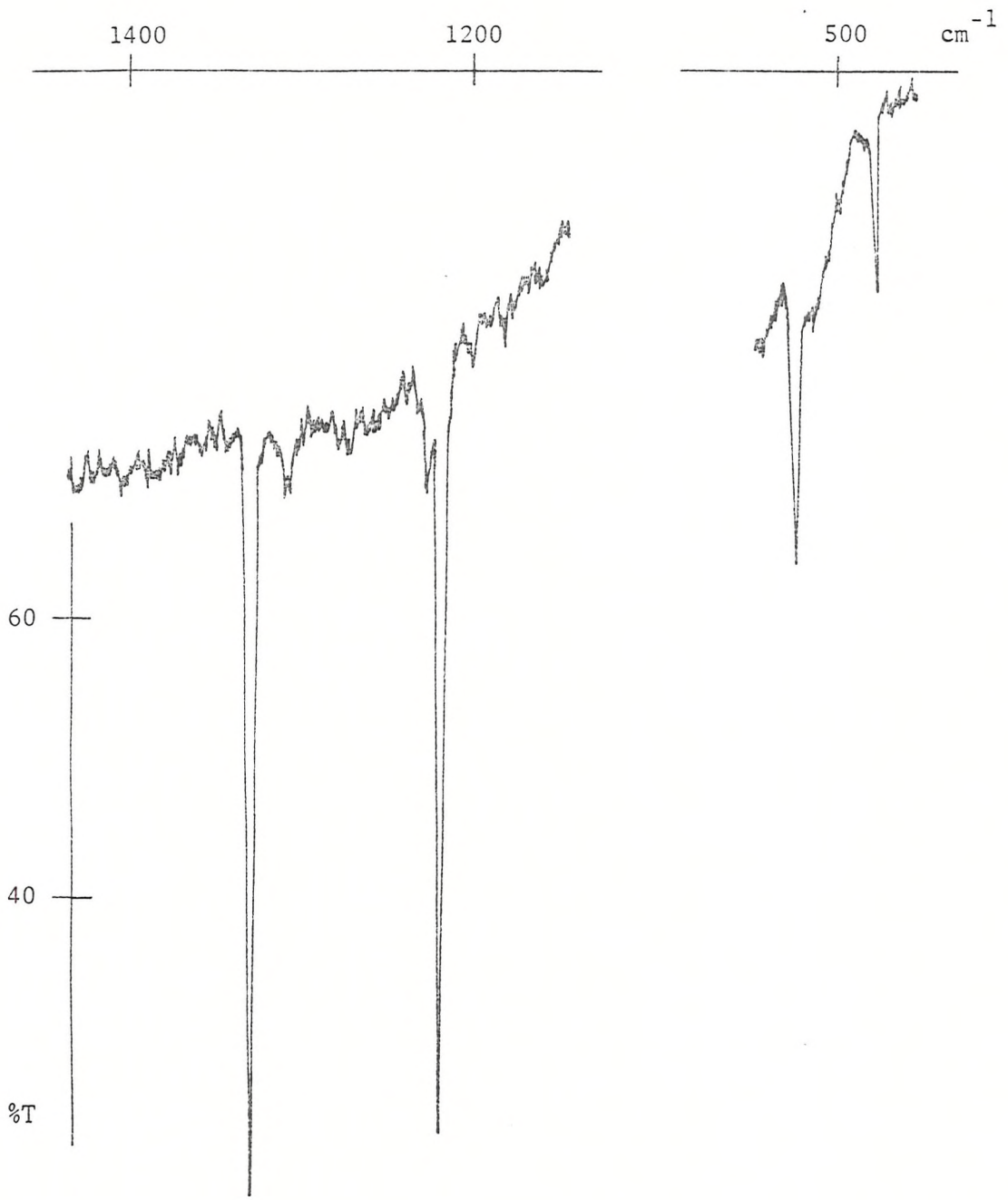

Figure 3.1(c) Infrared spectrum of matrix isolated potassium metaphosphate vapour (argon matrix).

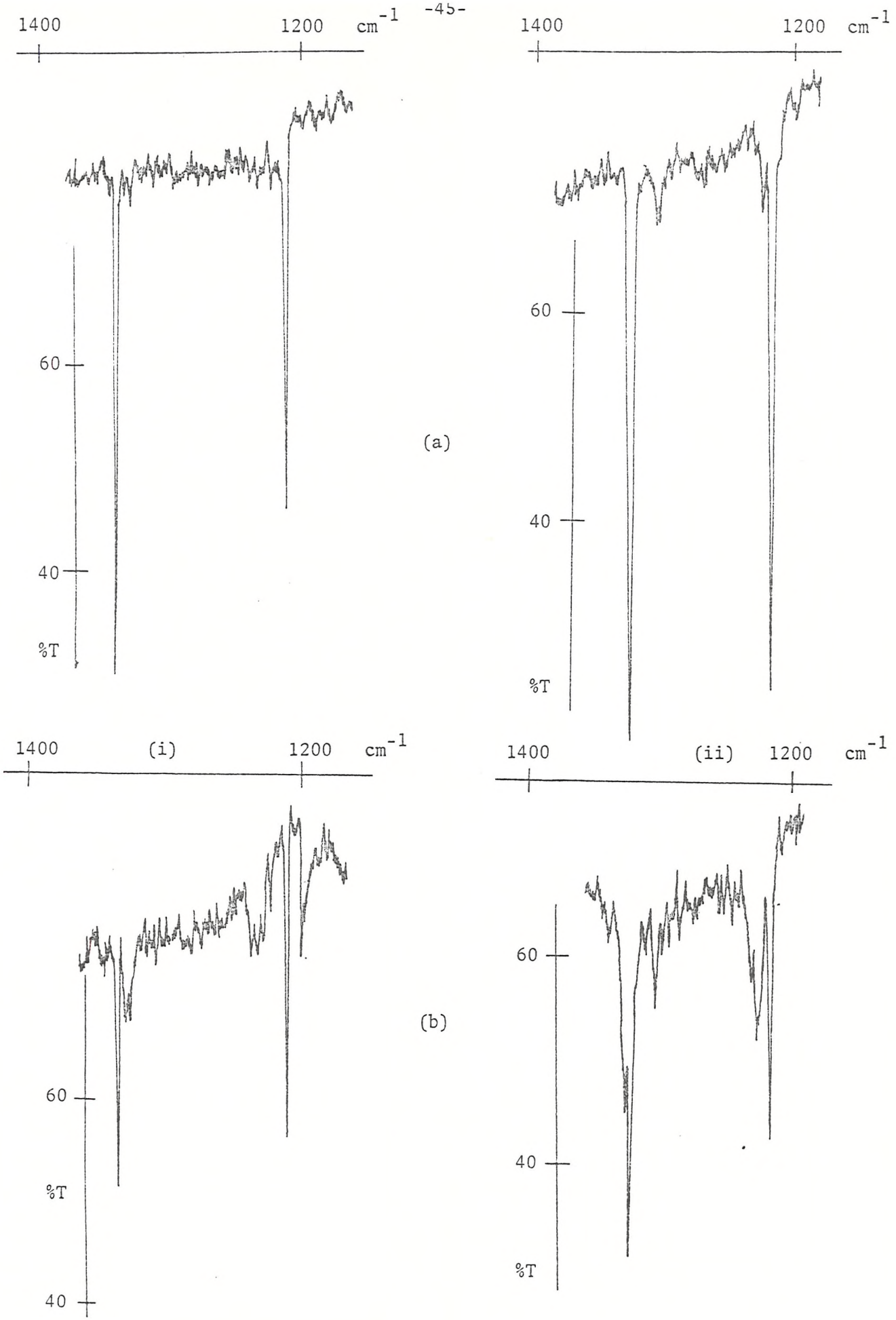

Figure 3.2 The result of controlled diffusion on the two highest frequency bands of matrix isolated sodium (i) and potassium (ii) metaphosphates (argon matrices); (a) before diffusion, (b) after diffusion.

similarity between these spectra and that of matrix isolated KNO_3 [15] would indicate that this is a reasonable interpretation, Figure 3.3. Secondly, the frequencies of corresponding bands of the sodium and potassium systems are cation dependent as would be expected, and would indicate that the presence of a simple phosphorus/oxygen species is unlikely and finally this interpretation is supported by the information gained using isotopic enrichment which is discussed in detail in subsequent sections. All observed bands and their qualitative assignments are given in Table 3.1.

Of the phosphate salts used the best spectral quality was obtained from vaporisation of sodium orthophosphate (Na_3PO_4) and for this reason, this salt was chosen for the subsequent ^{18}O enrichment studies.

3.3 THE DETERMINATION OF THE MODE OF COORDINATION IN MXO_3 SPECIES

A free XO_3^- ion will have D_{3h} symmetry and the normal modes of vibration will be distributed among the symmetry species according to:

$$\Gamma_{vib} = A_1' + A_2'' + 2E'$$

as is the case for planar MCl_3 species (see Chapter 2). Of these the A_1' mode is Raman active, the A_2'' mode is infrared active and the E' modes are both infrared and Raman active. Coordination of the metal atom can take place via oxygen in either monodentate or bidentate modes. Either of these two modes of coordination reduce the symmetry of the molecule to C_{2v} and the correlation of vibrations of such a molecule with those of the D_{3h} parent ion is as follows:

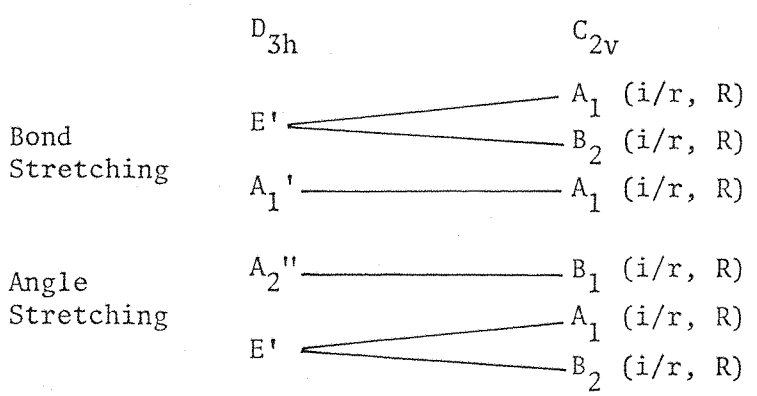

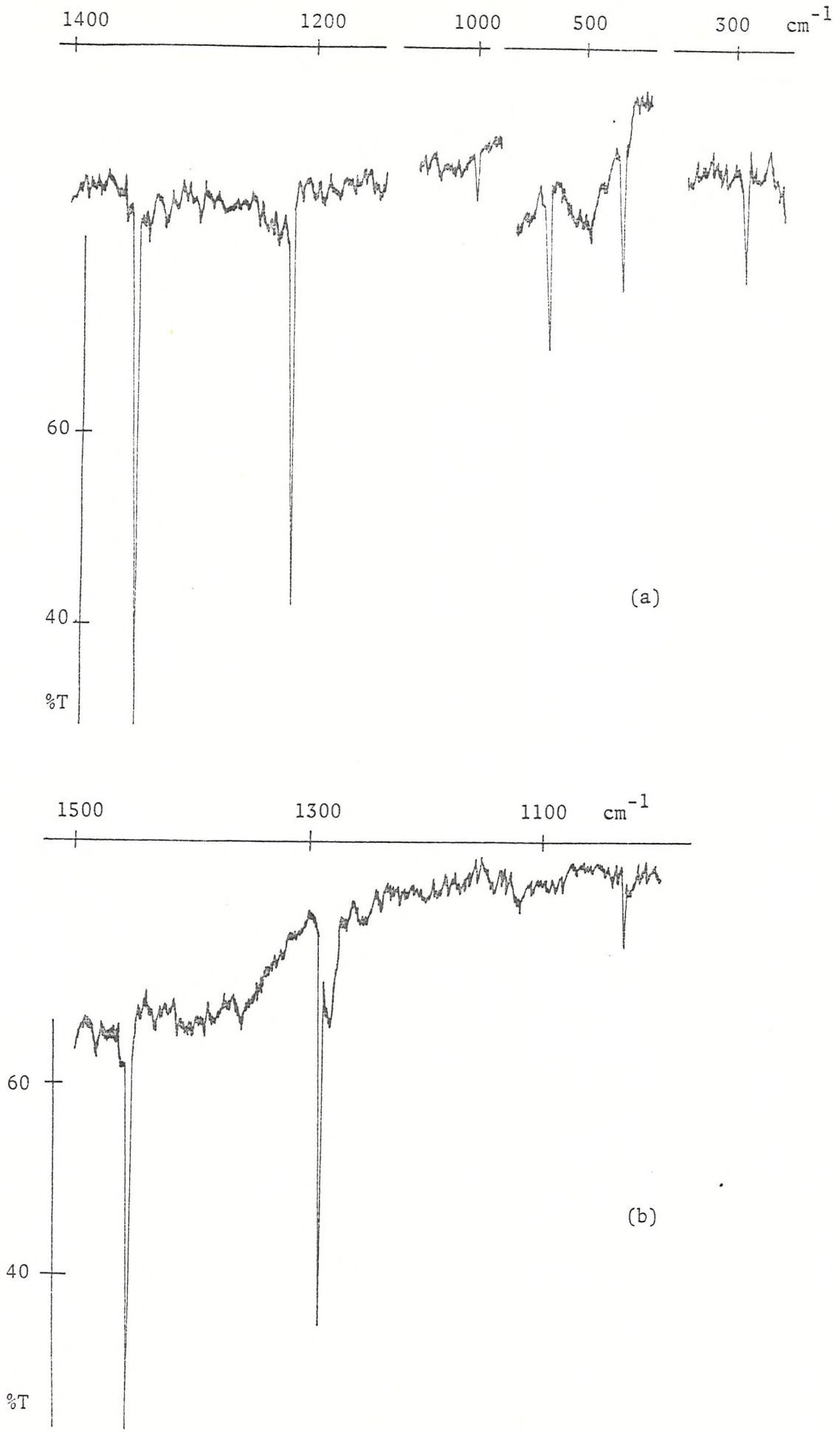

Figure 3.3 Infrared spectra of matrix isolated sodium orthophosphate vapour (a) (argon matrix) and potassium nitrate[15],

Table 3.1 Vibrational frequencies observed for some alkali-metal phosphate systems.

Sodium Orthophosphate Observed Frequencies (argon matrix) cm^{-1} (b)	Sodium Metaphosphate Observed Frequencies (argon matrix) cm^{-1} (b)	Assignment	$NaPO_2$ (a) Observed Frequencies (nitrogen matrix) cm^{-1}	Potassium Metaphosphate Observed Frequencies (argon matrix) cm^{-1} (b)	Assignment
1341.7	1341.7	$NaPO_3$		1333.8	KPO_3
1211.2	1211.2	$NaPO_3$		1221.0	KPO_3
	1144.0 1137.5	$NaPO_2$	1151.6		
	1058.0 1052.2	$NaPO_2$	1062.1		
1004.0	1004.0	$NaPO_3$		1085.0	KPO_3?
536.6	536.6	$NaPO_3$		521.5	KPO_3
474.0	474.0	$NaPO_3$		476.0	KPO_3
287.0		$NaPO_3$			

(a) from Reference 18.

(b) frequency accuracy ± 0.4 cm^{-1}

Coordination of the metal atom via phosphorus can be ruled out at this point since the resulting molecule will have C_{3v} symmetry and the degeneracy of the E' mode is not removed resulting in only a two line spectrum in the stretching region. Distinguishing between monodentate and bidentate binding is not therefore achieved by simple 'band counting' and another approach must be employed.

The general problem of distinguishing between monodentate and bidentate binding in molecules of this type has been extensively reviewed [19] and the work of Hester and co-workers[20,21] describes how an unequivocal distinction based upon spectroscopic data is theoretically possible if the symmetries of the X-O stretching modes, (in molecules of the type MXO_3) can be correctly assigned. In a C_{2v} bidentate complex the expected order of the X-O stretching modes is[20] $\nu A_1 > \nu B_2 > \nu A_1$ and this is different from that predicted for an idealised monodentate complex where $\nu B_2 > \nu A_1 > \nu A_1$. For both types of complex these three stretching modes are both infrared and Raman active and in principle, a definitive depolarisation study in the Raman should establish the assignments of the A_1 and B_2 modes and hence the type of coordination present. However the identification of even strongly polarised bands in matrix isolation spectra is regarded as at the least difficult by most experimentalists and consequently the approach developed recently for KNO_3, using isotopic substitution was employed to establish the mode of coordination in $NaPO_3$. This method has been described in detail,[15] but the essential features are as follows. Since the approach is concerned exclusively with the stretching region of the infrared spectrum an initial assumption is made that the stretching modes for both free and coordinated XO_3^- ions are uncoupled from the bending modes. Two stretching force constants then suffice to describe the A' and E' modes of a free D_{3h} XO_3^- ion, and these have been labelled K_r and K_{rr}, the principal and interaction stretching constants. The equivalence of the three X-O bonds is removed on coordination giving a unique bond with force constant K_1 and two other equivalent bonds with force constant K_2. Monodentate coordination can then be simulated by reducing K_1 and increasing K_2 and the reverse process simulates bidentate coordination. It is assumed that the XO_3 unit remains planar, with all interbond angles being set to 120^o. In the case of the

nitrate ion a series of calculations was carried out which ranged from 'strong' monodentate binding through 'free' nitrate to strong bidentate coordination, incorporating a 50% random distribution of ^{18}O atoms. The basic assumption is made that all frequency components arising from the parent E' mode in a D_{3h} molecule have equal absorbances. Thus in coordinated XO_3 where the degeneracy is lifted as a result of inequivalent force constants, the A_1 and B_2 components are taken to have the same intensity whilst in free XO_3^- where the degeneracy is removed as a result of inequivalent oxygen masses, the same assumption is made. This assumption has been shown to be reasonable.[22]

The free nitrate calculations yield an isotope pattern which appears as an almost equally spaced quartet characteristic of partial substitution of the E' stretching mode of a molecule of the type XY_3 [23] (see also Chapter 2). In the case of bidentate binding two groups of bands emerge which can be readily associated with the A_1 and B_2 components of the split E' mode, the highest frequency group appearing under high resolution essentially as a 1:1 doublet, each doublet consisting of a closely spaced 1:2:1 triplet. The highest frequency (A_1) mode in bidentate coordination thus gives rise to a total of six bands on ^{18}O substitution. These arise from the terminal X=O modes and are derived from the possible isotopic species as follows:

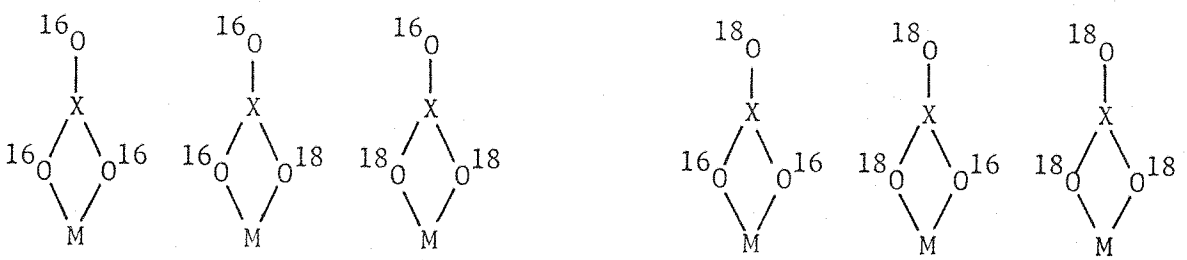

← increasing frequency

For monodentate binding the highest frequency mode is of B_2 symmetry and is calculated to appear as a 1:2:1 triplet and this arises from the three different types of terminal groups present. The calculation predicts superposition of B_2 frequencies for species which differ only in the nature of the bridging isotope.

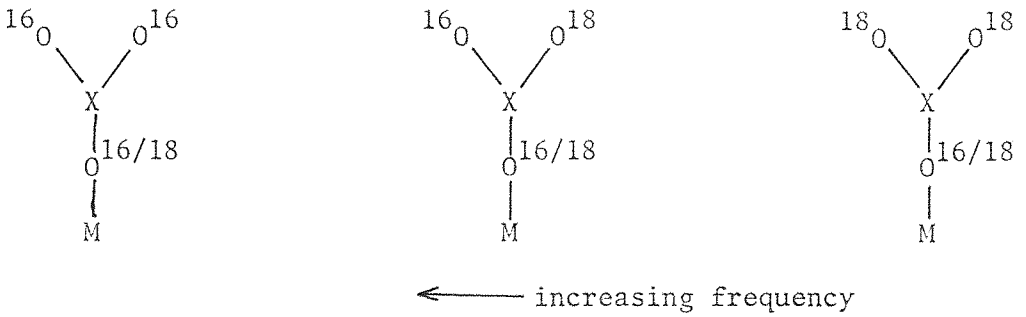

A diagramatic representation of the isotope patterns expected for mono- and bidentate binding and their derivation from the D_{3h} $[XO_3]^-$ ion is shown in Figure 3.4.

The observation of isotopic splitting patterns can therefore result in unequivocal distinction between monodentate and bidentate coordination in molecules of the type MXO_3. It was decided at this stage to attempt to prepare isotopically substituted Na_3PO_4 and to subsequently record the high resolution infrared spectrum of $^{16}O/^{18}O$ $NaPO_3$, with a view to determining the mode of cation binding.

3.4 THE INFRARED SPECTRUM OF $NaPO_3$ (^{16}O:^{18}O = ~3:1)

Samples of ^{18}O enriched phosphate were obtained by elemental oxidation of the metal phosphide in a reaction sequence initially explored using $^{16}O_2$. A stoichiometric (3:1) mixture of sodium and freshly distilled white phosphorus was gently warmed in an atmosphere of argon until reaction was complete. After removal of the argon the resulting black-red phosphide (Na_3P) was reacted with an excess of oxygen gas of known isotopic abundance until there was no further take-up. During this stage it was necessary to apply gentle heat from time to time to ensure continuous reaction. The product of this oxidation was typically a colourless glassy solid containing small amounts of embedded dark material which was almost certainly unreacted phosphide, covered with an impervious layer of phosphate. However, although this reaction only occasionally went to completion, all ^{16}O samples prepared in this way ultimately yielded matrix infrared spectra identical to those obtained from commercial samples of Na_3PO_4.

The effect on the infrared spectrum of ^{18}O enrichment is shown in Figure 3.5. Here a phosphate sample enriched with ca 28 atom % ^{18}O

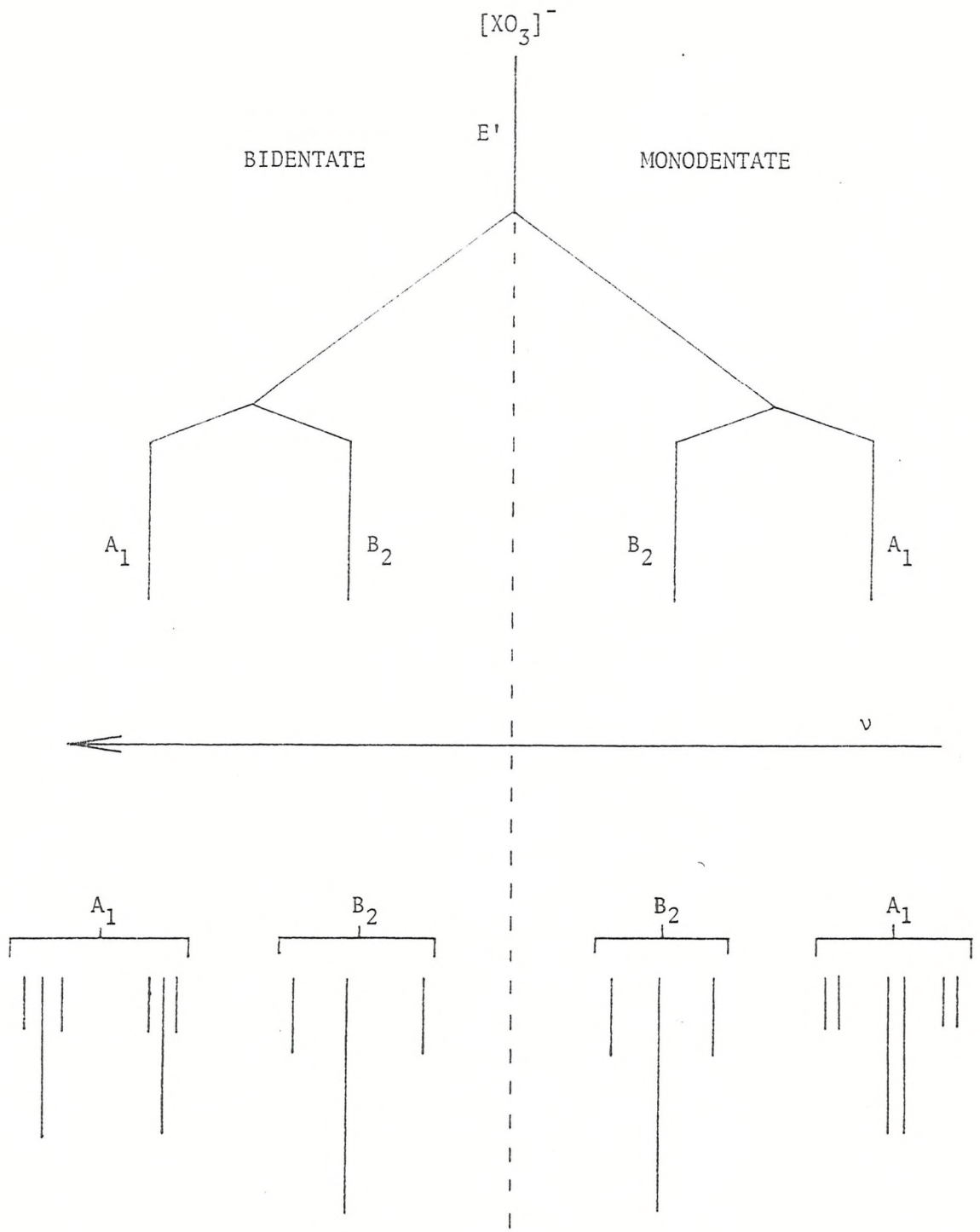

Figure 3.4 Expected isotope patterns for mono- and bi-dentate binding in coordinated $[XO_3]^-$ species.

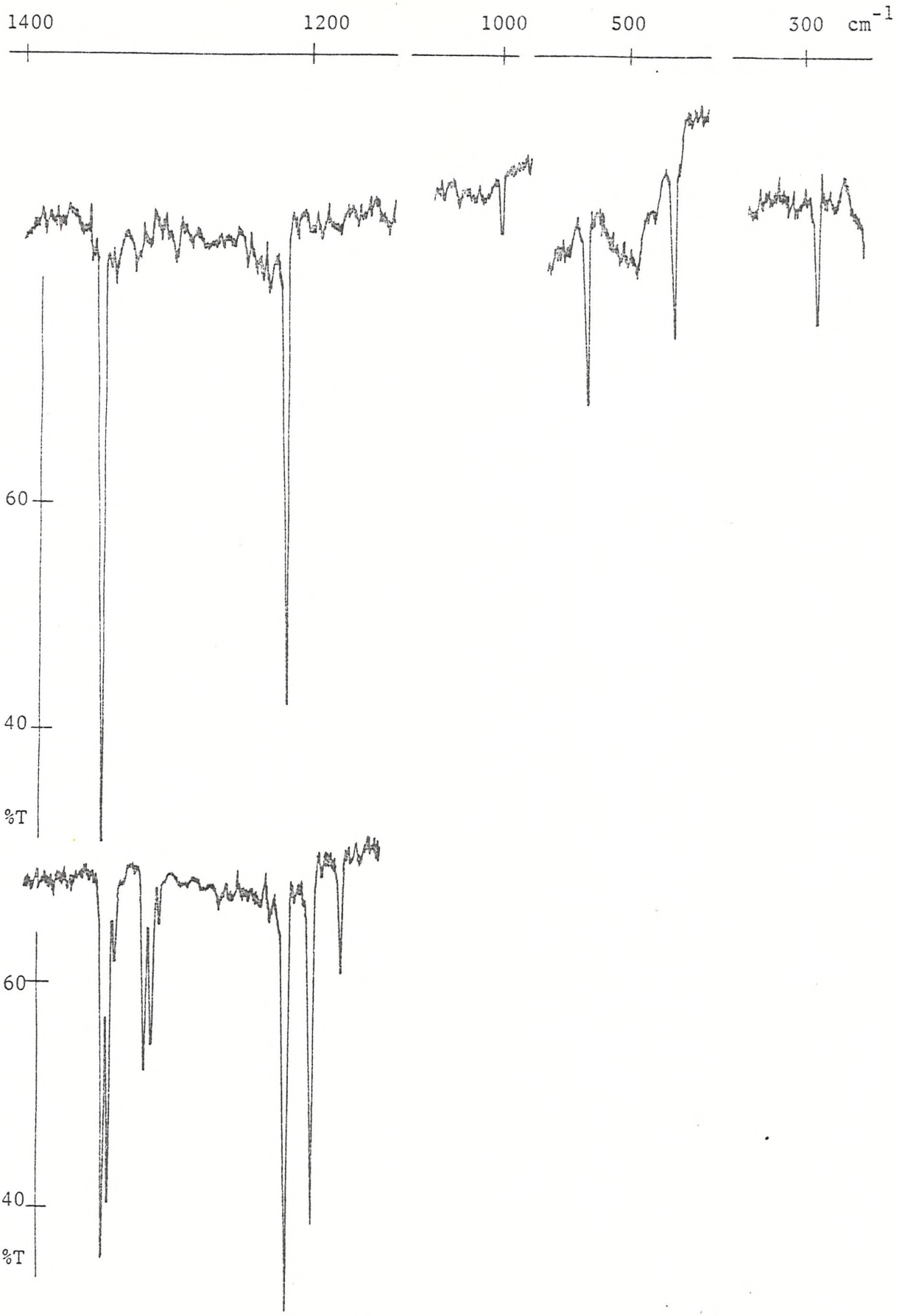

Figure 3.5 The effect of ^{18}O enrichment on the infrared spectrum of matrix isolated $NaPO_3$ (argon matrices).

has been isolated in an argon matrix, and it is evident that extensive isotope fine structure is present. In particular, the band at 1341.7 cm^{-1} now appears as a basic doublet each component of which consists of a closely spaced triplet whilst the second intense band at 1211.2 cm^{-1} appears as a well spaced triplet. Isotope fine structure was also observed for the weaker 474.0 cm^{-1} band (under high resolution only) but could not be satisfactorily obtained for the remaining bands. High resolution studies were carried out on the bands observed at 1341.7 cm^{-1}, 1211.2 cm^{-1} and 474.0 cm^{-1}. These spectra are shown in Figure 3.6(a)(b)(c). The remaining bands were not of sufficiently high intensity to yield meaningful isotope patterns. The nature of the spectra obtained and of the isotope patterns observed would clearly indicate a frequency order $\nu A_1 > \nu B_2 > \nu A_1$ for the P-O stretching modes (see Section 3.3) and consequently a bidentate structure for the molecule $NaPO_3$. The following force constant analysis is based on this assignment. The observed $NaPO_3$ (^{16}O) fundamentals are listed in Table 3.2 together with their assignments on the basis of a C_{2v} bidentate structure. Table 3.2 also contains the frequencies of the bands observed on isotopic substitution, along with the isotopic species from which they originate.

3.5 SPECTRAL INTERPRETATION AND FORCE CONSTANT ANALYSIS

The quantitative analysis of the spectra obtained on isotopic substitution is concerned first with the in-plane motion of the PO_3^- ion, neglecting cation motion. The overall approach is concerned with the calculation of frequencies from an appropriate model which are in agreement with the frequencies observed for the eleven distinct bands assigned to the isotopically substituted species $NaP^{16}O_n{}^{18}O_{3-n}$ (n = 0-3).

It has been shown that[15] for KNO_3 the two principal stretching force constants (F_R and F_D) and the principal interaction constant (F_{RD}) calculated from the three observed stretching frequencies in the all ^{16}O spectrum generate an isotope pattern whose frequency fit is well outside experimental error. A more realistic force field was used for KNO_3 and satisfactory agreement between observed and calculated frequencies was obtained, and this force field was applied to $NaPO_3$.

Table 3.2 Vibrational Frequencies (cm^{-1}) of isotopically substituted $NaPO_3$ isolated in argon matrices.

Observed[a]	Calculated[b]	Assignment[c]
1341.7	1341.7	$Na^{16}O^{16}OP^{16}O$ (A_1)
1338.0	1337.6	$Na^{16}O^{18}OP^{16}O$
1333.2	1332.8	$Na^{18}O^{18}OP^{16}O$
1312.2	1311.9	$Na^{16}O^{16}OP^{18}O$
1307.5	1306.8	$Na^{16}O^{18}OP^{18}O$
1302.0	1300.5	$Na^{18}O^{18}OP^{18}O$
1211.2	1211.2	$Na^{16}O^{16}OP^{16}O$ (B_2)
	1211.2	$Na^{16}O^{16}OP^{18}O$
1193.3	1193.4	$Na^{16}O^{18}OP^{16}O$
	1192.8	$Na^{16}O^{18}OP^{18}O$
1173.5	1173.3	$Na^{18}O^{18}OP^{16}O$
	1173.3	$Na^{18}O^{18}OP^{18}O$
1004.0	1004.0	$NaP^{16}O_3$ (A_1)
536.6	536.6	$NaP^{16}O_3$ (B_2)
474.0	474.0	$NaP^{16}O_3$ (B_1)
470.4	470.5	$NaP^{16}O_2{}^{18}O$
466.8	467.1	$NaP^{16}O^{18}O_2$
463.3	463.6	$NaP^{18}O_3$
287.0		νNa-O (?)

(a) Frequency accuracy 0.3 cm^{-1}.

(b) Calculated using force field and model shown in Table 3.2.

(c) Assuming C_{2v} bidentate structure.

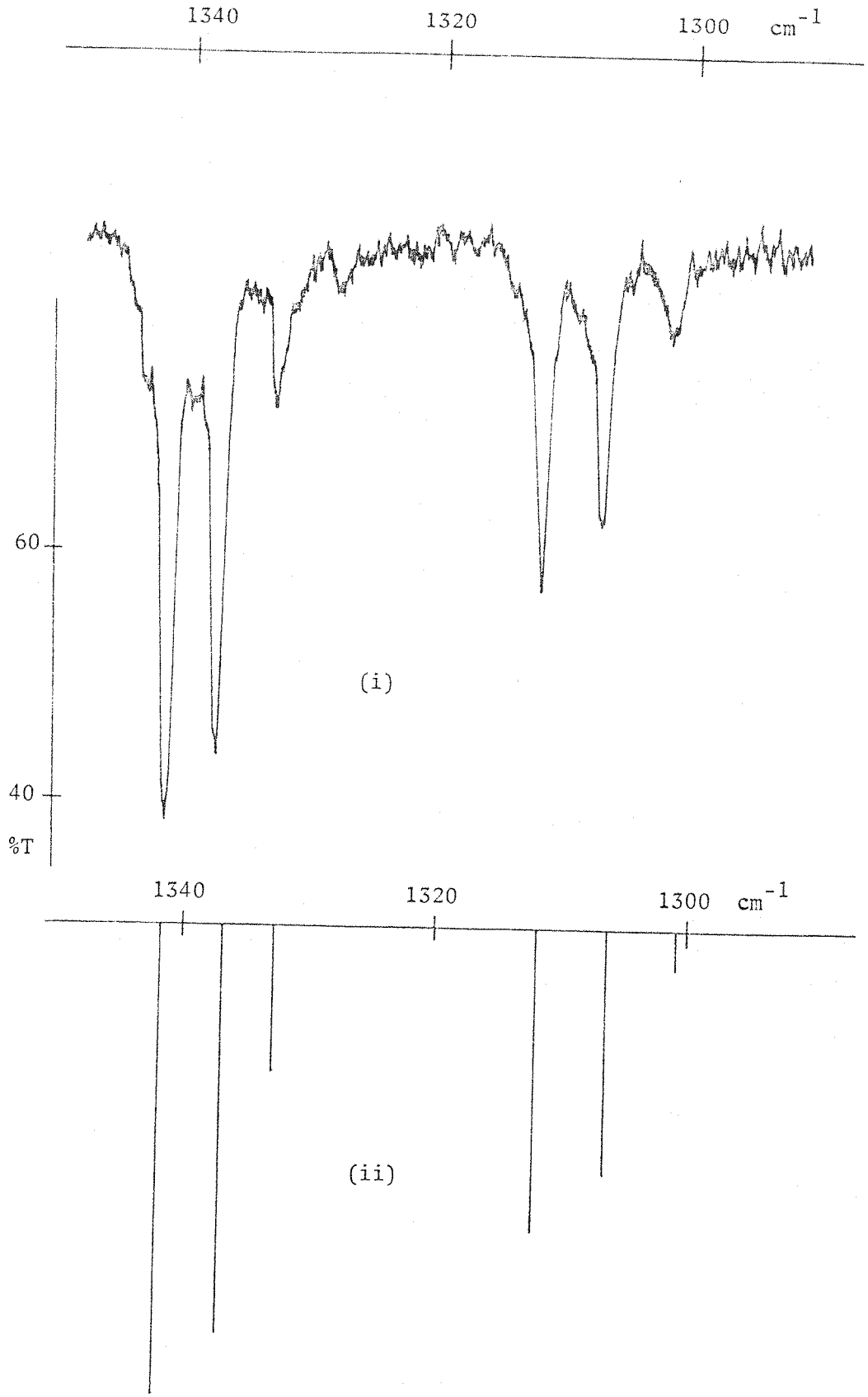

Figure 3.6(a) (i) High resolution infrared spectrum of the highest frequency A_1 modes of matrix isolated $NaPO_3$ (^{18}O enriched) - argon matrix.
(ii) Calculated spectrum.

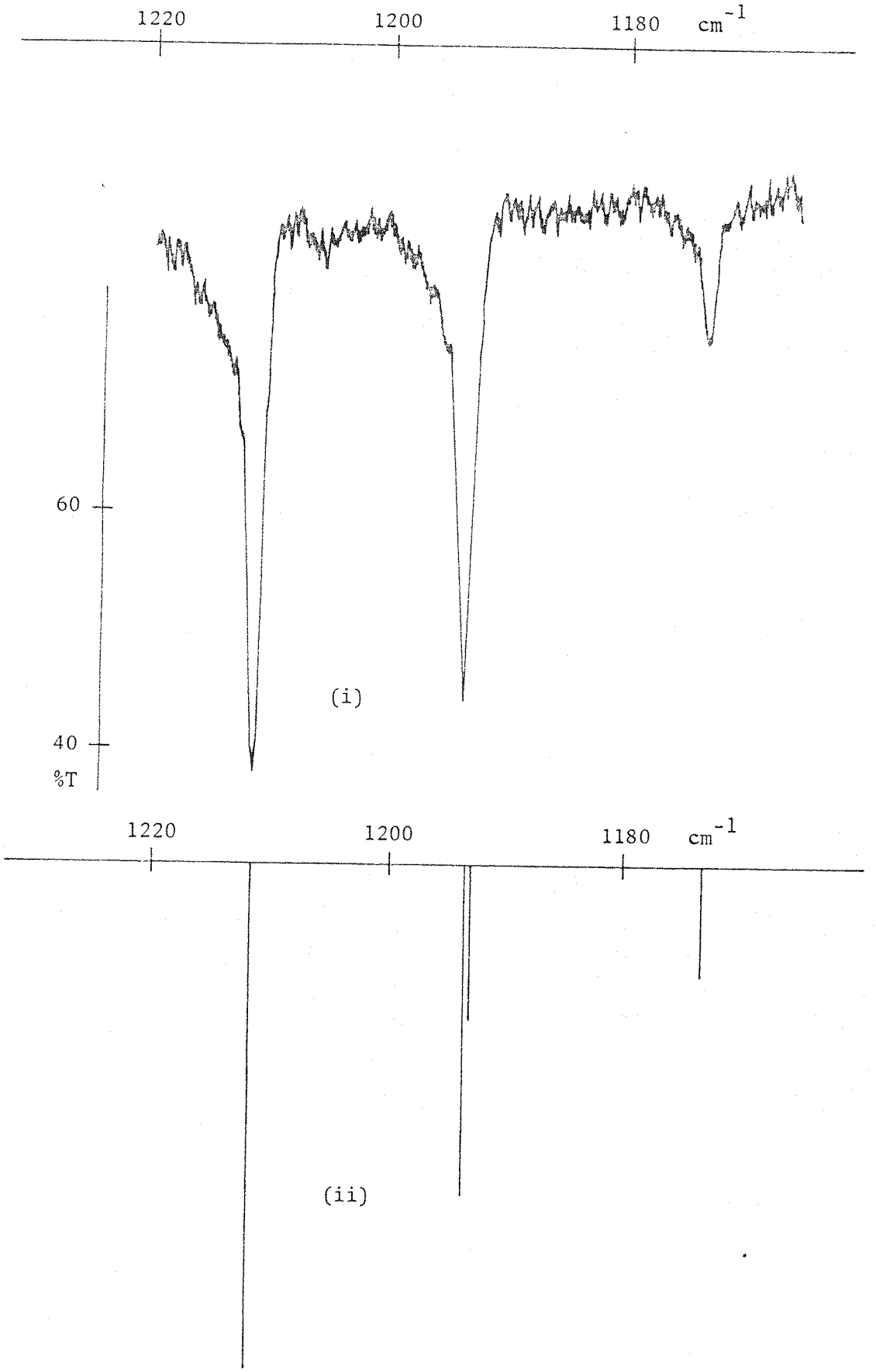

Figure 3.6(b) (i) High resolution infrared spectrum of the highest frequency B_2 mode of matrix isolated $NaPO_3$ (^{18}O enriched) - argon matrix.
(ii) Calculated spectrum.

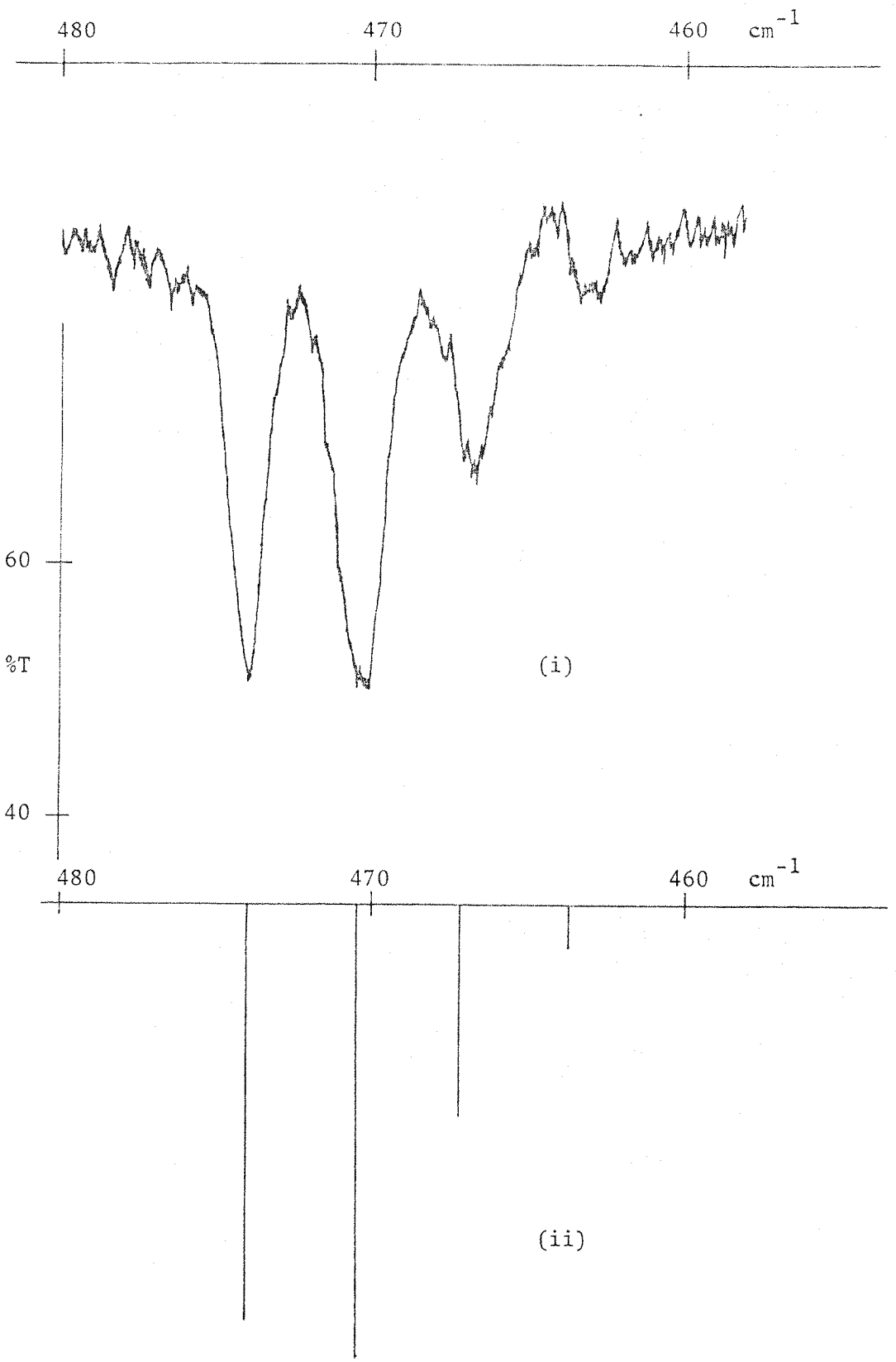

Figure 3.6(c) (i) High resolution infrared spectrum of the out of plane bending mode of matrix isolated $NaPO_3$ (^{18}O enriched) - argon matrix.
(ii) Calculated spectrum.

Using the standard FG matrix method (see Section 2.6) the following symmetry coordinates can be written down to represent the three A_1 and two B_2 vibrations of the PO_3^- unit, ignoring cation motion:

$$S_1 = \Delta R \qquad (A_1)$$

$$S_2 = \frac{1}{\sqrt{2}}(\Delta D_1 + \Delta D_2) \quad (A_1)$$

$$S_3 = \frac{1}{\sqrt{2}}(\Delta \theta_1 + \Delta \theta_2) \quad (A_1)$$

$$S_4 = \frac{1}{\sqrt{2}}(\Delta D_1 - \Delta D_2) \quad (B_2)$$

$$S_5 = \frac{1}{\sqrt{2}}(\Delta \theta_1 - \Delta \theta_2) \quad (B_2)$$

where the internal coordinates θ, D and R are defined as below:

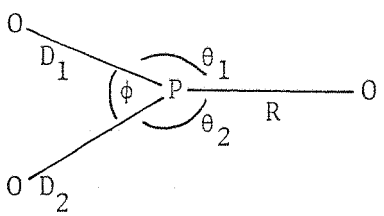

It is impossible for the angle θ and ϕ to all increase simultaneously, resulting in a redundancy, so the above symmetry coordinates omit the angle ϕ. From these symmetry coordinates the F matrix elements can be calculated. Use was made of the C_{2v} symmetry of the molecule to simplify the F matrix. Consequently $f_{D_1\theta_1} = f_{D_2\theta_2} = f_{D\theta cis}$ and $f_{D_1\theta_2} = f_{D_2\theta_1} = f_{D\theta trans}$. Similarly $f_{RD_1} = f_{RD_2}$. The resulting F matrix was simplified further by neglecting $f_{D\theta trans}$ and the interaction constant $f_{\theta\theta}$. The force field used was then:

$$2V = F_R\Delta R^2 + F_D(\Sigma\Delta D^2) + F_\theta(\Sigma\Delta\theta^2) + 2F_{RD}(\Sigma\Delta R\Delta D)$$
$$+2F_{R\theta}(\Sigma\Delta R\Delta\theta) + F_{D\theta cis}(\Delta D_1\Delta\theta_1 + \Delta D_2\Delta\theta_2)$$

The F and G matrices are factored into a 3 x 3 block (A_1 modes) and a 2 x 2 block (B_2 modes). If the secular equation for the two B_2 modes is calculated, it is found to contain three unknowns, F_{44}, F_{55} and F_{45}; for only two observed frequencies:

$$|GF - E\lambda| = \begin{vmatrix} (G_{44}F_{44} + G_{45}F_{45} - \lambda)(G_{44}F_{45} + G_{45}F_{55}) \\ (G_{45}F_{44} + G_{55}F_{45})(G_{45}F_{45} + G_{55}F_{55} - \lambda) \end{vmatrix}$$

where G_{44}, G_{55} and G_{45} are the corresponding G matrix elements and $\lambda = 4\pi^2c^2\nu^2$. A quadratic of the type:

$$\lambda^2 - (G_{44}F_{44} + G_{55}F_{55} + 2G_{45}F_{45})\lambda + (G_{44}G_{55} - G_{45}^2)(F_{44}F_{55} - F_{45}^2) = 0$$

can be constructed where the roots of the equation are the B_2 frequencies. A computer was used to calculate F_{44} and F_{55} for a given value of F_{45}. The B_2 frequency of the species $NaP^{18}O_3$ was then calculated for each set of $F_{44}F_{55}$ and F_{45}. The final set of force constants was then chosen to be that which calculated the overall isotopic shift accurately. Since $F_{44} = f_D - f_{DD}$, $F_{55} = f_\theta$ and $F_{45} = f_{D\theta}$, this set of values determines f_θ, $f_{D\theta}$ and $(f_D - f_{DD})$. These force constant values were then used in the SOTONVIBP program along with f_R, f_D, f_{RD}, f_ϕ, $f_{R\theta}$ and $f_{D\theta}$, as defined in Table 3.3. A frequency fit for the molecule $NaP^{16}O_3$ was obtained, and subsequent calculation of the isotopic frequencies gave good agreement with observed frequencies using the final force constant values shown in Table 3.3. The line diagrams accompanying the high resolution spectra of the stretching modes (Figure 3.6(a) and (b)) of isotopically substituted $NaPO_3$ were calculated using this force field and excellent agreement was observed.

There remains the problem of the assignment of the out-of-plane (B_1) mode of the PO_3 group. KNO_3 shows two relatively weak features of 827.3 and 721.1 cm^{-1} which have been assigned[15] as the B_1 out-of-plane and B_2 in-plane bending modes of the NO_3 group respectively. For $NaPO_3$, corresponding features are observed at 536.6 and 474.0 cm^{-1} and these are similarly assigned as deformations of the PO_3 group. However the following discussion shows that the isotopic fine structure observed for the 474.0 band indicates a reversal of the assignment for $NaPO_3$ with νB_2 lying above νB_1

The out-of-plane bending mode is a non degenerate mode involving the in-phase motion of three oxygen atoms and for a free $[PO_3]^-$ ion with

Table 3.3 Force field and model used for the calculation of the line diagrams in Figure 3.4.

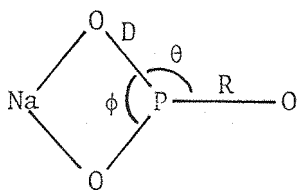

$D = 1.65$ Å
$R = 1.40$ Å
$\phi = \theta = 120^{o}$

$F_R = 10.14$ mdyn Å^{-1}
$F_D = 8.42$ mdyn Å^{-1}
$F_{RD} = 0.35$ mdyn Å^{-1}
$F_{DD} = 0.183$ mdyn Å^{-1}
$F_\theta = 1.36$ mdyn Å rad^{-2}
$F_\phi = 1.23$ mdyn Å rad^{-2}
$F_{R\theta} = 0.63$ mdyn rad^{-1}
$F_{D\theta} = 0.62$ mdyn rad^{-1}

(1 dyn = 10^{-5} N)

idealised D_{3h} symmetry 28% ^{18}O enrichment would yield a 17:20:8:1 quartet related to the A_2'' vibration. These four bands arise from the four distinct species $P^{16}O_n{}^{18}O_{3-n}$ (n = 0-3) and the frequencies are obtainable from the following expression, derived using the standard Wilson GF matrix approach:

$$4\pi^2\nu^2 = \frac{K\Delta}{l^2}\left(\frac{9}{mp} + \frac{1}{mo'} + \frac{1}{mo''} + \frac{1}{mo'''}\right)$$

Here $\frac{K\Delta}{l^2}$ is an out-of-plane bending constant, mo', mo'' and mo''' are the masses of the three oxygen atoms and mp is the mass of phosphorus. On coordination this equation will no longer hold exactly, but it may nevertheless be used to predict the general appearance of the isotope pattern since the B_1 mode is almost certainly well removed from the perturbing influence of out-of-plane cation motion. The line diagram accompanying the high resolution spectrum of the 474.0 cm^{-1} band (Figure 3.6(c)) calculated using this equation shows excellent agreement with the observed fine structure.

A more general relationship has recently been derived for describing the out-of-plane motion of the coordinated $[CO_3]^-$ ion.[24] If one considers the out-of-plane mode of a planar molecule AXYZ in which atom A is centrally bound to X, Y and Z by bonds of length ℓ_1, ℓ_2 and ℓ_3 respectively it may be shown that the frequency of this mode is given by:

$$4\pi^2\nu^2 = \frac{F}{R^2}\left(\frac{R^2}{MA} + \frac{\sin^2\theta_1}{\ell_1{}^2M_X} + \frac{\sin^2\theta_2}{\ell_2{}^2M_Y} + \frac{\sin^2\theta_3}{\ell_3{}^2M_Z}\right)$$

where θ_1, θ_2 and θ_3 are the angles YAZ, XAZ and XAY, $R = \left(\frac{\sin\theta_1}{\ell_1} + \frac{\sin\theta_2}{\ell_2} + \frac{\sin\theta_2}{\ell_3}\right)$ and F is the force constant for an out of plane potential function $2V = F(\Delta S)^2$ in which ΔS represents a small displacement of atom A out of the XYZ plane. This equation should be more generally applicable for describing this type of molecular vibration. A full derivation of this equation is given in Appendix 1.

The agreement between calculated and observed isotopic splitting patterns provides excellent quantitative evidence to support a bidentate

structure for the molecule $NaPO_3$. Moreover it would appear that the general approach used here for $NaPO_3$ and previously for KNO_3 [15] should be applicable to other coordinated $[XO_3]^-$ ions.

3.6 CONCLUSIONS

These infrared matrix studies indicate that molecular $NaPO_3$ is an important species in the vaporisation of Na_3PO_4 and that this species has a bidentate C_{2v} structure in low temperature argon matrices. However the identification of $NaPO_3$ as a result of vaporisation of Na_3PO_4 raises the question of whether the residual 2Na + O remains behind (possibly as sodium aluminate) or is present in the vapour, remaining undetected by infrared spectroscopy. In general, the experiments carried out on this system involved degassing of samples at ca 1400 K before deposition. A dark film which slowly formed on the cold parts of the vacuum jacket during this process was thought initially to arise from impurities in the tantalum susceptor. Subsequent tests however showed that this film reacted vigorously with water to yield a strongly alkaline solution containing sodium ions, implying that when Na_3PO_4 is heated under these conditions, some sodium is lost as elemental vapour.

By comparison with the spectra obtained from Na_3PO_4, the vibrational frequencies observed for the potassium metaphosphate (KPO_3) system can be confidently assigned to the molecular species KPO_3, and similarly $NaPO_3$ can be considered to be an important product of the vaporisation of sodium metaphosphate ($NaPO_3$) together with $NaPO_2$. The presence of $NaPO_2$ in the spectra of sodium metaphosphate is probably due to reduction of $NaPO_3$ during the vaporisation process by hot tantalum. Later experiments carried out in which the sample was contained in a platinum boat (to prevent contact with the tantalum susceptor) overcame this problem.[25]

Finally although the synthetic route used for the preparation of isotopically enriched Na_3PO_4 typically starts from a non-random distribution of oxygen atoms (principally $^{16}O_2$ + $^{18}O_2$ with little $^{16}O^{18}O$) the resulting infrared spectra indicate that complete isotope scrambling has taken place. It is not possible from these experiments to decide upon the mechanism by which this scrambling occurs. Two mechanisms would appear to

be possible. First, scrambling may be the result of breaking the O-O bond during the oxidation of the phosphide. Secondly, if the O-O bond remains intact, scrambling may arise by exchange processes occurring in the melt. The mechanism of scrambling could be investigated by mixing together $NaP^{18}O_3$ and $NaP^{16}O_3$ and recording the spectrum obtained from the vapour above the resulting melt.

REFERENCES

1. J R Van Waser, 'Phosphorus and its Compounds', Vol 1, Interscience (1958).

2. D E C Corbridge, 'The Structural Chemistry of Phosphorus', Elsevier, Amsterdam, (1974).

3. I Haidue, 'The Chemistry of Inorganic Ring Systems', Pt II, Interscience, NY (1970), p819.

4. e.g. E Steger, Z Anorg Allgem Chem, (1958), 296, 305.
A Simon E Steger, Naturweiss, (1954), 41, 186.

5. See Reference 2 and V Fawcett, D A Long, L H Taylor, Proc 5th Int Conf Raman Spec, (1976), 112.

6. D E C Corbridge, E J Lowe, J Chem Soc, (1954), 493.

7. e.g. H C Ko, O J Kleppa, Inorg Chem, (1970), 10, 771.

8. A Buchler, J L Stauffer, J Phys Chem, (1966), 70, 4092.

9. A V Steblevskii, A S Alikhanyan, I D Sokolva, V I Gargoraki, Russ J Inorg Chem, (1974), 19, 789.

10. A S Alikhanyan, A V Steblevski, V I Gargoraki, I D Sokolva, Dokl Akad Nauk SSSR, (Phys Chem), (1975), 222, 629.

11. A V Steblevskii, A S Alikhanyan, I D Sokolva, V I Gargoraki, Russ J Inorg Chem, (1977), 22, 11.

12. K A Gingerich, F Miller, J Chem Phys, (1975), 63, 1211.

13. A V Steblevskii, A S Alikhanyan, I D Sokolva, V I Gargoraki, Russ J Inorg Chem, (1978), 23, 173.

14. I A Ratkovskii, V A Ashuiko, V A Urikh, V A Sinyaev, L Ya Krisko, Khim Khim Tekhnol (Minsk), 1976, 10, 3.

15. I R Beattie, J S Ogden, D D Price, J Chem Soc Dalton Trans, (1979), 1640.
D D Price, Ph.D. Thesis, Southampton University, (1980).

16. D E Milligan, M E Jacox, W A Gruillory, J Chem Phys, (1970), 52, 3864.

17. W C Schroeder, A A Berk, A Gabriel, J Amer Chem Soc, (1937), 59, 1783.

18. J S Ogden, S J Williams, J Chem Phys, (1980), 73(4), 2007.

19. See e.g. C C Addison, N Logan, S C Wallwork, C D Garner, Quart Rev, (1971), 25, 289.

P B Gilchlow, S D Robinson, Coordination Chem Rev, (1978), 25, 69.

20. R E Hester, W E L Grossman, Inorg Chem, (1966), 5, 1308.

21. H Brintzinger, R E Hester, Inorg Chem, 1966, 5, 980.

22. J S Ogden, Ber Bunsen Phys Chem, (1978), 82, 76.

23. I R Beattie, H E Blayden, S M Hall, S N Jenny, J S Ogden, J Chem Soc Dalton Trans, (1976), 666.

24. J S Ogden, S J Williams, J Chem Soc Dalton Trans, (1980), 456.

25. S J Williams, personal communication.

CHAPTER 4

MATRIX ISOLATION STUDIES OF THE VAPOUR ABOVE HEATED ARSENIC AND ANTIMONY OXIDES

4.1 INTRODUCTION

Group V oxides containing the M_4O_6 (T_d) cage structural unit have been the subject of investigation by many researchers in recent years. Of this series of compounds by far the most popular subjects for study have been the oxides of phosphorus (P_4O_6, P_4O_{10}) and of arsenic (As_4O_6). Considerable information is available pertaining to the nature of these compounds in the vapour phase, including vapour phase vibrational analyses. In contrast, in the case of the oxide of antimony (Sb_4O_6), although there is some information available for this molecule in the solid state, there has been very little work published relating to the nature of antimony oxide species in the vapour phase, and no definitive vapour phase vibrational data has appeared.

The work described in this chapter was carried out primarily in an attempt to identify and fully characterise the species present in the vapour above heated antimony trioxide and to obtain a complete vibrational analysis of these species. Parallel studies on arsenic trioxide were also carried out in order to confirm vibrational assignments made by previous workers, where uncertainty exists, and for the purpose of comparison with the antimony system. ^{18}Oxygen enrichment studies were also carried out as an aid to spectral interpretation, and an approach to the location of inactive vibrational modes using isotopic splitting patterns is also discussed. Results obtained from the oxides of phosphorus are discussed in Chapter 5.

Arsenic trioxide vapour is known to be composed of tetrahedral (Td) As_4O_6 molecules up to 1073 K and this has been demonstrated by vapour density measurements[1] and electron diffraction investigations of the vapour.[2,3] These also show that As_4O_6 (g) has the same bond angles and interatomic distances as As_4O_6 units in solid arsenolite[4,5] and a more recent mass spectroscopic investigation also confirmed the presence of As_4O_6 in the vapour.[6] Electron diffraction studies of the vapour above antimony trioxide also have shown it to consist of tetrahedral Sb_4O_6 molecules having the same interatomic distances and bond angles as those of senarmonite[5,7]. These observations are supported by vapour density measurements up to 928 K[8,9,10] and by a more recent mass spectro-

scopic study by Norman and Staley.[6] However Boerboom et al report preliminary mass spectroscopic results which indicate that the vapour above heated antimony trioxide consists of lower oxides than Sb_4O_6 (notably SbO) under what might have been reducing conditions.[11] The vapour pressure and thermodynamic functions of both As_4O_6 (g) and Sb_4O_6 (g) have also been measured using available vibrational data.[12,13] In the case of antimony trioxide this vibrational data was obtained from solid senarmonite.

As_4O_6 has been subjected to a number of vibrational analysis in both solid and vapour phases. Beattie et al[14] reported single crystal Raman spectra of As_4O_6 and gas phase Raman spectra of P_4O_6, P_4O_{10} and As_4O_6. The vibrational assignments for As_4O_6 resulting from this study have been supplemented and revised as a result of an in-cavity Raman investigation by Brumbach and Rosenblatt.[15] Some infrared studies, notably those of Cheremisinov[16] have provided further information as an aid to a complete vibrational assignment. More recently Muller et al[17] have reported a vibrational analysis of As_4O_6 employing the same approach used previously for P_4O_6 and P_4O_{10}.[18] Sourisseau and Mercier[19] have reported vibrational spectra of As_4O_6 powder (at 4 K, Raman) and infrared spectra of As_4O_6 in a nujol mull, as well as computed valence force fields for P_4O_6, As_4O_6 and Sb_4O_6. The Raman spectra of the vapour above heated arsenic trioxide up to 1200 K have also been reported.[20]

Once again, in the case of Sb_4O_6 the existing information as regards vibrational analyses is much less comprehensive than for the arsenic analogue. Single crystal Raman spectra have been reported for Sb_4O_6[14] as have infrared spectra of nujol mulls containing Sb_4O_6.[19] The published vibrational analyses and force field computations[17,19] rely on the single crystal results of Beattie et al and on the results obtained from nujol mulls, since no gas phase vibrational frequencies are available for Sb_4O_6. This fact highlights a possible inconsistency in the information available for these molecules. Moreover even in the case of As_4O_6, where more data are available, computed force fields have been calculated using a mixture of gas phase and solid phase vibrational frequencies.[17,19]

This chapter describes work carried out on the arsenic and antimony

trioxide systems with the principal aim of characterising the vibrational spectra of the species present in the vapour above heated antimony trioxide. A complete vibrational assignment is reported for molecular As_4O_6 and Sb_4O_6 trapped in inert gas matrices. Both infrared and Raman experiments were carried out and the technique of isotopic substitution was employed to provide further information as to the nature of these molecules, and to act as an aid to location of inactive fundamentals. Using the vibrational frequencies obtained, some of the principal force constants were calculated.

4.2 THE INFRARED AND RAMAN SPECTRA OF MATRIX ISOLATED $Sb_4{}^{16}O_6$ AND $As_4{}^{16}O_6$

The infrared and Raman spectra of both As_4O_6 and Sb_4O_6 were obtained employing similar experimental conditions and it is reasonable therefore to consider both infrared and Raman results together.

Figure 4.1(a) shows a typical infrared spectrum obtained after condensing the vapour above heated antimony trioxide (at ca 640 K) with a large excess of nitrogen at 12 K for about 60 minutes. The spectrum consists of absorptions at 796.0 cm^{-1} (802.0 shoulder), 424.0 cm^{-1} and 296.0 cm^{-1}. Very small frequency shifts ($\lesssim$ 2 cm^{-1}) were observed on changing the matrix gas to argon and Figure 4.1(b) shows the infrared spectrum obtained from a similar deposit when argon was used as the matrix gas. Absorption occurred at 800.0/795.0 cm^{-1} (doublet), 422.0 cm^{-1} and 296.0 cm^{-1}. Figure 4.2(a) shows the Raman spectrum obtained from a similar deposit of antimony trioxide vapour in a nitrogen matrix and bands were observed here at 466.5 cm^{-1}, 424.0 cm^{-1}, 281.2/272.0 cm^{-1} (doublet), 179.0 cm^{-1} and 133.2 cm^{-1}. Figure 4.2(b) shows the corresponding Raman spectrum obtained employing an argon matrix. Again, only very small frequency shifts were noted on changing the matrix gas from nitrogen to argon, and this spectrum exhibited bands at 466.1 cm^{-1}, 423.0 cm^{-1}, 272.1/281.0 cm^{-1} (doublet), 177.9 cm^{-1} and 132.0 cm^{-1}. All the vibrational frequencies observed for antimony trioxide are summarised in Table 4.1 where they are also compared with those observed by other researchers.

Figure 4.3(a) shows the infrared spectrum obtained by condensing the

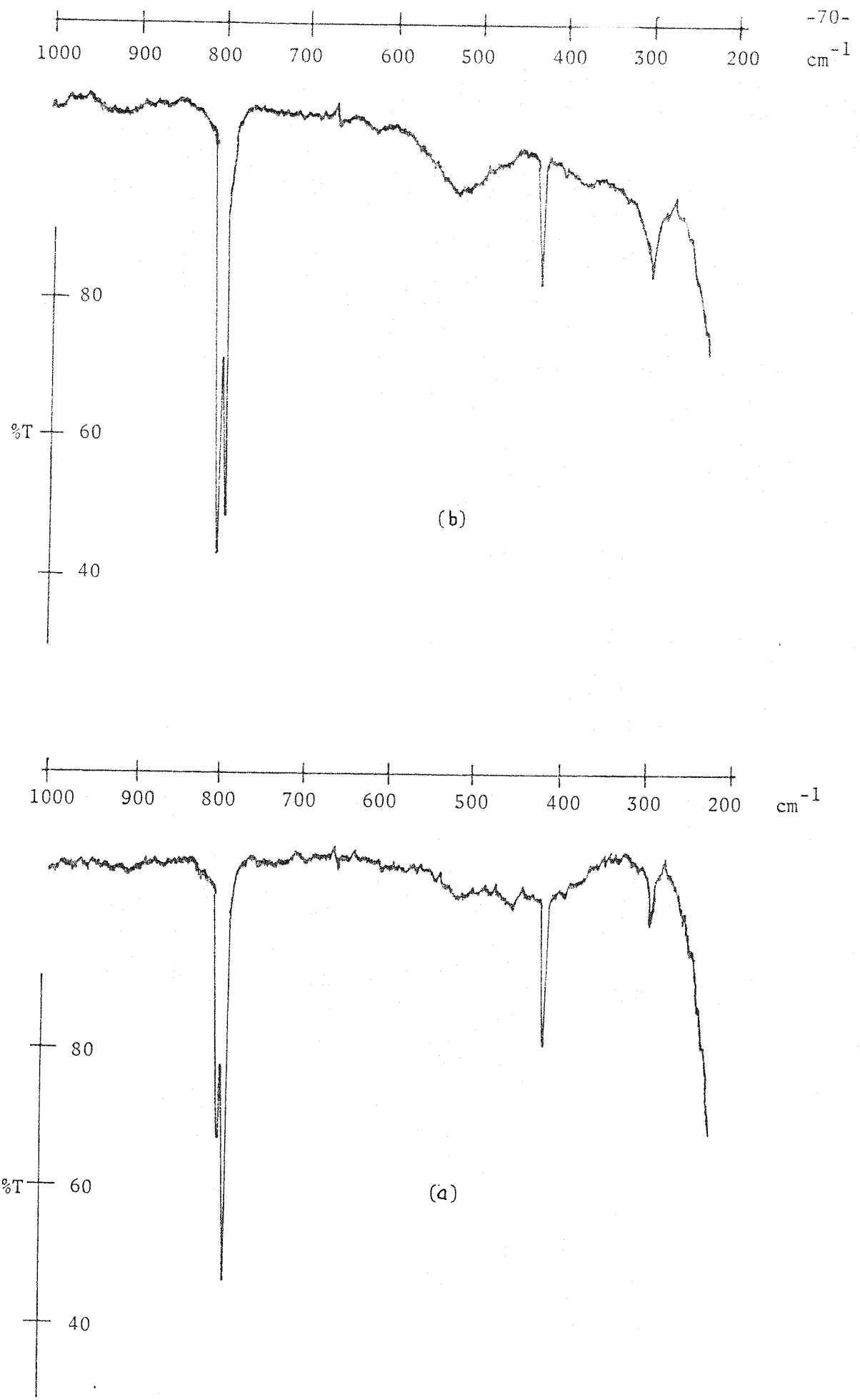

Figure 4.1 Infrared spectra of matrix isolated antimony trioxide
(a) argon matrix
(b) nitrogen matrix

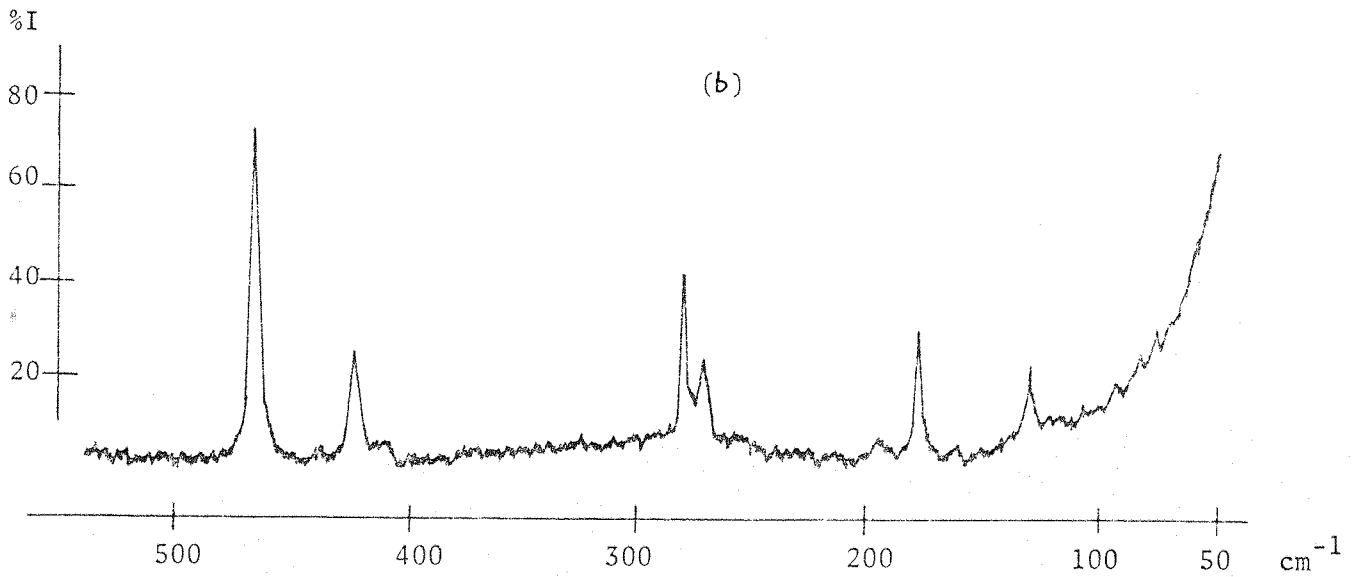

Figure 4.2 Raman spectra of matrix isolated antimony trioxide
(a) argon matrix
(b) nitrogen matrix

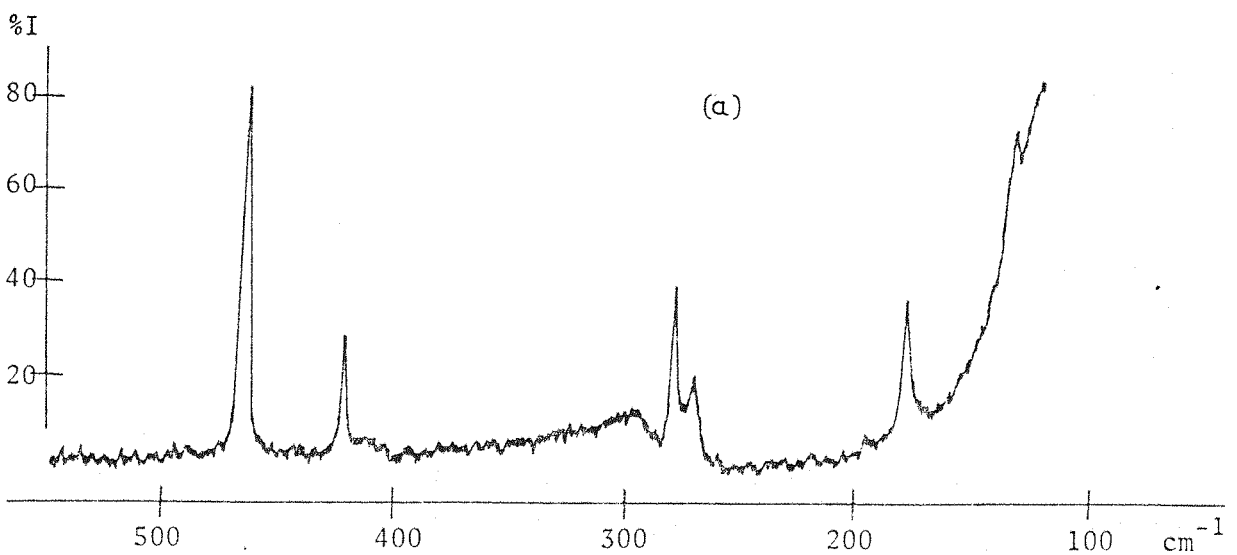

Table 4.1 Vibrational frequencies for Sb_4O_6 and assignments

IR* Argon Matrix (a) cm^{-1}	R* Argon Matrix (a) cm^{-1}	IR* Nitrogen Matrix (a) cm^{-1}	R* Nitrogen Matrix (a) cm^{-1}	R Solid (b) cm^{-1}	IR Nujol Mull (c) cm^{-1}	R Solid (c) cm^{-1}	Assign-ment
-	-	-	-	87	-	-	Lattice mode
	132		133	121		121	ν_4 E
-	178	-	179	193	179	193	$\nu_{10}F_2$
296	-	296	-	-	272	271	ν_9 F_2
	281		281	256		256	ν_2 A_1
	-		-	356		359	ν_3 E
422	423	424	424	376	404	376	ν_8 F_2
	466		466	452		452	ν_1 A_1
795	-	796	-	717	744	717	ν_7 F_2

(a) This work

(b) Ref 14

(c) Ref 19

* frequency accuracy ± 0.4 cm^{-1}

- = not observed

vapour above heated arsenic trioxide (at ca 373 K) with a large excess of nitrogen at 12 K. Absorptions were noted at 829.6 cm^{-1}, 498.0 cm^{-1}, 378.2 cm^{-1} and 255.0 cm^{-1}. As is the case with antimony trioxide, only very small frequency shifts were noted for the arsenic system on changing the matrix gas and Figure 4.3(b) shows the infrared spectrum obtained from a similar deposit of arsenic trioxide vapour in an argon matrix. Here absorptions were observed at 830.1 cm^{-1} (832.0 shoulder), 499.0 cm^{-1}, 378.0 cm^{-1} and 256.0 cm^{-1}. Figure 4.4(a) and (b) show the corresponding Raman spectra obtained from deposits of arsenic trioxide vapour (nitrogen and argon matrices respectively) and bands were observed at 558.0 cm^{-1}, 497.0 cm^{-1}, 386.0/381.0 cm^{-1} (doublet), 255.0 cm^{-1} and 191.0 cm^{-1} (nitrogen matrix) and 558.0 cm^{-1}, 498.0 cm^{-1}, 387.0/382.0 cm^{-1} (doublet), 257.0 cm^{-1} and 192.0 cm^{-1} (argon matrix). All the vibrational frequencies observed for arsenic trioxide are summarised in Table 4.2 where they are compared with the results of previous workers.

In view of the similarity between the frequencies observed in argon and nitrogen matrices, the following discussion will only include data obtained using nitrogen matrices, since these spectra were of marginally better quality than those obtained using argon as the matrix gas.

4.3 SPECTRAL INTERPRETATION AND ASSIGNMENT

Infrared experiments carried out on the antimony trioxide system in which the sample temperature was varied, but with the same matrix gas flow rate (i.e. effective matrix ratio variation) failed to yield evidence of any relative intensity variations. As a consequence of this and in view of the conflicting mass spectroscopic evidence which exists for antimony trioxide vapour,[6,11] it is as well to consider first the antimony trioxide results in qualitative terms.

The infrared spectrum of matrix isolated antimony trioxide vapour exhibits only three absorptions. Relative intensity variations were at no time observed, even when deliberate attempts were made to achieve this. This would indicate that these three absorptions are due to a single species. Indeed, if it were the case, as Boerboom et al suggest,[11] that the major species above heated antimony trioxide was the simple diatomic

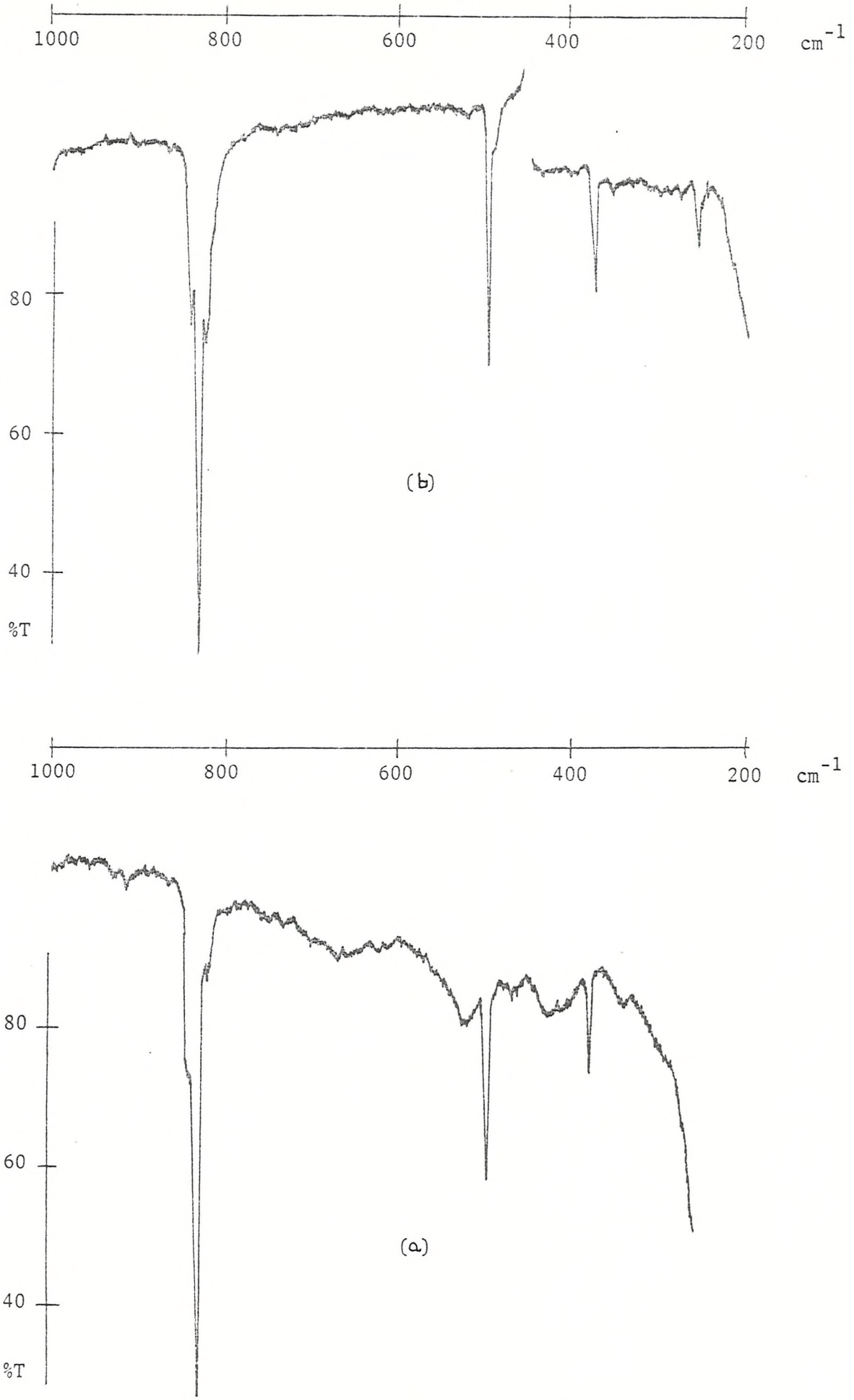

Figure 4.3 Infrared spectra of matrix isolated arsenic trioxide (a) argon matrix, (b) nitrogen matrix

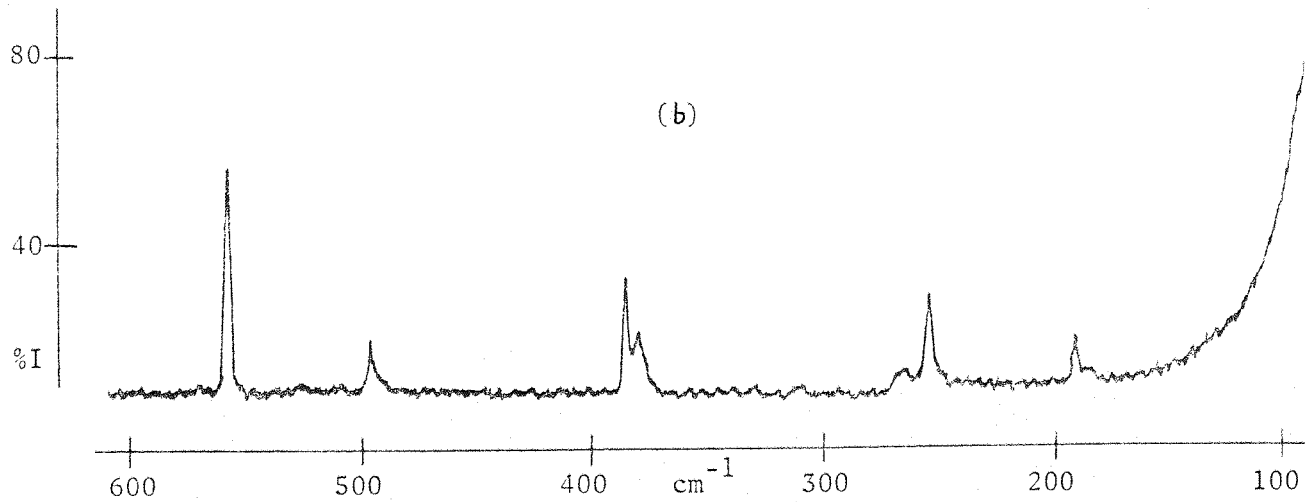

Figure 4.4 Raman spectra of matrix isolated arsenic trioxide
(a) argon matrix
(b) nitrogen matrix

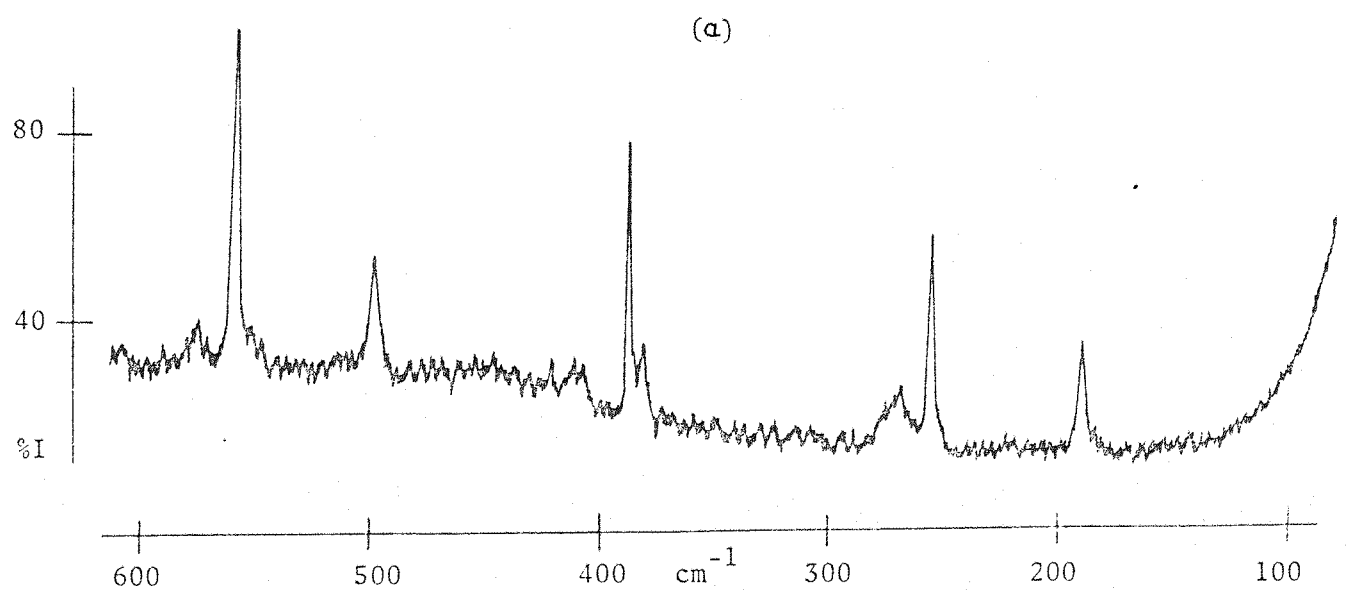

Table 4.2 Vibrational frequencies for As_4O_6 and assignments

IR+ Argon Matrix (a) cm^{-1}	R+ Argon Matrix (a) cm^{-1}	IR+ Nitrogen Matrix (a) cm^{-1}	R+ Nitrogen Matrix (a) cm^{-1}	R Vapour (b) cm^{-1}	R Vapour (c) cm^{-1}	R Solid (b) cm^{-1}	R Solid (c) cm^{-1}	R Vapour (d) cm^{-1}	IR Vapour (e) cm^{-1}	R Solid (f) cm^{-1}	Assignment
-	-	-	-	99	-	86	85	-	-	92	Lattice mode
	192		191	184	185	184	189	187		184	ν_4 E
256	257	255	255	253	253	268	269	253	-	270	$\nu_{10} F_2$
378	-	378	-	-	-	-	-	365	356	-	ν_9 F_2
	387		386	381	381	370	371	379		371	ν_2 A_1
									395		
	-		-	409	409	417	416	410 * 470 *		418	ν_3 E
499	498	498	497	492	496	470	470	492	-	471	ν_8 F_2
								505		536†	
	558		558	556	555	560	560	551		561	ν_1 A_1
								747			
830	-	829	-	-	-	780	782	814	830	783	ν_7 F_2

(a) this work

(b) Ref 14

(c) Ref 15

(d) Ref 20

(e) Ref 24

(f) Ref 19

* 410 cm^{-1} band explained as $2\nu_6$ (A_1 + E + F_2) (Ref 20). Fermi resonance enhanced by ν_2; 470 assigned as ν_3 (E).

† assigned as 2 x ν_{10} in Ref 19.

- = not observed.

+ frequency accuracy ± 0.4 cm^{-1}.

SbO, then a complex system of polymer formation might be expected, as is the case with the oxides of silicon and tin,[21,22] together with highly significant relative intensity variations which such a system should exhibit. On the basis of this fact, and the similarity between corresponding spectra obtained from the antimony and arsenic trioxide systems, it would seem reasonable to suggest that the spectra which appear in Figures 4.1 and 4.2 are due to matrix isolated molecular Sb_4O_6 units. This qualitative assignment is supported by the evidence provided by the spectra obtained from isotopically substituted Sb_4O_6 ($^{16}O/^{18}O$) and As_4O_6 ($^{16}O/^{18}O$) which is discussed in Section 4.4. It would appear then, that the major species present in the vapour above heated antimony trioxide is Sb_4O_6 and the spectra obtained are subsequently assigned on this basis.

A simple group theoretical treatment of an M_4O_6 cage type molecule (belonging to the point group T_d) leads to the following irreducible representation for the vibrational modes, of which the $2A_1$ and 2E modes are

$$\Gamma_{vib} = 2A_1 + 2E + 2F_1 + 4F_2$$

Raman active only, the $4F_2$ modes are both infrared and Raman active, and the $2F_1$ modes are both infrared and Raman inactive. Therefore for antimony trioxide, on the basis that the spectra obtained are due to molecular Sb_4O_6, the three observed infrared absorptions at 796 cm^{-1}, 424 cm^{-1} and 296 cm^{-1} are readily assigned as three of the four F_2 fundamentals. One of these, namely the band at 424 cm^{-1} is also observed in the Raman spectrum. Similarly in the case of As_4O_6, all four F_2 fundamentals are seen in the infrared spectrum (at 829.5 cm^{-1}, 497 cm^{-1}, 378.2 cm^{-1} and 255.1 cm^{-1}) of which two (at 497.0 cm^{-1} and 255.0 cm^{-1}) are also present in the Raman spectrum. Comparison of the As_4O_6 spectrum with previous work by Beattie et al[14] and Brumbach and Rosenblatt[15] enables assignment of the bands observed in the Raman spectrum of As_4O_6 at 558 cm^{-1} as A_1, at 386 cm^{-1} as A_1 and at 191 cm^{-1} as E. Moreover, comparison of the Sb_4O_6 spectra with those of As_4O_6 allows assignments of the bands observed in the Raman spectrum of Sb_4O_6 at 466.5 cm^{-1} as A_1, 281.2 cm^{-1} as A_1 and 133.2 cm^{-1} as E. The band observed at 179 cm^{-1} in this spectrum is assigned as the remaining F_2 fundamental of Sb_4O_6, not observed in the infrared spectrum owing to the 200 cm^{-1} limit on the spectrometer used.

The small shoulder on the low frequency side of the 386 cm^{-1} A_1 fundamental of As_4O_6 could be explained by more than one possibility. These are as follows:

(1) the F_2 fundamental observed at 378 cm^{-1} in the infrared spectrum;

(2) an overtone or combination band enhanced by Fermi-Resonance;

(3) due to the presence of some aggregate species in the matrix.

Explanations (1) and (2) are best dealt with together. At first sight both these possibilities seem likely. Fermi-resonance between the first overtone of the E mode at 191 cm^{-1}, which contains the totally symmetric representation[23] could be evoked as a possible explanation (2 x 191 cm^{-1} = 382 cm^{-1}) and this effect could be present along with the possibility of the presence of a discrete F_2 fundamental.

However, Figure 4.5(a) shows the effect of a controlled diffusion experiment carried out on a deposit of As_4O_6 in an argon matrix and it is clear that the lower frequency component of the doublet has grown in intensity relative to the high frequency component. Moreover Figure 4.5(b) shows the Raman spectrum obtained from a deposit of As_4O_6 in an argon matrix where the matrix gas flow rate was significantly reduced (i.e. effectively a more concentrated matrix) and here again relative intensity variation of this doublet is noted together with the appearance of small bands at the sides of two of the remaining four fundamentals. This evidence would seem to suggest that the low frequency component of this doublet is in fact due to some aggregate species. Indeed, no relative intensity variations would be expected if this band was a discrete F_2 fundamental. This evidence however, does not entirely rule out the possibility of Fermi-resonance where variation of the degree of coupling may be a consequence of varying matrix gas perturbations. This effect would be expected to be more marked on changing the matrix gas, although this was noted, this effect would also be expected if the low frequency component was due to some aggregate species. Explanations (1) and (2) seem to be finally ruled out when the corresponding doublet appearing in the Raman spectrum of Sb_4O_6 is examined in more detail. Here the lower frequency component has no coincident band in the infrared spectrum (F_2 at 296 cm^{-1}) so it cannot be an F_2 fundamental; Fermi-resonance enhancement

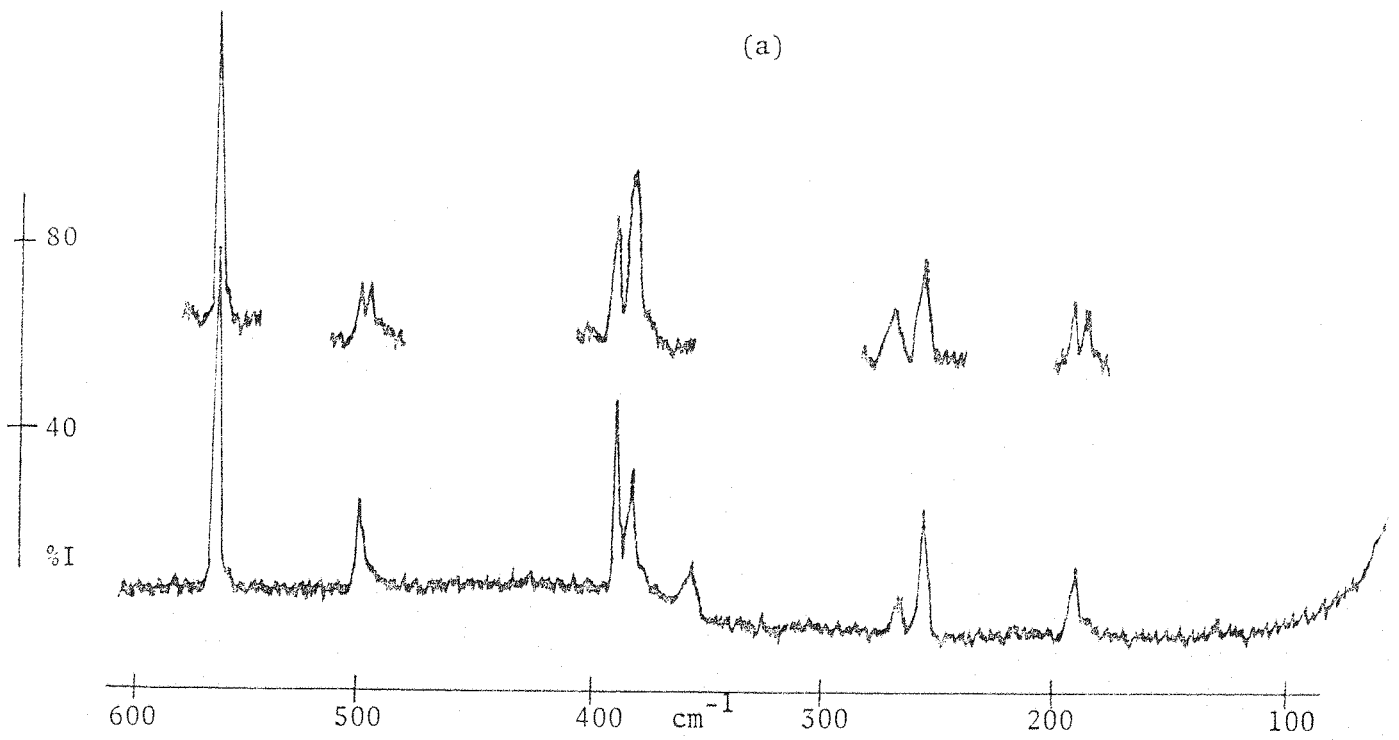

Figure 4.5 (a) Raman spectrum of arsenic trioxide isolated in an argon matrix with the results of a controlled diffusion experiment.

(b) Raman spectrum of arsenic trioxide isolated in an argon matrix with lower matrix ratio.

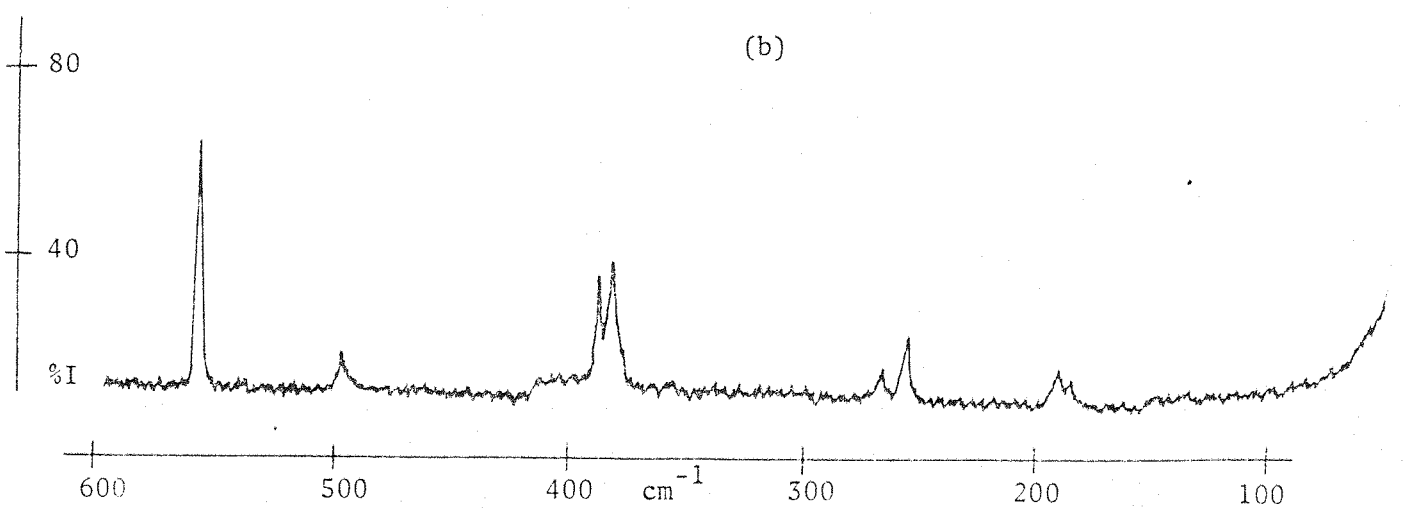

can be rejected as an explanation in this case as there is no band of similar energy to the A_1 mode for resonance to occur (2 x 133 cm^{-1} = 266 cm^{-1}). Consequently, the presence of aggregate Sb_4O_6 units would seem to be the only reasonable explanation in the case of Sb_4O_6 and this would also account for the weak broad shoulders observed on these spectra from time to time. The occurrence of aggregation is then invoked as the explanation of these doublets, but the basic assignment is not affected by the presence of these doublets.

Tables 4.1 and 4.2 contain a complete assignment for the spectra obtained in this work based on the previous discussion, as well as a comparison with assignments made by previous workers.

The 829.0 cm^{-1} band of As_4O_6 (ν_7F_2) and the 796.0 cm^{-1} band of Sb_4O_6 (also ν_7F_2) were not observed in the Raman spectra obtained in this work, and the same is true for the 378.2 cm^{-1} (ν_9F_2, As_4O_6) and 296.0 cm^{-1} (ν_9F_2, Sb_4O_6) bands, although all should be Raman active. ν_7 has however been observed in the Raman spectrum of solid Sb_4O_6 and of solid and vapour-phase As_4O_6.[14,15,19,20] The main uncertainty regarding the assignments until now has been concerned with the location of ν_9 for both As_4O_6 and Sb_4O_6. Brumbach and Rosenblatt[15] have shown that the bands previously observed at 86 cm^{-1} and 99 cm^{-1} for As_4O_6 in the solid and vapour phase spectra respectively[14] (assigned as $\nu_{10}F_2$[14]) is not a fundamental of As_4O_6 by reason of its temperature dependent frequency variation and its disappearance in their work on going from solid phase to vapour phase. They suggest that this band is associated with the crystal lattice and this assignment is consistent with low temperature vibrational studies of solid CO, CO_2, N_2O, N_2, O_2, Br_2 and Cl_2 whose lattice mode frequencies have been shown to be temperature dependent.[24-26] As a consequence of this and the observation in this work of F_2 fundamental at 378.2 cm^{-1} for As_4O_6 and 296.0 cm^{-1} for Sb_4O_6 in the infrared spectra these bands are assigned as $\nu_9(F_2)$, and the 255.0 cm^{-1} (As_4O_6) and 179.0 cm^{-1} (Sb_4O_6) bands are assigned as $\nu_{10}(F_2)$. This assignment is supported by previous infrared observations of a band at 395 cm^{-1} for As_4O_6[27] although only once has this band been reported as appearing in the Raman spectrum.[20]

There remains the problem associated with the location of $\nu_3(E)$ which was not observed in this work. Most investigators have placed this

fundamental at $\sim$ 409 cm^{-1} for As_4O_6 and $\sim$ 355 cm^{-1} for Sb_4O_6 although the 409 cm^{-1} band has also been assigned as being due to Fermi-resonance enhancement between ν_2 and $2\nu_6$.[20] There would however, seem to be insufficient evidence for the rejection of the previous assignment, which has remained consistent over a number of investigations. This band (ν_3E) has been reported as being of very weak intensity and as a result its non-appearance in the Raman spectra of this work is not altogether unexpected.

This work then, provides a vibrational assignment for As_4O_6 and Sb_4O_6 trapped in inert matrices with the exception of ν_3(E), and the inactive F_1 fundamentals. The non-appearance in the Raman spectra of the F_2 mode ν_9 noted by workers before, remains unexplained as does the non-appearance of $\nu_7(F_2)$ in the Raman spectra obtained in this work.

At this stage it was decided to obtain vibrational spectra of ^{18}O enriched arsenic and antimony trioxides, as an aid to structural confirmation, and as a method of locating the infrared and Raman inactive F_1 modes. Isotopic splitting patterns obtained from a particular vibration have been shown to be affected by the presence of a fundamental of similar energy which gives rise to vibrations of the same symmetry types on partial substitution. Here intensity 'borrowing' may affect the observed intensity ratios and the absolute frequencies observed may also be affected,[28] (also see Chapter 2). Consequently the observation of a highly perturbed isotopic splitting pattern, where no observed frequency is of similar energy, may be evidence for the presence of an F_1 fundamental. Suitable calculations could then be performed to give an estimate of the frequency of the F_1 vibration, as the proximity of the two vibrations governs the degree of perturbation of the isotopic splitting pattern. Previously, researchers have relied on the observation of overtone or combination bands as a means for locating inactive modes. The use of isotopic substitution would appear to present an alternative approach where overtone or combination bands are not observed.

4.4 FORCE CONSTANT ANALYSIS

Using the computer program SOTONVIBP an exact frequency fit for the

seven observed frequencies was sought for both $As_4{}^{16}O_6$ and $Sb_4{}^{16}O_6$. To achieve this an eight parameter force field was used to describe the potential energy function of the molecule. The eight force constants used are defined as below:

$F_1 = F_r$ (principal stretching constant, M-O)
$F_2 = F_\alpha$ (principal bending constant, O-M-O)
$F_3 = F_{rr}$ (interaction constant through common 'M' atom)
$F_4 = F'_{rr}$ (interaction constant through common 'O' atom)
$F_5 = F_\beta$ (principal bending constant M-O-M)
$F_6 = F_{\alpha\alpha}$ (interaction bending constant O-M-O/O-M-O)
$F_7 = F_{r\alpha}$ (stretch/bend interaction constant M-O/O-M-O)
$F_8 = F_{r\beta}$ (stretch/bend interaction constant M-O/M-O-M)

This force field resulted in an exact fit between observed and calculated frequencies for the all ^{16}O species. The observed and calculated frequencies for $As_4{}^{16}O_6$ and $Sb_4{}^{16}O_6$ appear in Table 4.3. Table 4.4 gives the final force constant values which reproduced the observed frequencies.

4.5 INFRARED SPECTRA OF MATRIX ISOLATED $Sb_4{}^{16/18}O_6$ AND $As_4{}^{16/18}O_6$

Samples of ^{18}O enriched Sb_4O_6 and As_4O_6 were prepared containing 40% and 50% ^{18}O respectively. This was achieved by direct reaction of the metal with oxygen under controlled conditions. The antimony or arsenic, contained in a platinum boat, was heated using a resistive furnace to 750-800°C in the presence of ca 300Torr of a $^{16}O/^{18}O$ mixture of known composition. When oxygen uptake was complete (about 1-2 hours) the residual pressure of oxygen was usually found to be 20-40Torr. The resulting white crystalline oxide was then sublimed in the presence of oxygen into pyrex 'break-seal' ampoules, leaving any unreacted metal behind in the reaction chamber. The ampoules were then evacuated finally being 'sealed off' under vacuum.

Figure 4.6(a) and (b) shows the infrared spectra obtained from ^{18}O enriched samples of Sb_4O_6 and As_4O_6 employing nitrogen matrices. It is clear that the highest frequency mode in each case now appears as a sextet,

Table 4.3 Observed and calculated frequencies for $As_4{}^{16}O$ and $Sb_4{}^{16}O$. Frequencies were calculated using the force field and model described in the text and in Table 4.4.

$As_4{}^{16}O_6$		Assignment	$Sb_4{}^{16}O_6$	
Obs cm^{-1}	Calc cm^{-1}		Obs cm^{-1}	Calc cm^{-1}
829.6	829.6	F_2	796.0	796.0
498.0	498.0	F_2	424.0	424.0
378.0	378.0	F_2	296.0	296.0
255.5	255.5	F_2	179.0	179.0
558.0	558.0	A_1	466.5	466.5
386.0	386.0	A_1	281.0	281.0
-	507.4	E	-	435.5
191.0	191.0	E	133.0	133.0
-	778.3	F_1	-	734.4
-	191.3	F_1	-	144.0

Table 4.4 Force field and model used for the calculation of frequencies shown in Table 4.8 and the line diagrams in Figure 4.9.

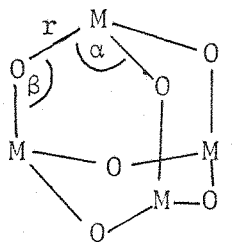

M = As, Sb

r (As) = 1.8 Å, r (Sb) = 2.0 Å
α (As) = 100.0°, α Sb = 100.0°
β (As) = 126.0°, β (Sb) = 126.0°

	As_4O_6	Sb_4O_6	
F_r =	3.33	2.80	mdyn $Å^{-1}$
F_α =	1.30	1.23	mdyn Å rad^{-2}
F_{rr} =	0.37	0.10	mdyn $Å^{-1}$
F'_{rr} =	0.04	0.02	mdyn $Å^{-1}$
F_β =	0.49	0.41	mdyn Å rad^{-2}
$F_{\alpha\alpha}$ =	0.42	0.51	mdyn Å rad^{-2}
$F_{r\alpha}$ =	-0.23	-0.45	mdyn rad^{-1}
$F_{r\beta}$ =	0.17	0.14	mdyn rad^{-1}

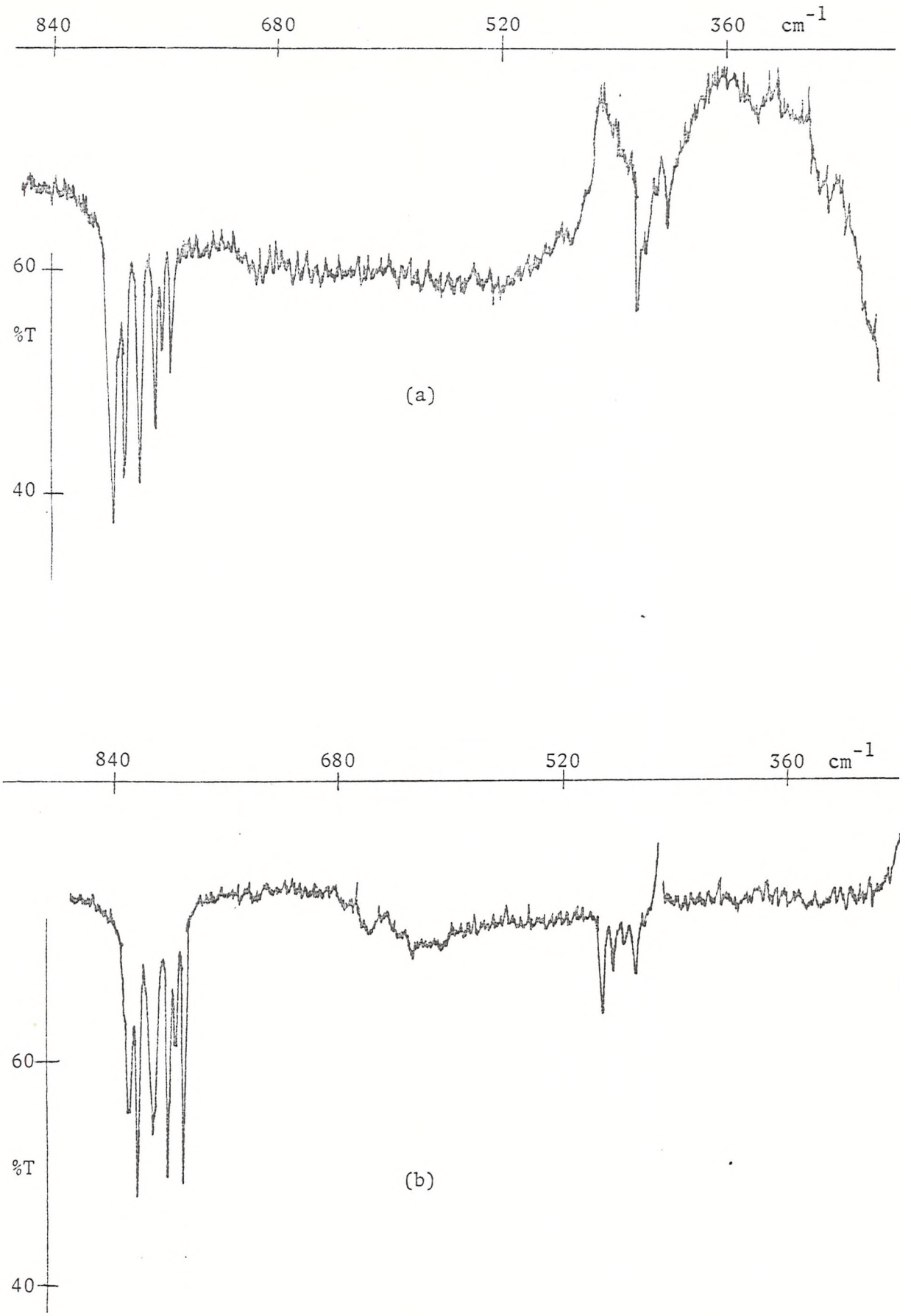

Figure 4.6 Infrared spectra of matrix isolated ^{18}O enriched Sb_4O_6 and As_4O_6

and Figure 4.7(a) and (b) show high resolution spectra of the highest frequency bands of Sb_4O_6 and As_4O_6 respectively. Under high resolution the 424.0 cm^{-1} and 498.0 cm^{-1} bands of $^{16}O/^{18}O$ Sb_4O_6 and As_4O_6 yielded isotope patterns but these were of lower spectral quality, Figure 4.8(a) and (b). It is clear on a qualitative level that these isotope patterns would suggest the presence of Sb_4O_6 units in the matrix owing to the similarity between the spectra produced from the arsenic and antimony systems. The complexity of the isotope patterns clearly rules out the possibility of the presence of molecules such as SbO and associated polymers. All observed frequencies for $^{16/18}O$ As_4O_6 and Sb_4O_6 are listed in Tables 4.5(a) and (b).

4.6 ISOTOPIC SPLITTING PATTERN ANALYSIS

A more stringent test of the validity of a particular force field is its ability to reproduce isotopic splitting patterns accurately. This force field was used to calculate theoretical isotope patterns for the two highest frequency F_2 modes of As_4O_6 and Sb_4O_6.

For a molecule of the type M_4O_6 there are eleven possible combinations of $^{18}O/^{16}O$ incorporation in going from $M_4(^{16}O)_6$ to $M_4(^{18}O)_6$. These include the existence of different geometrical isomers when di- and tri-substitution is considered. In the case of di-substitution two isomers are possible, the cis isomer (where the two ^{18}O atoms are adjacent) and the trans isomer (where the two ^{18}O atoms are diametrically opposed). For tri-substitution, three isomers are possible, the 'apical' (A) isomer (where the three ^{18}O atoms are bonded to a common M atom) the 'facial' (fac) isomer (where the three ^{18}O atoms form a 'face' of the molecule) and the meridional (mer) isomer (where the three ^{18}O atoms are common to one 'edge' of the molecule). Diagrams of the possible geometrical isomers are shown in Figure 4.9. The computational problem is complicated further by the fact that the partially substituted molecules will no longer have T_d symmetry, and as a consequence the three-fold degeneracy of the F_2 modes will be removed. Using the force field described above separate calculations were carried out for each possible combination of $^{18}O/^{16}O$ and for each isomer, changing only the necessary isotopic masses,

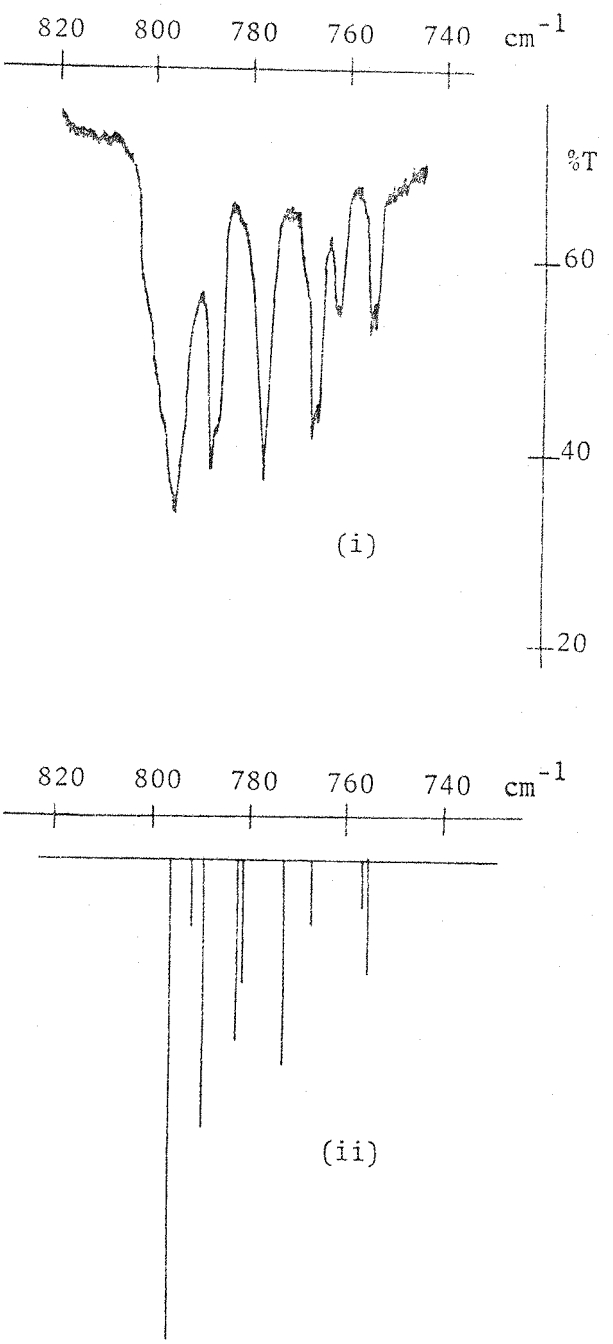

Figure 4.7(a) High resolution spectrum of part of Figure 4.6(a)
(i) Observed spectrum
(ii) Calculated spectrum

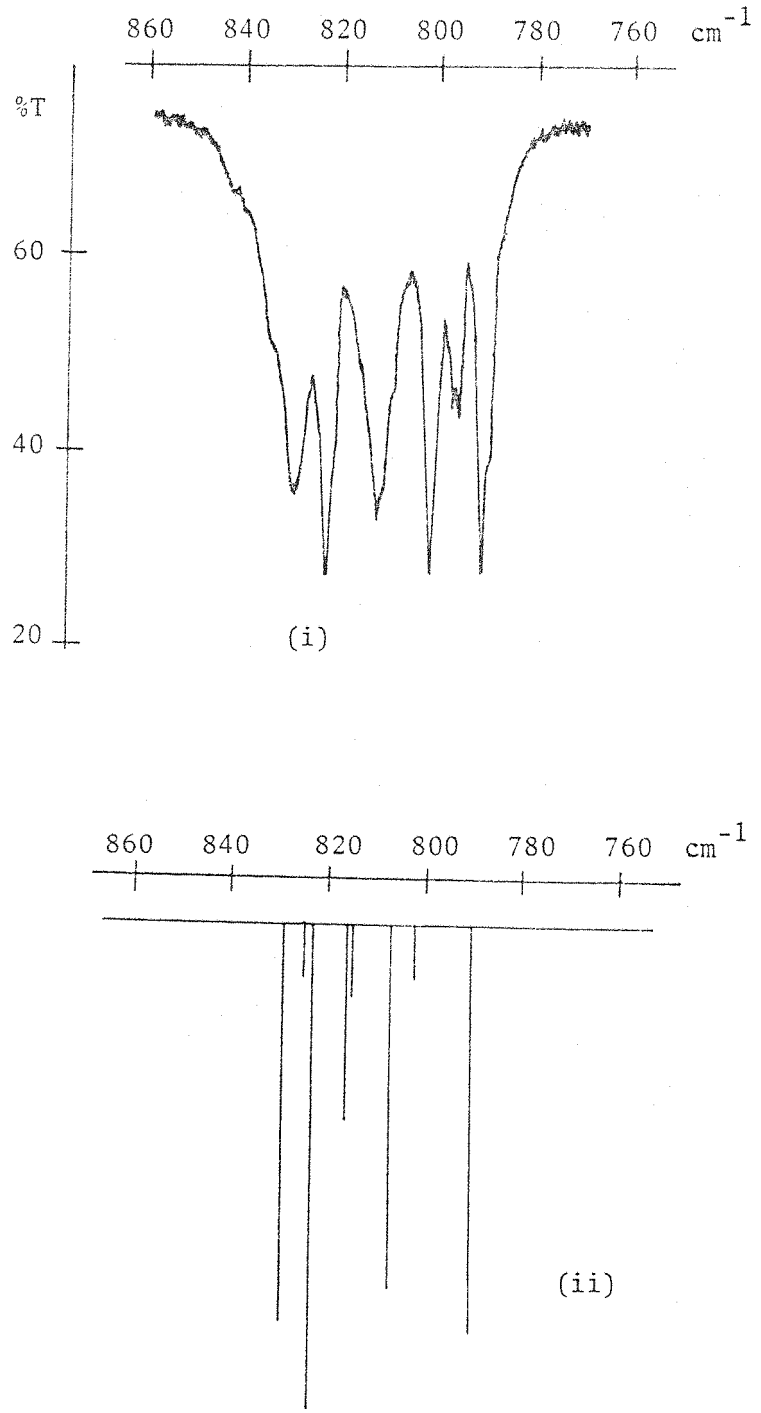

Figure 4.7(b) High resolution spectrum of part of Figure 4.6(b)
(i) Observed spectrum
(ii) Calculated spectrum

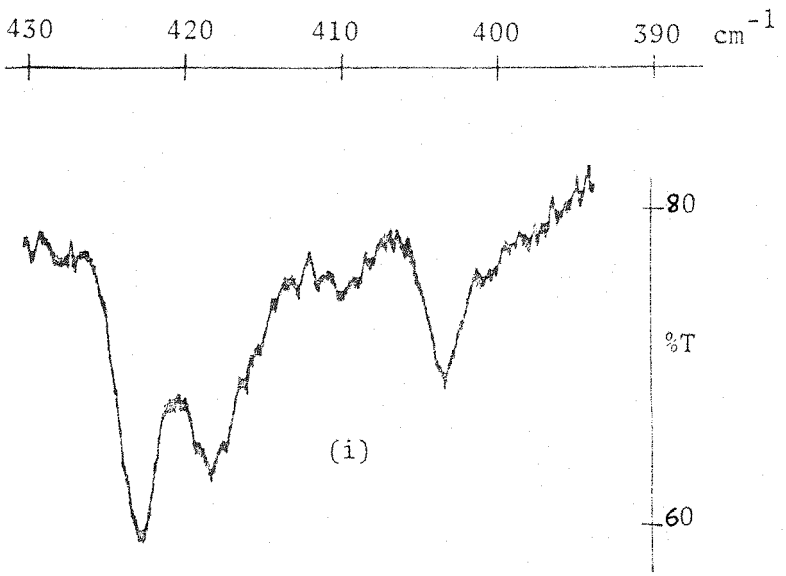

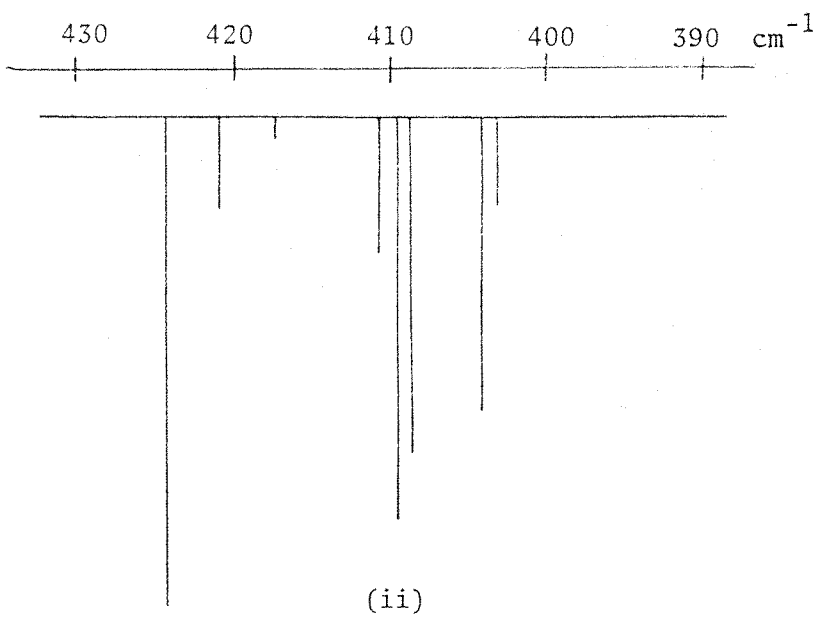

Figure 4.8(a) High resolution spectrum of part of Figure 4.6(a)

(i) Observed spectrum

(ii) Calculated spectrum

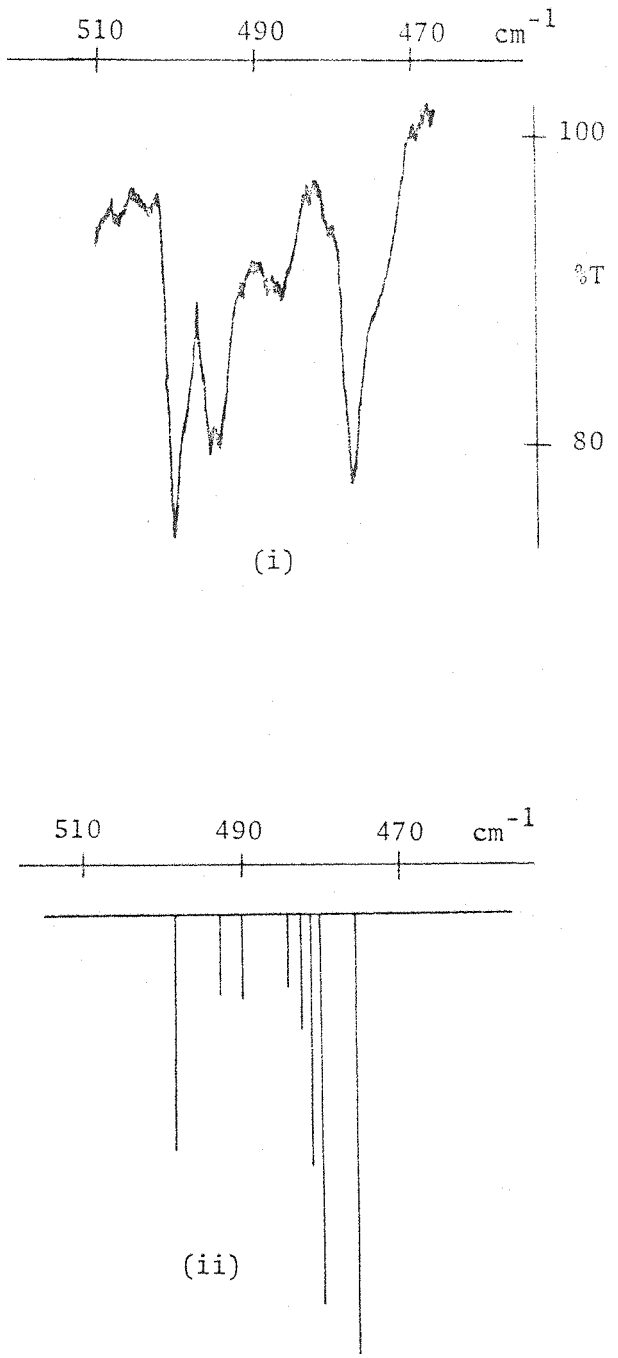

Figure 4.8(a) High resolution spectrum of part of Figure 4.6(b)
(i) Observed spectrum
(ii) Calculated spectrum

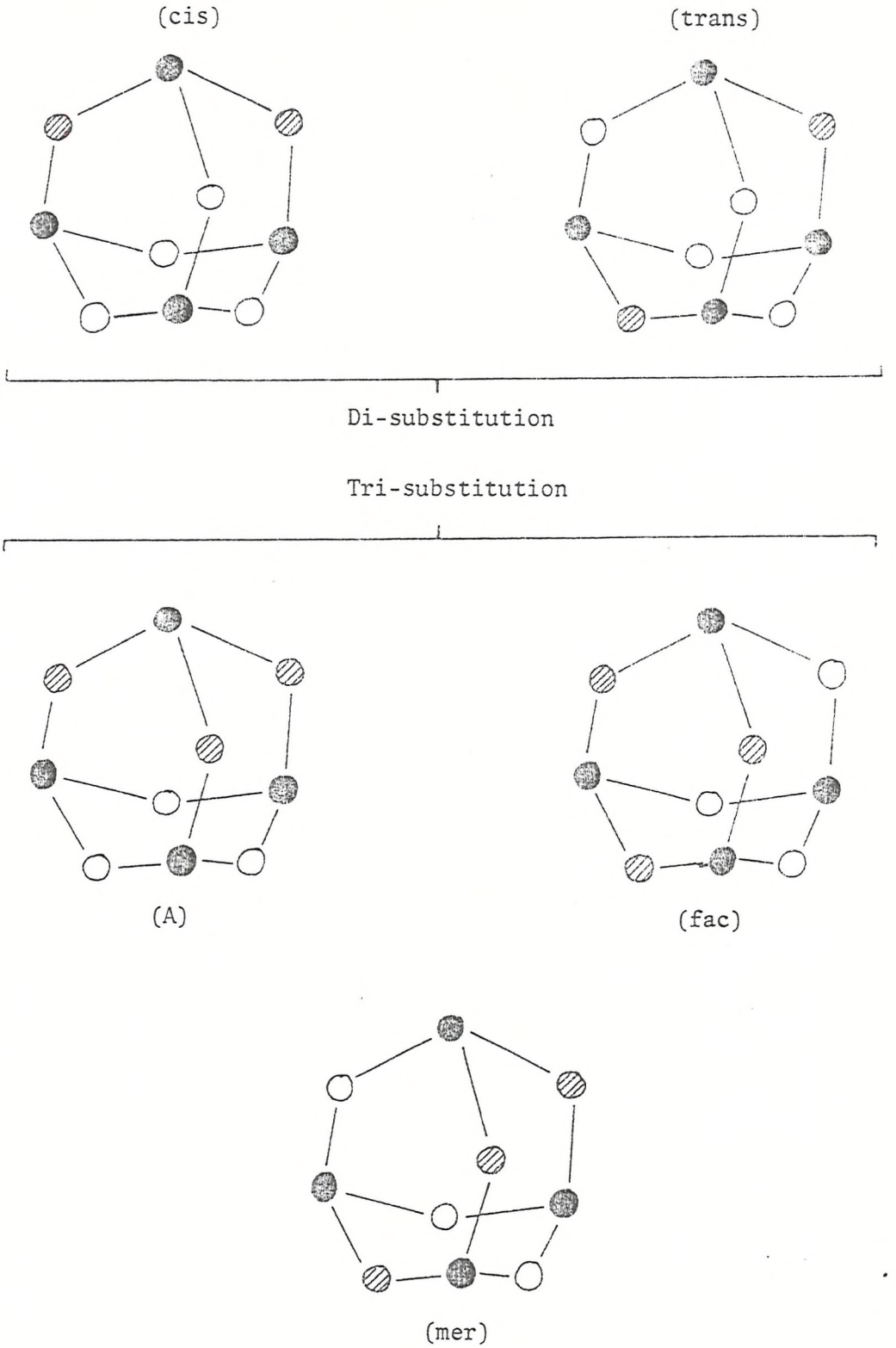

Figure 4.9 Isotopomers produced for di- and tri-substitution of ^{18}O into an M_4O_6 cage.

● = P

◍ = ^{18}O

○ = ^{16}O

Table 4.5(a) Vibrational frequencies of isotopically substituted arsenic trioxide for the two highest frequency F_2 modes

Molecule	Pt Grp	Vib modes	Frequencies cm^{-1}
$As_4(O^{16})_6$	T_d	F_2	829.6 829.6 829.6 498.0 498.0 498.0
$As_4(O^{16})_5(O^{18})$	C_{2v}	A_1,B_1,B_2	829.1 829.5 816.5 498.0 497.5 481.8
$As_4(O^{16})_4(O^{18})_2$(cis)	C_s	2A',A''	829.2 807.4 823.1 497.5 482.7 480.6
$As_4(O^{16})_4(O^{18})_2$(trans)	D_{2d}	B_2,E	816.4 816.4 828.7 497.5 497.5 475.7
$As_4(O^{16})_3(O^{18})_3$(A)	C_{3v}	A_1,E	823.1 823.1 790.2 480.6 480.6 483.2
$As_4(O^{16})_3(O^{18})_3$(mer)	C_2	A_1,B_1,B_2	816.0 825.3 802.3 492.9 481.2 475.5
$As_4(O^{16})_3(O^{18})_3$(fac)	C_{3v}	A_1,E	807.1 807.1 829.0 480.3 480.3 483.9
$As_4(O^{16})_2(O^{18})_4$(trans)	D_{2d}	B_2,E	815.5 815.5 790.6 475.3 475.3 488.7
$As_4(O^{16})_2(O^{18})_4$(cis)	C_s	2A',A''	822.7 807.0 790.0 481.7 480.3 475.3
$As_4(O^{16})(O^{18})_5$	C_{2v}	A_1,B_1,B_2	815.5 790.0 789.6 474.9 475.5 488.7
$As_4(O^{18})_6$	T_d	F_2	790.2 790.2 790.2 475.5 475.5 475.5

Table 4.5(b) Vibrational frequencies of isotopically substituted antimony trioxide for the two highest frequency F_2 modes

Molecule	Pt Grp	Vib modes	Frequencies cm^{-1}
$Sb_4(O^{16})_6$	T_d	F_2	796.0 796.0 796.0 424.0 424.0 424.0
$Sb_4(O^{16})_5(O^{18})$	C_{2v}	A_1,B_1,B_2	795.6 795.9 781.8 424.0 423.6 409.5
$Sb_4(O^{16})_4(O^{18})_2$(cis)	C_s	2A',A''	795.5 789.0 772.1 423.6 410.0 408.7
$Sb_4(O^{16})_4(O^{18})_2$(trans)	D_{2d}	B_2,E	781.6 781.6 795.1 423.6 423.6 404.1
$Sb_4(O^{16})_3(O^{18})_3$(A)	C_{3v}	A_1,E	788.9 788.9 756.1 408.6 408.6 410.4
$Sb_4(O^{16})_3(O^{18})_3$(mer)	C_2	A_1,B_1,B_2	791.4 781.2 766.9 403.9 420.6 409.1
$Sb_4(O^{16})_3(O^{18})_3$(fac)	C_{3v}	A_1,E	795.3 771.8 771.8 410.9 408.4 408.4
$Sb_4(O^{16})_2(O^{18})_4$(trans)	D_{2d}	B_2,E	780.8 780.8 756.3 403.7 403.7 417.1
$Sb_4(O^{16})_2(O^{18})_4$(cis)	C_s	2A',A''	788.5 771.6 755.8 409.5 408.4 403.7
$Sb_4(O^{16})(O^{18})_5$	C_{2v}	A_1,B_1,B_2	780.7 755.8 755.4 403.4 403.7 408.7
$Sb_4(O^{18})_6$	T_d	F_2	755.3 755.3 755.3 403.4 403.4 403.4

but retaining the same equilibrium internal coordinate values. The results of these calculations are given in Table 4.5(a) and (b) where each isomer, its point group and the vibrational species originating from the parent F_2 mode are listed together with the calculated frequencies for the two highest frequency F_2 modes. These calculated isotopic frequencies are represented in the line diagram accompanying the high resolution spectra shown in Figure 4.7 and 4.8. These line diagrams incorporate isotopic enrichment of 40% for Sb_4O_6 and 50% for As_4O_6. For the highest frequency F_2 fundamental agreement between observed and calculated isotope patterns is excellent, providing further evidence of the validity of the force field used. The line diagrams were derived assuming that the intensity of the F_2 mode is shared equally among all components for the partially substituted molecules. This has been shown to be not too gross an assumption where there is no close proximity between bands belonging to the same symmetry species[29] (see Chapter 2).

Although the F_2 and F_1 modes of an M_4O_6 molecule give rise to bands of the same symmetry species for certain partially substituted molecules, the separation for the highest frequency F_2 and F_1 modes ($\sim$ 50 cm^{-1} for As_4O_6 and $\sim$ 60 cm^{-1} for Sb_4O_6) would appear to be sufficient to reduce the possibility of mixing of these bands to a minimum. Moreover, a series of calculations carried out recently for the molecule V_4O_{10} shows that perturbation of the F_2 isotope pattern only become significant when the separation is of the order of 20 cm^{-1}.[30] In the derivation of predicted isotopic splitting patterns assumptions are made regarding the distribution of intensity between components of the triply degenerate F_2 modes for partially substituted molecules (see above and Chapter 2). This could render estimation of the frequency of the F_1 modes on the basis of relative intensity variations between components of the isotope pattern, unreliable. However, if any assymetry in the observed pattern (i.e. small frequency shifts) could be successfully modelled by deliberate incorporation of a nearby F_1 fundamental, this might prove to be a relatively sensitive method for the estimation of frequencies for inactive fundamentals. At worst, this approach would appear to provide an alternative to frequency estimation by observations of overtone bands. Of course little

positive information could be obtained in cases where no assymmetry is detected in the observed pattern.

Owing to the uncertainty in the frequency of the highest frequency E mode, and its non-appearance in the Raman spectra obtained in this work, no value for the frequency of this fundamental was used when the initial force field was calculated. These calculations predict its frequency to be at 507.4 cm^{-1} and 435.5 cm^{-1} for As_4O_6 and Sb_4O_6 respectively. Although too much emphasis should not be placed on these predictions, the close proximity of these fundamentals and the F_2 fundamentals observed at 498 cm^{-1} (As_4O_6) and 424 cm^{-1} (Sb_4O_6) is interesting in view of the poor agreement between observed and calculated isotope patterns for this F_2 fundamental. Here the E mode is likely to produce significant mixing with components of the F_2 mode in the symmetries C_{2v}, C_{3v}, C_s or C_2 which occur in partially substituted species. If this is the case, the fact that the calculations performed made no allowance for this could be the reason for the poor agreement between observed and calculated isotope patterns.

It is interesting to compare the force field used in this work with those recently reported for P_4O_6, P_4O_{10}, Sb_4O_6 and As_4O_6.[17,18] In the case of Sb_4O_6 these calculations were based on the single crystal frequencies of Beattie et al[12] whereas for As_4O_6 gas phase frequencies were used. A valence force field has also been calculated[19] for Sb_4O_6 using vibrational frequencies obtained from nujol mulls together with those obtained from single crystal Raman spectra.[14] In view of these inconsistencies it would seem reasonable to suggest that the force field used in this work for Sb_4O_6 will be more realistic as all frequencies were recorded in the same molecular environment. Moreover, Cyvin and Cyvin[18] attempted a force constant analysis for P_4O_6, P_4O_{10} and As_4O_6 using only a three parameter force field consisting of a principal stretching constant and two angle bending constants. This simple force field was found to be inadequate and interaction constants had to be introduced to adequately define the problem. Finally further evidence in support of the validity of the eight parameter force field used in this work is provided by the fact that a similar set of force constants has been used successfully in a recent investigation of the molecule V_4O_{10}.[31]

4.7 CONCLUSIONS

The species Sb_4O_6 has been identified as the major constituent in the vapour above heated antimony trioxide. With the exception of $\nu_3(E)$ a complete vibrational assignment has been made for Sb_4O_6 and As_4O_6 isolated in low temperature matrices, and the isotope patterns obtained on ^{18}O substitution for the highest frequency F_2 modes have been successfully interpreted. An eight parameter force field has been developed which reproduces both observed frequencies and isotope patterns accurately, and the isotope pattern observed for the F_2 fundamental of Sb_4O_6 and As_4O_6 has facilitated identification of this type of vibration in similar molecules.[31]

The sensitivity of these isotope patterns to the proximity of inactive F_1 modes has been shown to be a possible approach to the estimation of frequencies for inactive fundamentals.

It is interesting to compare the difference between matrix and solid frequencies for the series of compounds M_4O_6 (M = P, As, Sb). In particular the frequency for the top F_2 modes are listed below:

	Solid frequency[(a)] cm^{-1}	Matrix frequency cm^{-1}	Frequency shift cm^{-1}
P_4O_6*	959	954	5
As_4O_6	829	780	51
Sb_4O_6	796	717	79

(a) Ref 14. * See Chapter 5.

It is clear that although in the case of Sb_4O_6 the solid must be structurally similar to the matrix isolated species, it could not be described as containing 'isolated molecules' to the same extent as say P_4O_6. This would suggest that in the case of As_4O_6 and Sb_4O_6, the use of vibrational data from solid and gaseous phases in subsequent calculations might result in misleading results. In particular thermodynamic functions derived from vibrational data are liable to be more reliable if a consistent (i.e. obtained from the same phase) set of frequencies is used. This work provides for Sb_4O_6 for the first time such a set of consistent vibrational frequencies.

REFERENCES

1. H Biltz, Z Phys Chem (Leipzig), (1896), 19, 417.

2. L R Maxwell, S B Hendricks, L S Deming, J Chem Phys, (1937), 5, 626.

3. G C Hampson, A J Stosick, J Amer Chem Soc, (1938), 60, 1814.

4. P A Akishin, V P Spiridonev, Zh Struckt Khim, (1961), 2, 542.

5. K E Almin, A Westgren, Chem Zentralble, (1942), 2, 9.

6. J H Norman, H G Staley, J Chem Phys, (1964), 41, 5, 1503.

7. P A Akishin, N G Rambidi, V P Spiridonev, 'The Characterisation of High Temperature Vapours', Ed J L Margrave, Wiley NY, (1967).

8. H Z Biltz, Phys Chem, (1896), 19, 385.

9. V Meyer, H Henshing, Ber, (1879), 12, 1282.

10. A Smits, E Beljaars, J Phys Chem A, (1933), 167, 273.

11. A J Boerboom, H W Reyn, H F Vugts, J Kistemaker, J Adv Mass Spec, (1966), 3, 945.

12. R G Behrens, G M Rosenblatt, J Chem Thermodyn, (1972), 4, 175.

13. R G Behrens, G M Rosenblatt, J Chem Thermodyn, (1973), 5, 173.

14. I R Beattie, K M S Livingstone, G A Ozin, D J Reynolds, JCS, (1970), 449.

15. S B Brumbach, G M Rosenblatt, J Chem Phys, (1972), 56, 6, 3110.

16. V P Cheremisinov, Opt Spectrosc, (1959), 7293.

17. A Muller, B N Cyvin, S J Cyvin, S Pohl, B Krebs, Spectrochim Acta, (1976), 32A, 67.

18. S J Cyvin, B N Cyvin, Z Naturforsch, (1971), 26A, 901.

19. C Sourisseau, R Mercier, Spectrochim Acta, (1978), 34A, 173.

20. S R Goates, G N Papatheodorou, J Chem Phys, (1978), 8, 67, 3717.

21. J S Ogden, M J Ricks, J Chem Phys, (1970), 53, 3, 896.

22. J S Anderson, J S Ogden, J Chem Phys, (1967), 51, 10, 4189.

23. G Herzberg, 'Infrared and Raman Spectra', Van Nostrand NY, p127.

24. J E Cahill, G E Leroi, J Chem Phys, (1969), 51, 1324.

25. J E Cahill, G E Leroi, J Chem Phys, (1969), 51, 97.

26. J E Cahill, G E Leroi, J Chem Phys, (1969), 51, 4114.

27. W T McDevitt, W L Baun, Spectrochim Acta, (1964), 20, 799.

28. J S Ogden, Spectrochim Acta, (1977), 33A, 1059.

29. J S Ogden, Ber Bunsen Phys Chem, (1978), 82, 76.

30. D D Price, Ph.D. Thesis, Southampton University, (1980).

31. I R Beattie, J S Ogden, D D Price, Inorg Chem, (1978), 17, 11, 3296.

CHAPTER 5

MATRIX ISOLATION/MASS SPECTROSCOPIC STUDIES OF VAPOUR PHASE OXIDES OF PHOSPHORUS

5.1 INTRODUCTION

The oxides of phosphorus P_4O_6 and P_4O_{10} are well known and have been the subjects of many investigations in previous years. Recent gas phase electron diffraction data exists for P_4O_6 [1] and for P_4O_{10} [2-5] in addition to earlier studies.[6,7] There also exists considerable information regarding the nature of the vibrational spectra of P_4O_6 and P_4O_{10}. An infrared (CS_2 solution) and Raman investigation (liquid) has been carried out for P_4O_6 and infrared (nujol mull) and single crystal Raman investigation for P_4O_{10},[8] as part of a series of articles dealing with phosphorus compounds.[8-10] This study supplements previous investigations of the spectra of P_4O_6 [11-13] and P_4O_{10},[13-16] and more recently, these molecules have been the subjects of a detailed Raman study[17]. Normal coordinate analyses using infrared and Raman vibrational frequencies have also been computed.[18,19] Much data are also available for the analogous Group V compounds As_4O_6 and Sb_4O_6 (see Chapter 4).

As far as the intermediate oxides of phosphorus are concerned (P_4O_x, x = 7-9) there is much less data available. Oxidation of P_4O_6 was thought to yield only P_4O_{10}, but recently the oxides P_4O_8 and P_4O_9 were shown to exist in mixed crystal phases.[20,21] Additionally X-ray crystallographic space group determination indicated that P_4O_7 exists in crystal phase mixtures with P_4O_8.[22,23] Little chemical characterisation of these compounds was made however, and the synthetic techniques used (pyrolysis flow-quench[20] and gas phase oxidation[22]) led to mixtures and/or low yields. Renewed interest in these compounds in recent years has been made apparent by the appearance of the results from some new investigations. A high yield synthesis of P_4O_7 (by the thermal decomposition of P_4O_6) has been developed and this compound has been analysed by ^{31}P nuclear magnetic resonance spectroscopy and mass spectrometry.[24] Its structure has been shown to retain the cage associated with P_4O_6. An improved synthesis of P_4O_7 has since been reported[25] where P_4O_7 is the major product of reaction between P_4O_6 and P_4O_{10}. A sample of P_4O_7, prepared according to this method has been investigated by X-ray crystallography[26] where the molecular dimensions obtained are compared with those obtained previously for P_4O_8 and P_4O_9.[1,2]

Vibrational data relating to these intermediate oxides are however very limited. No detailed vibrational study has appeared although there is some information available for P_4O_7 obtained from CS_2 solution (IR) and crystalline P_4O_7 (R).[24]

The purpose of the work carried out in this chapter was to initially obtain good quality infrared and Raman spectra of matrix isolated P_4O_6 and P_4O_{10} and their ^{18}oxygen substituted derivatives as an extension to the techniques of isotopic splitting pattern analysis used in the characterisation of As_4O_6 and Sb_4O_6 described in the previous chapter. Accurate assignment of vibrational frequencies to these molecules allowed the identification of intermediate oxides present in the samples used, and the subsequent assignment of vibrational frequencies to the molecules P_4O_7, P_4O_8 and P_4O_9. A sampling technique was devised so that parallel mass spectroscopic and matrix isolation studies could be carried out using the same sample and this is shown to be a powerful method for determining the composition of the vapour obtained from a heated sample, particularly where a mixture of products results.

Finally, the force field developed in the previous chapter to reproduce accurately observed frequencies and isotopic splitting patterns for As_4O_6 and Sb_4O_6 is shown to be successful in the same respects for P_4O_6 and with some extension for P_4O_{10}.

5.2 EXPERIMENTAL

5.2(i) Sampling techniques for mass spec/matrix isolation studies

The identification of the molecules P_4O_7, P_4O_8 and P_4O_9, described in subsequent sections, was greatly facilitated by the ability to be able to carry out both mass spectroscopic and matrix isolation studies on the same sample. Provided, in the case of mass spectroscopic results, spectrometer induced reactions are taken into account and their subsequent products identified, the major vapour phase species can be identified first by preliminary mass spectroscopic experiments, enabling subsequently observed vibrational spectra to be assigned with some confidence. This is particularly useful where more than one species is present in the vapour phase. The problems of species identification can be further complicated when the species present in the vapour exhibit

vibrational bands at similar frequencies. This complication arises when considering the series of compounds P_4O_x (x = 6-10) where vibrational transitions of similar frequency would be expected for all these molecules. Indeed extremely complex spectra would be expected (and were observed) when mixtures of these molecules were present. However, the use of mass spectroscopy enabled the identification of P_4O_7 which in turn facilitated the identification of P_4O_8 and P_4O_9.

The essential features of the mass spectroscopic sampling apparatus is shown in Figure 5.1. The sample contained in a sample holder (a) (described in Chapter 2) complete with greaseless tap (b) was supported in the mounting collar (c) using an 'o' ring (d) and retaining clamp (e). The dimensions of the mounting collar were identical to that used for infrared experiments (see Chapter 2). The sample was heated using a loosely wound resistive heater (f) wound directly onto the pyrex sample holder. A gate valve (g) was placed between the sample and the spectrometer ionisation chamber (h). This allowed isolation of the sample chamber prior to an experiment being carried out so that this part of the apparatus could be pumped out via a port (i) using a separate pumping system. This allowed the vacuum in the spectrometer itself to be maintained at all times. The gate valve also acted as an effective shutter during the course of an experiment allowing or intercepting passage of vapour into the ionisation chamber of the spectrometer as desired. Although there was considerable condensation of the vapour on the 'off axis' parts of the apparatus, sufficient vapour reached the ionisation chamber for samples which had a significant vapour pressure in the region 0-100°C. Modification of this sampling technique would clearly be required for less volatile samples. The mass spectrometer used throughout this work was an AEI MS 12.

5.2(ii) Sample preparation

Preparative methods developed for the molecule P_4O_6 and the intermediate oxides of phosphorus have usually involved the use of 'flow' techniques or gas phase oxidation.[20,22] More recently a high yield preparation of P_4O_7 has been developed[24] from the thermal decomposition of P_4O_6, and has been shown to be the major product of reaction between

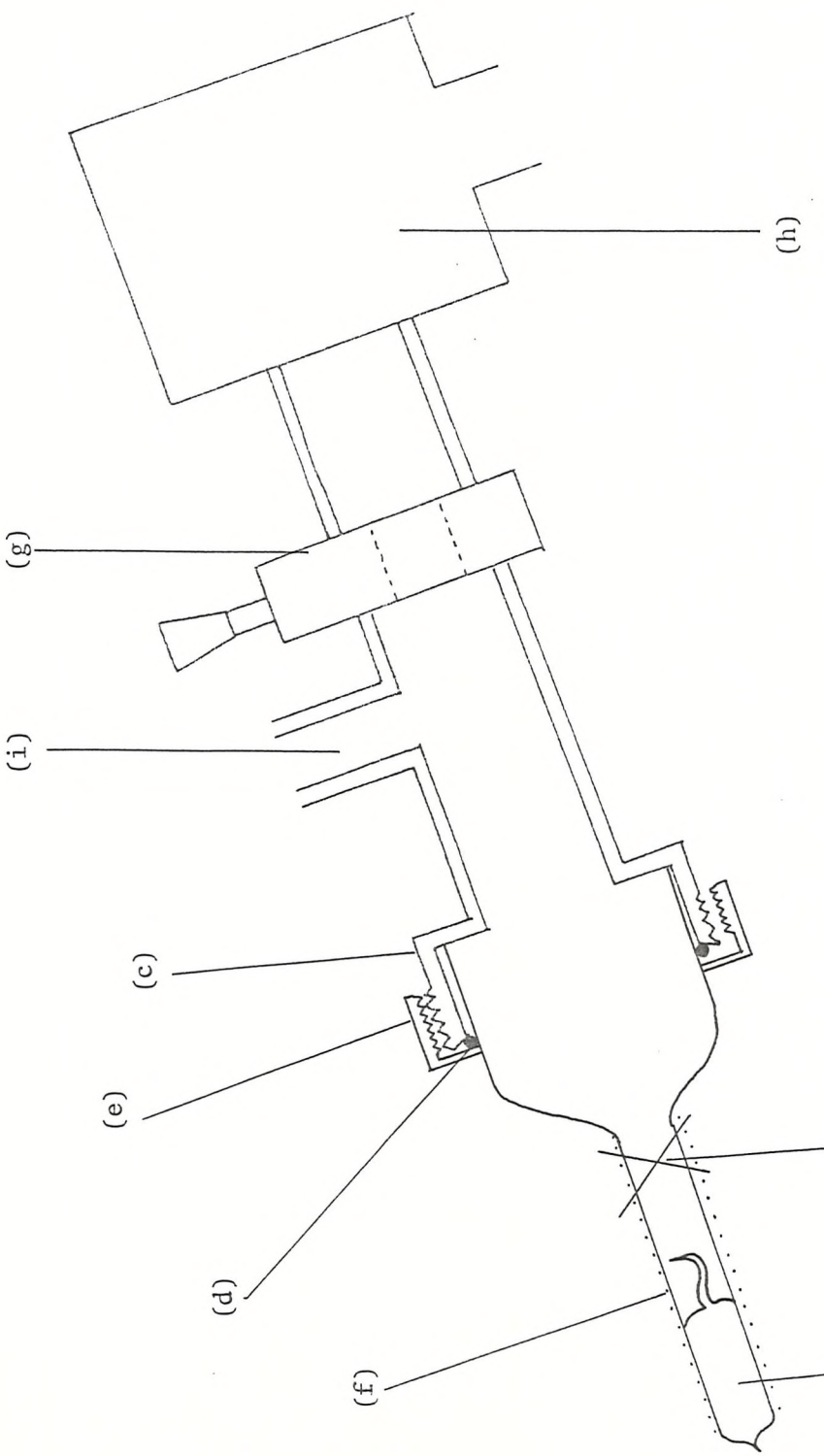

Figure 5.1 The sampling apparatus used for the mass spectroscopic experiments

P_4O_6 and P_4O_{10}.[25]

A requirement in this work was that any synthesis used should be economical enough in its use of oxygen, that ready incorporation of ^{18}O could be easily achieved. This clearly rules out the use of flow techniques and an approach via the controlled oxidation of elemental phosphorus was sought. The preparation of P_4O_{10} is the most straightforward and involved the oxidation of a weighed quantity of freshly sublimed white phosphorous by an excess of oxygen. P_4O_{10} was the only major product of reactions of this type and ^{18}O substituted samples of P_4O_{10} could be readily prepared using an $^{16}O/^{18}O$ mixture of known composition. The P_4O_{10} was vacuum sublimed into 'break seal' ampoules in the presence of oxygen, at which time any unreacted phosphorus was oxidised.

Complications arose however when this preparative method was extended to P_4O_6. Although P_4O_6 was a major product when the above reaction was carried out in a deficit of oxygen, only rarely was P_4O_6 isolated alone. Separation of P_4O_6 from small quantities of P_4O_{10} could be achieved owing to the high volatility of P_4O_6, but all samples of P_4O_6 prepared contained small quantities of unreacted phosphorus. More often, mixtures of P_4O_6, P_4O_7, P_4O_8, P_4O_9 and P_4O_{10} were produced. The differential volatilities of these species however, simplified greatly analysis where mixtures were produced and the use of mass spectroscopy enabled the major vapour phase species to be identified at any stage of the vaporisation. The fact that mixtures were generally produced in this way also enabled the production of an ^{18}O substituted sample of P_4O_7, although P_4O_6 was often present.

Finally it is interesting to note that freshly sublimed white phosphorus frequently had to be warmed before reaction with oxygen occurred, even when the partial pressure of oxygen was in the region of 250 torr.

5.3 THE INFRARED AND RAMAN SPECTRA OF MATRIX ISOLATED $P_4{}^{16}O_{10}$ AND $P_4{}^{16}O_6$

As is the case for As_4O_6 and Sb_4O_6, both infrared and Raman spectra of P_4O_6 and P_4O_{10} were obtained using similar experimental conditions, and

they are therefore dealt with together.

Figure 5.2(a) shows a typical infrared spectrum obtained after condensing the vapour above heated P_4O_{10} at ca 373K (sample prepared as in Section 5.2) with a large excess of argon for about 30 minutes. The spectrum consists of absorptions at 1403.0 cm^{-1}, 1024.0 cm^{-1}, 765.0 cm^{-1}, 575.1 cm^{-1}, 410.0 cm^{-1} and 272.0 cm^{-1}. Negligible frequency shifts were observed on changing the matrix gas and therefore nitrogen was used for Raman experiments owing to its production of optically clear matrices. Figure 5.2(b) shows a typical Raman spectrum obtained after condensing the vapour from a similar sample with an excess of nitrogen (again at ca 373K) for about 45 minutes. Here bands are observed at 1428.0 cm^{-1}, 1402 cm^{-1}, 716.0 cm^{-1}, 555.0 cm^{-1}, 410.0 cm^{-1}, 273.0 cm^{-1} and 255 cm^{-1}. The molecule P_4O_{10} retains Td symmetry and the normal modes of vibration are distributed among the symmetry species according to:

$$\Gamma_{vib} = 6F_2 + 3A_1 + 3E + 3F_1$$

Here, the F_1 modes are infrared and Raman inactive, the F_2 modes are infrared and Raman active, and the A_1 and E modes are Raman active only. Comparison of these observed frequencies with those of previous investigations allows assignments to be made of:

F_2		A_1		E	
ν_{10}	1403.0 cm^{-1}	ν_1	1428.0 cm^{-1}	ν_6	255 cm^{-1}
ν_{11}	1024.0 cm^{-1}	ν_2	716.0 cm^{-1}		
ν_{12}	765.0 cm^{-1}	ν_3	555.0 cm^{-1}		
ν_{13}	575.1 cm^{-1}				
ν_{14}	410.0 cm^{-1}				
ν_{15}	272.0 cm^{-1}				

All observed frequencies for $P_4{}^{16}O_{10}$ appear in Table 5.1 where they are compared with those observed by previous workers. The location of two of the E modes (ν_4 and ν_5) remains in doubt, and these modes were not observed in this work. There is however considerable agreement with regard to the assignments of the remaining active fundamentals for P_4O_{10}. No estimates of the frequencies of the infrared and Raman inactive F_1

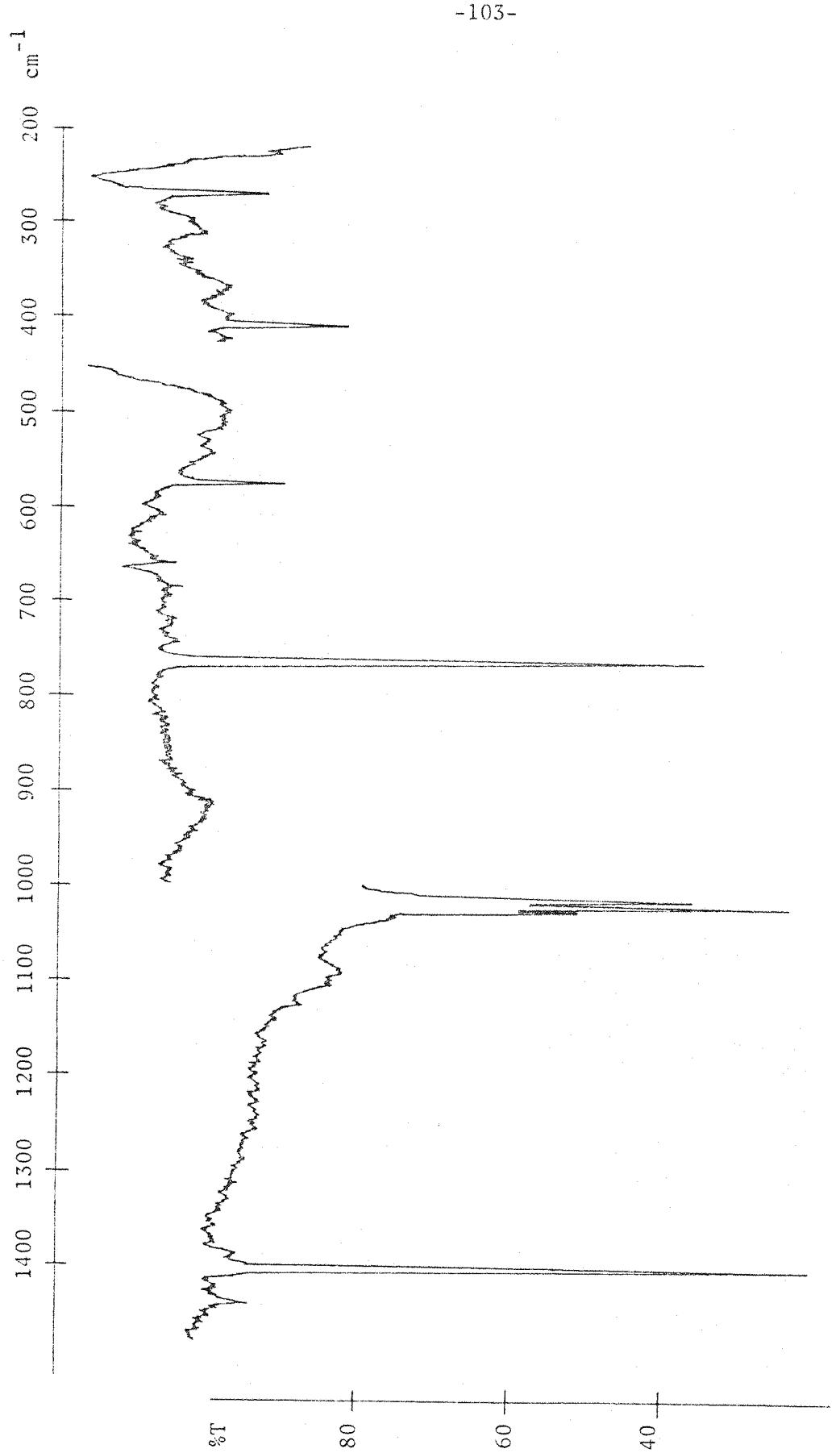

Figure 5.2(a) Infrared spectrum of matrix isolated $P_4{}^{16}O_{10}$ (argon matrix)

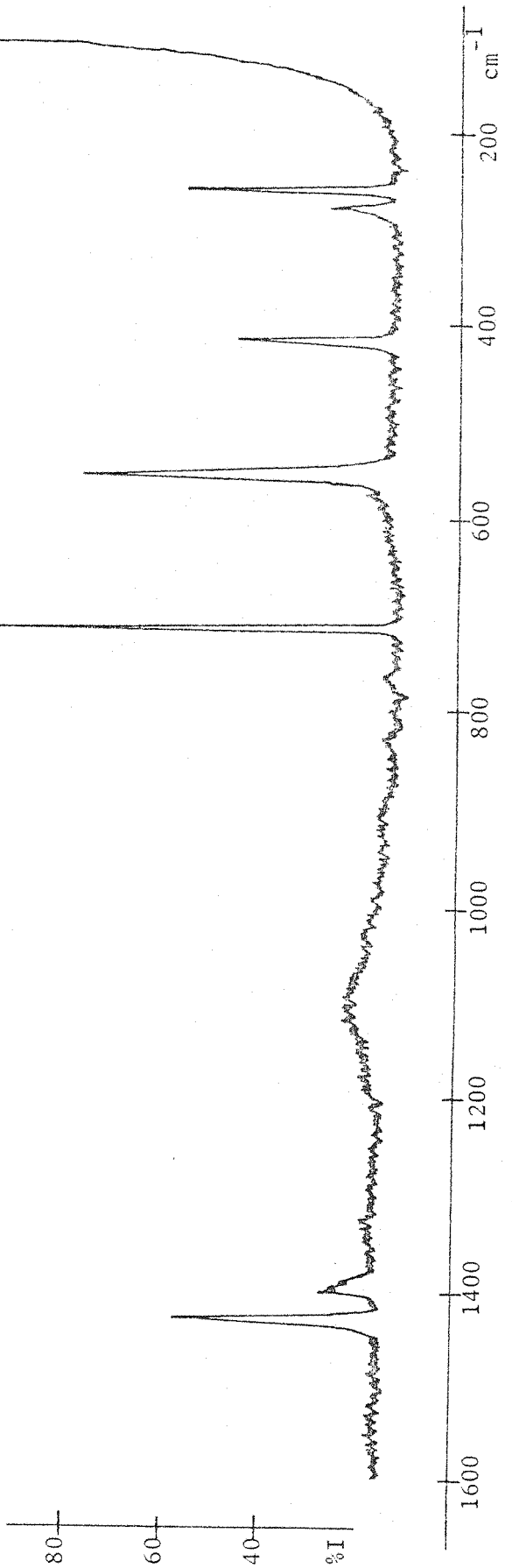

Figure 5.2(b) Raman spectrum of matrix isolated $P_4{}^{16}O_{10}$ (nitrogen matrix)

Table 5.1 Vibrational frequencies for $P_4{}^{16}O_{10}$ and Assignments

IR Argon matrix cm^{-1} (a)	R Nitrogen matrix cm^{-1} (a)	IR Nujol mull cm^{-1} (b)	R Solid cm^{-1} (b)	IR Nujol mull cm^{-1} (c)	R Solid cm^{-1} (d)	R Gas phase cm^{-1} (e)	Assignments
	1428.0		1413		1417	1440	ν_1 A_1
1403.0	1402.0	1390		1390	1386	1406	ν_{10} F_2
1024.0		1010		1015			ν_{11} F_2
	-		-		952	-	ν_4 E
765.0		760		764			ν_{12} F_2
	716.0		720		721	717	ν_2 A_1
	-		-		650	662	ν_5 E
575.1		573		573			ν_{13} F_2
	555.0		556		559	553	ν_3 A_1
410.0	410.0	414 421			424	411	ν_{14} F_2
272.0	273.0	270 280				264	ν_{15} F_2
	255.0		257		257	254	ν_6 E

(a) This work (frequency accuracy ± 0.4 cm^{-1})
(b) Reference 8
(c) Reference 16
(d) Reference 13
(e) Reference 17
- = not observed

modes have previously been made and information regarding these vibrations is not available from these results.

P_4O_6 is volatile at room temperature (mpt 22°C) and the deposition rate of a sample prepared according to the method described in section 5.2 was controlled using a greaseless needlevalve. Figure 5.3(a) shows a typical infrared spectrum obtained by condensing the vapour above P_4O_6 (ambient temperature) with a large excess of argon for about 15 minutes. Absorptions were observed at 954.8 cm^{-1}, 640.7 cm^{-1}, 406.2 cm^{-1} and 301.3 cm^{-1}. Again, negligible frequency shifts were noted on changing the matrix gas to nitrogen, and for similar reasons as before nitrogen was used as the matrix gas for the Raman experiments. Figure 5.3(b) shows a typical Raman spectrum obtained after condensing the vapour above P_4O_6 (again at ambient temperature) with a large excess of nitrogen for about 30 minutes. Bands were observed at 640.0 cm^{-1}, 619.1 cm^{-1}, 406.0 cm^{-1} and 301.3 cm^{-1}.

Comparison of these observed frequencies with those of previous workers allows assignments to be made as follows:

F_2		A_1	
ν_7	954.8 cm^{-1}	ν_1	619.1 cm^{-1}
ν_8	640.7 cm^{-1}		
ν_9	406.2 cm^{-1}		
ν_{10}	301.3 cm^{-1}		

All the observed frequencies for $P_4{}^{16}O_6$ appear in Table 5.2 where together with their assignments they are compared with those of previous workers. Although these observed frequencies are in agreement with previously reported values[8,17] it is interesting to note the non-appearance in the Raman spectra of ν_2 (A_1). Gerding et al[11] suggested that the two A_1 modes were coincident at 613 cm^{-1} in the liquid. This would appear not to be the case as Chapman[8] observed a weak polarised Raman band from liquid P_4O_6 at 569 cm^{-1}. This observation is supported by the presence of Raman bands at 599 cm^{-1} (solid P_4O_6) and 562 cm^{-1} (gaseous P_4O_6, 150°) in the spectra reported by Beattie et al.[17] Moreover if a coincidence

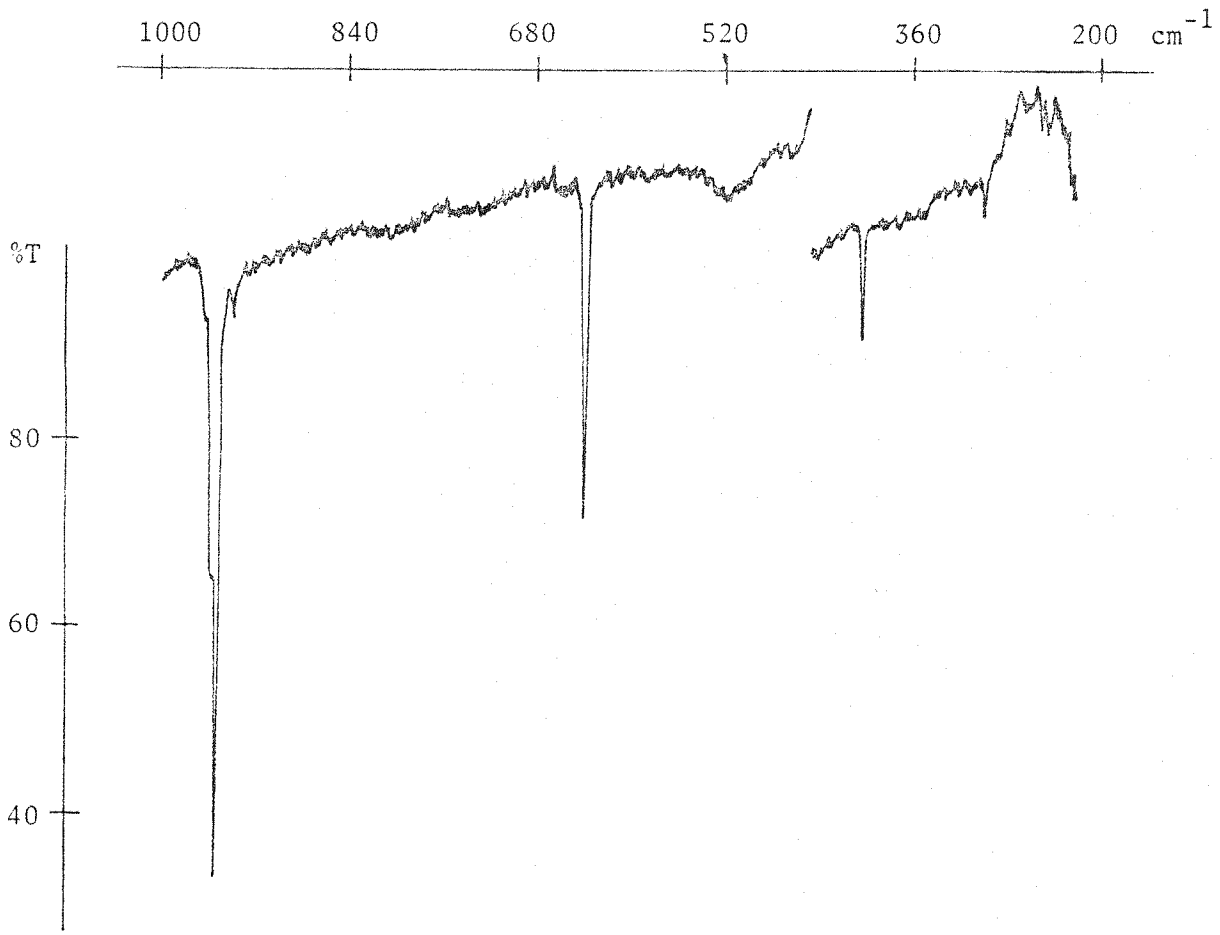

Figure 5.3(a) Infrared spectrum of matrix isolated $P_4{}^{16}O_6$ (argon matrix)

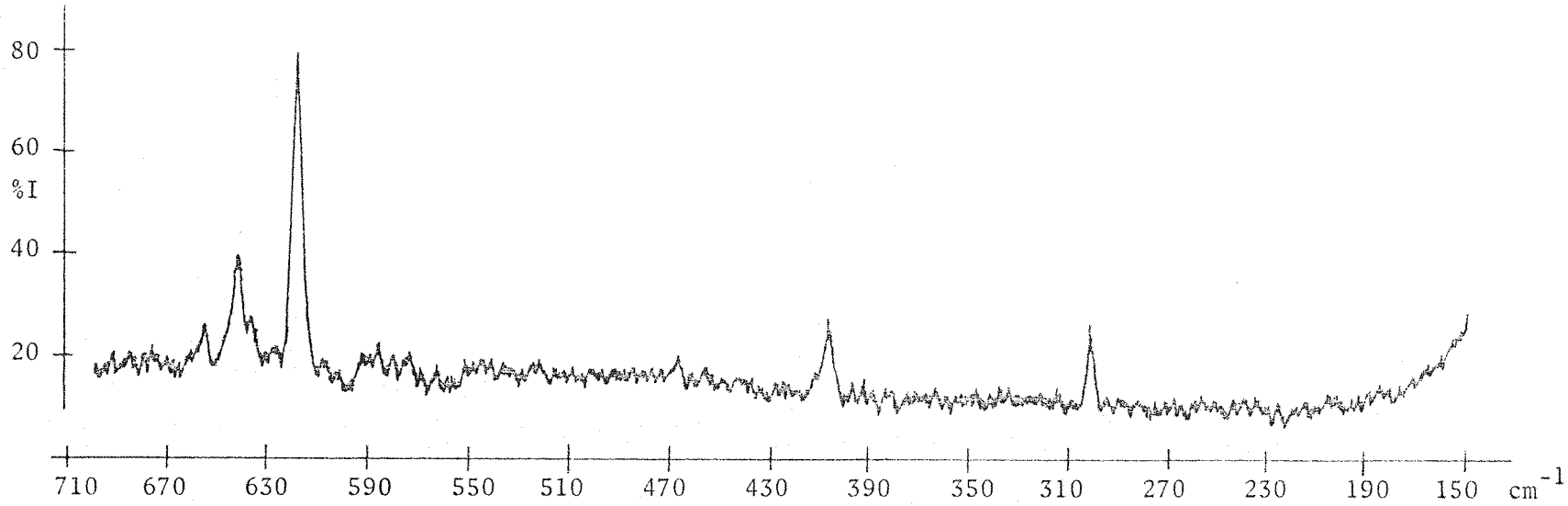

Figure 5.3(b) Raman spectrum of matrix isolated $P_4{}^{16}O_6$ (nitrogen matrix)

Table 5.2 Vibrational frequencies and assignments for $P_4{}^{16}O_6$

IR Argon matrix cm^{-1} (a)	R Nitrogen matrix cm^{-1} (a)	IR CS_2 soln cm^{-1} (b)	R Liquid cm^{-1} (b)	R Solid cm^{-1} (c)	R Gas 150° cm^{-1} (c)	Assignment
954.8	-	919	919	891	959	ν_1 F_2
-	-	832	-	-	-	ν_5
	-		691	-	-	ν_3 E
640.7	640.5	643	643	638	642	ν_8 F_2
	619.1		613	609	620	ν_1 A_1
	-		569	599	562	ν_2 A_1
406.2	406.2	407	407	413	408	ν_9 F_2
301.3	301.3	302	302	302	305	ν_{10} F_2
	-		285	285	-	ν_4 E

(a) This work (frequency accuracy ± 0.4 cm^{-1})
(b) Reference 8
(c) Reference 17
- = not observed

does exist it would seem unlikely that it would persist in all phases and consequently the assignment of Chapman[8] is accepted. His assignment of ν_4 (E) at 691 cm^{-1} would also seem to be correct as a band previously assigned to this vibration at 1029 cm^{-1} [11] has not been observed by other workers. Chapman includes in his work a tentative assignment for the highest frequency infrared and Raman inactive F_1 mode, on the basis of an infrared absorption observed at 832 cm^{-1} in CS_2 solution. Although no information regarding the frequencies of these F_1 modes is available from the spectra obtained from matrix isolated P_4O_6 in this work, subsequent calculations (see section 5.4) place the frequency of this vibration at 866.2 cm^{-1}, and this is significant in the light of spectra obtained from P_4O_7, P_4O_8 and P_4O_9 (see section 5.6).

Finally it is interesting to compare the spectra obtained from P_4O_6 with those obtained from samples of As_4O_6 and Sb_4O_6. In particular, although all the infrared spectra appear similar, in the Raman spectra the relative intensities and frequencies of the P_4O_6 fundamentals varies appreciably from those observed for As_4O_6 and Sb_4O_6, whose Raman spectra are very similar in these respects. This is not altogether surprising however if the relative masses of ^{31}P, ^{75}As, ^{121}Sb and ^{16}O are considered. It would seem reasonable to suggest that in the case of P_4O_6 the lighter phosphorus will exhibit greater motion during the course of the molecular vibrations with consequent relative intensity and frequency variations.

5.4 FORCE CONSTANT ANALYSIS

As a further test of the force field used to describe the potential energy function of Sb_4O_6 and As_4O_6, this force field was used to calculate frequencies for both P_4O_6 and P_4O_{10}. This process for P_4O_{10} required extension of the force field to include the four terminal P=O bonds. Besides the eight force constants used to describe the motion of the M_4O_6 cage (F_r, F_α, F_{rr}, F'_{rr}, F_β, $F_{\alpha\alpha}$, $F_{r\alpha}$ and $F_{r\beta}$) two new force constants were introduced for P_4O_{10} these being:

F_d - principal stretching constant P=O

F_{rd} - interaction constant O-P=O

This force field was found to be adequate to accurately reproduce

observed frequencies and the observed and calculated frequencies for P_4O_{10} are contained in Table 5.3.

For P_4O_6, the eight parameter force field used for As_4O_6 and Sb_4O_6 was successfully used without modification to reproduce the observed frequencies and the calculated and observed frequencies for P_4O_6 are also shown in Table 5.3. Table 5.4 gives the final force constant values used for P_4O_6 and P_4O_{10}, together with the sets of internal coordinates used. The successful use of this force field to describe the vibrations of the molecules P_4O_6, P_4O_{10}, As_4O_6 and Sb_4O_6 together with its recent use in the characterisation of V_4O_{10} [27] would seem to lend weight to the validity of this approach.

5.5 INFRARED SPECTRA OF MATRIX ISOLATED $P_4{}^{16/18}O_6$ AND $P_4{}^{16/18}O_{10}$

In order to obtain a more complete characterisation of the molecules P_4O_6 and P_4O_{10} and as a further test of the validity of the force field used for the calculations carried out on these molecules, it was decided to obtain high resolution spectra of $^{16/18}O$ substituted samples of P_4O_6 and P_4O_{10}.

Figure 5.4 shows the infrared spectrum obtained from a sample of P_4O_{10} prepared using a 3:2 mixture of ^{16}O:^{18}O. Figure 5.5 shows a similar spectrum of a sample of P_4O_6 prepared using a similar isotopic mixture. Although this P_4O_6 sample contained some unreacted phosphorus, this did not seem to degrade the quality of the spectra obtained. Moreover no absorbtion due to P_4 were observed in the spectrum.

It is clear from Figure 5.4 that the high frequency (terminal) F_2 mode of P_4O_{10} now appears basically as a doublet and that the highest frequency cage F_2 mode (1024 in $P_4{}^{16}O_{10}$) appears as the characteristic multiplet similar to the patterns observed for As_4O_6 and Sb_4O_6. Figure 5.5 shows that the highest F_2 mode for P_4O_6 also appears as a multiplet characteristic of an F_2 M_4O_6 cage vibration. Figure 5.6 shows the high resolution spectra of the two highest frequency F_2 modes of P_4O_{10}, while Figure 5.7 shows a similar spectrum of the highest frequency F_2 mode of P_4O_6. High resolution spectra could not be obtained from other absorptions in either case, owing to the low intensities of these bands.

Table 5.3 Observed and calculated frequencies for $P_4{}^{16}O_{10}$ and $P_4{}^{16}O_6$. Frequencies were calculated using the force field and model described in the text and in Table 5.4.

P_4O_6		Assignment		P_4O_{10}	
Obs cm^{-1}	Calc cm^{-1}			Obs cm^{-1}	Calc cm^{-1}
954.8	954.8	F_2	F_2	1403.0	1403.0
640.7	640.7	F_2	F_2	1024.0	1024.0
406.2	406.2	F_2	F_2	765.0	765.0
301.3	301.3	F_2	F_2	575.1	575.1
619.1	619.1	A_1	F_2	410.0	410.0
-	562.1	A_1	F_2	272.0	272.0
-	647.9	E	A_1	1428.0	1428.0
-	285.4	E	A_1	716.0	716.0
-	855.2	F_1	A_1	555.0	555.0
	209.9	F_1	E	-	880.2
			E	-	378.4
			E	255.0	255.0
			F_1	-	1122.8
			F_1	-	449.2
			F_1	-	267.9

- = not observed

Table 5.4 Force field and model used for the calculations of frequencies shown in Table 5.3 and the line diagrams in Figure 5.

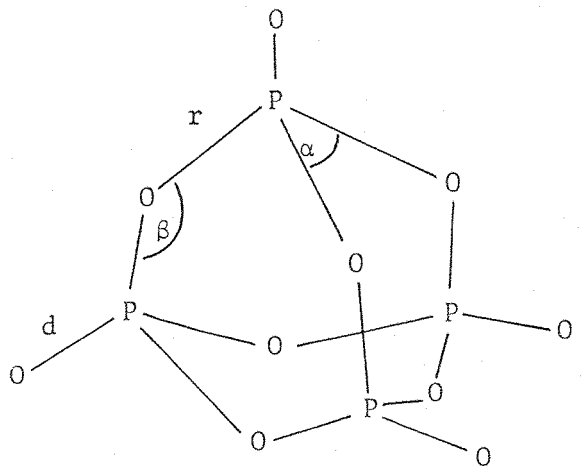

P_4O_6	P_4O_{10}
r = 1.65 Å	r = 1.6 Å
α = 99°	α = 101.6°
β = 128°	β = 123.5°
	d = 1.4 Å

P_4O_6	P_4O_{10}
F_r = 3.51	F_r = 5.64 mdyn Å^{-1}
F_α = 0.53	F_α = 1.24 mdyn Å rad^{-2}
F_{rr} = -0.23	F_{rr} = 0.46 mdyn Å^{-1}
F'_{rr} = 0.56	F'_{rr} = -0.24 mdyn Å^{-1}
F_β = 1.5	F_β = 1.56 mdyn Å rad^{-2}
$F_{\alpha\alpha}$ = -0.21	$F_{\alpha\alpha}$ = -0.13 mdyn Å rad^{-2}
$F_{r\alpha}$ = 0.1	$F_{r\alpha}$ = 0.21 mdyn rad^{-1}
$F_{r\beta}$ = 0.13	$F_{r\beta}$ = 0.9 mdyn rad^{-1}
	F_d = 11.16 mdyn Å^{-1}
	F_{rd} = 1.07 mdyn Å^{-1}

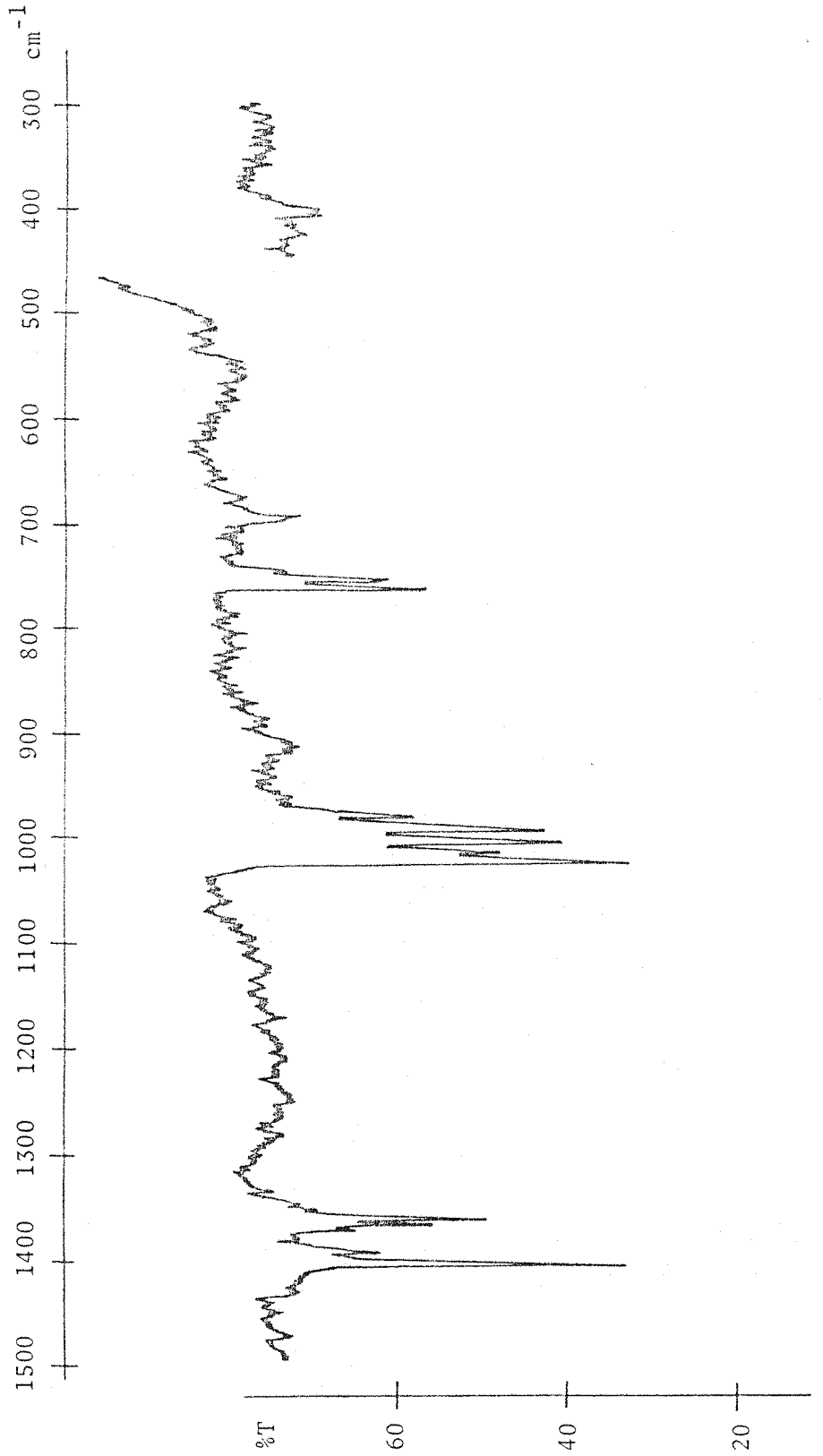

Figure 5.4 Infrared spectrum of matrix isolated $P_4{}^{16/18}O_{10}$ (argon matrix)

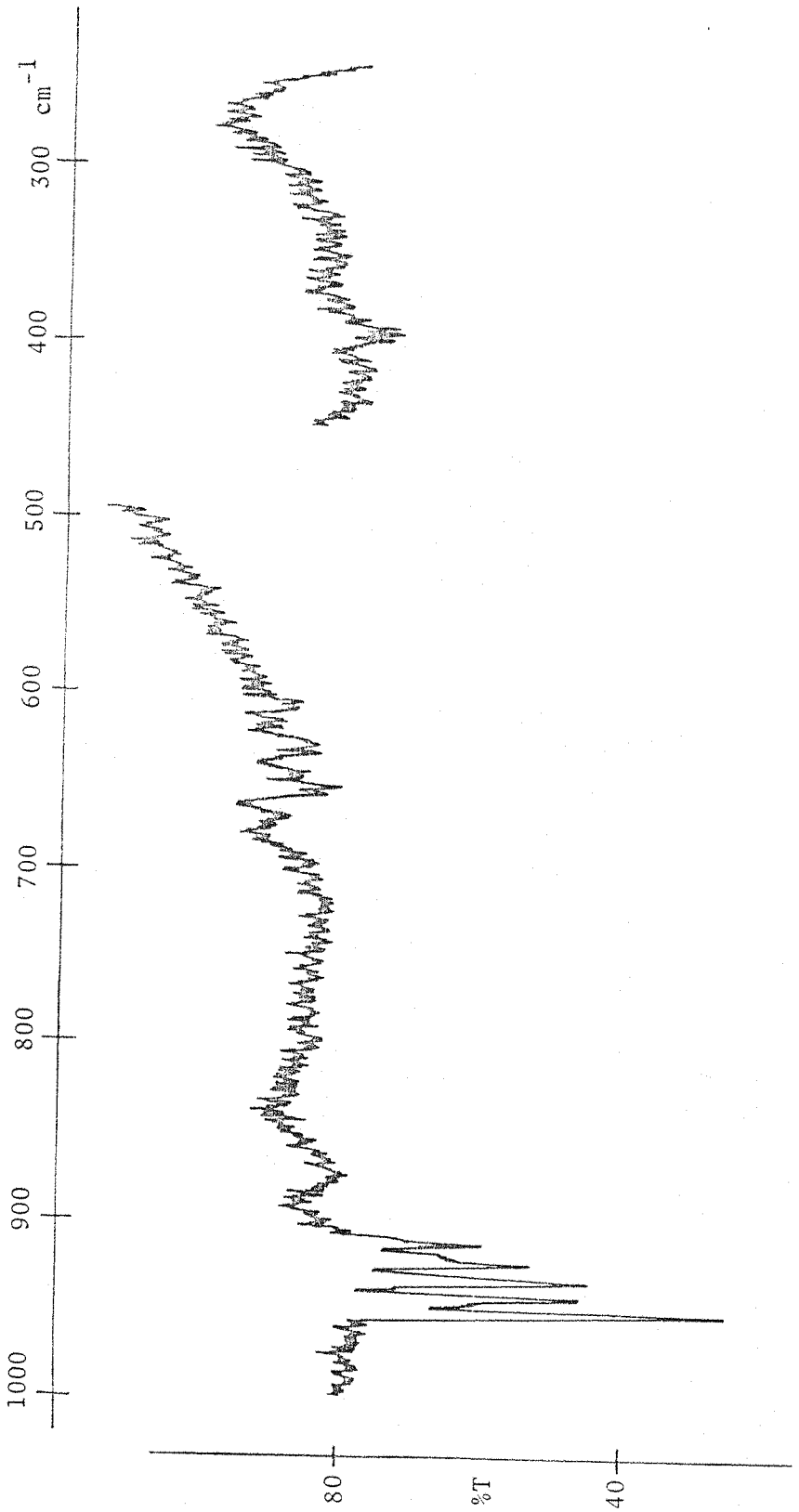

Figure 5.5 Infrared spectrum of matrix isolated $P_4{}^{16/18}O_6$ (argon matrix)

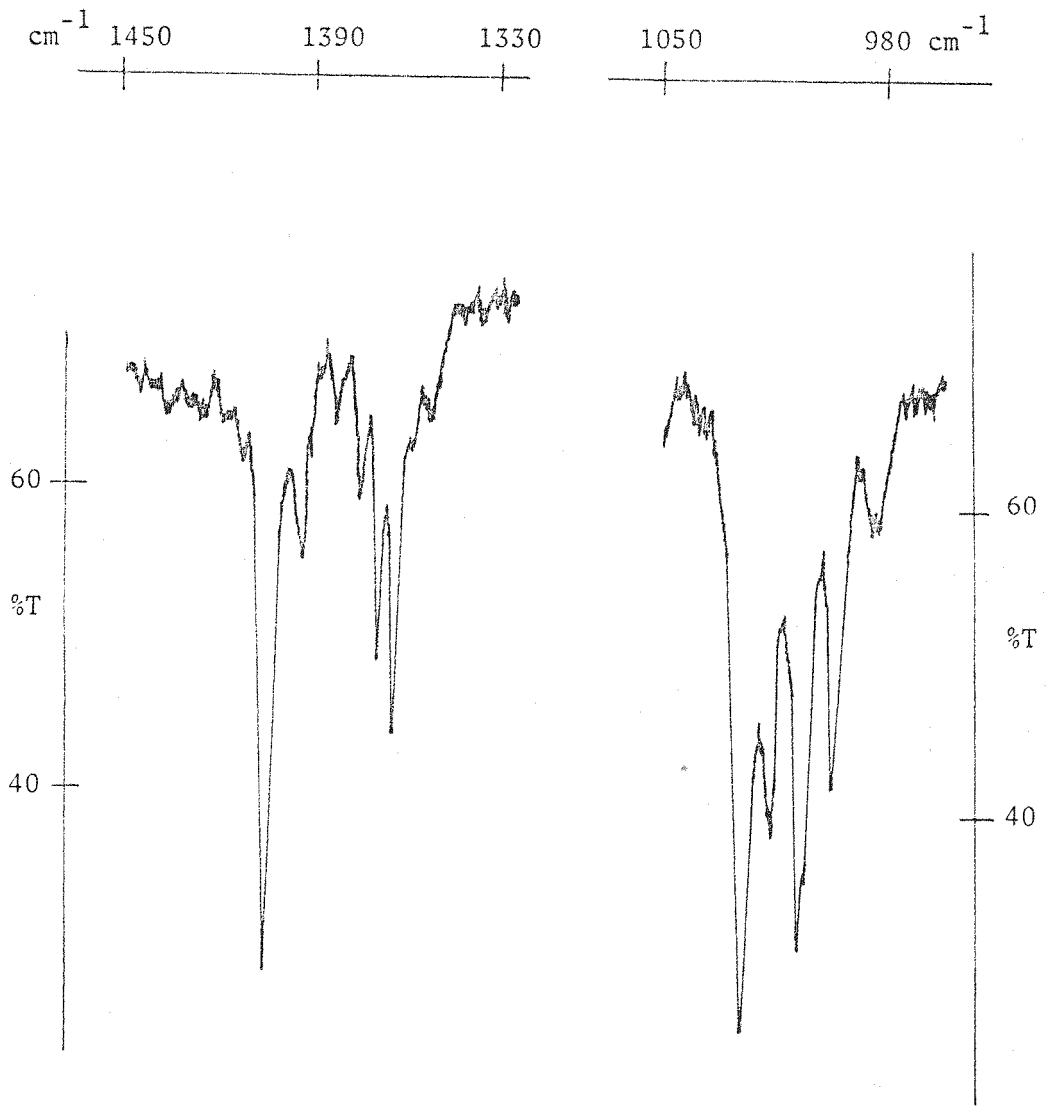

Figure 5.6 High resolution spectrum of part of Figure 5.4

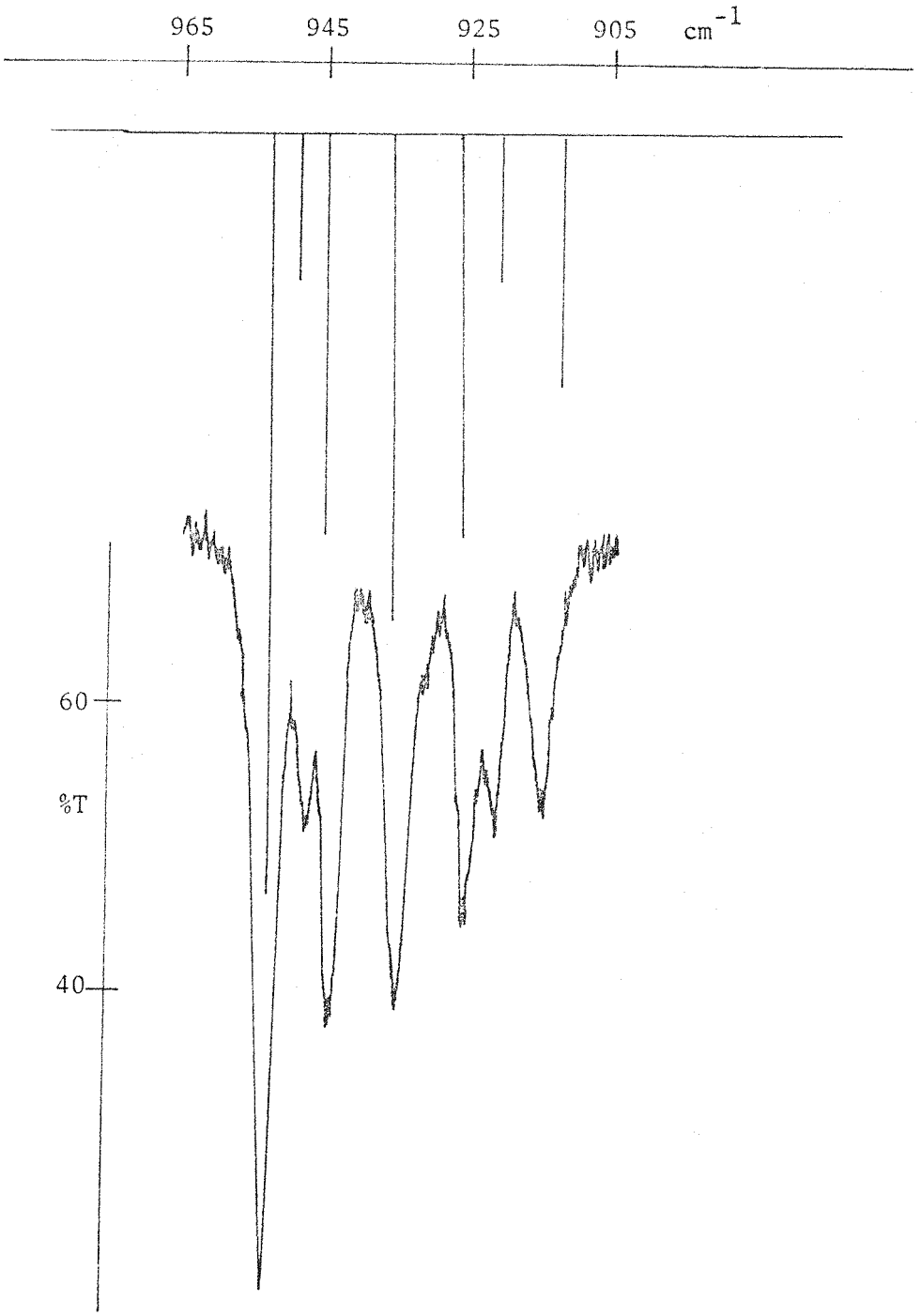

Figure 5.7 High resolution spectrum of part of Figure 5.5 together with calculated spectrum

Turning first to P_4O_6, it is clear that the high resolution isotope pattern obtained is identical to those observed for As_4O_6 and Sb_4O_6. This appears as a septet which is expected for the presence of six equivalent oxygen atoms. Using a procedure exactly analogous to that used for As_4O_6 and Sb_4O_6 and utilising the force field described earlier the frequencies of the bands derived from the highest frequency F_2 mode of P_4O_6 were calculated for all isotopic variants. The results of these calculations appear in Table 5.5 and in Figure 5.7, where they take the form of a computed line diagram. Agreement between calculated and observed spectra is excellent, again indicating the reliability of this approach to characterisation of M_4O_6 cage vibrations.

For the molecule P_4O_{10}, a quantitative analysis of the spectrum of isotopically (^{18}O) enriched P_4O_{10} is understandably more complex. Random incorporation of ^{18}O into this molecule results in the generation of 90 isotopomers. Consequently, the computational problem is vast and although individual isotopic frequency calculations were carried out for all 90 isotopomers (using the SOTONVIBP program) a complete analysis was not attempted and a realistic simplification of the problem sought. This simplification rests on the assumption that the four terminal bonds can be effectively decoupled from the rest of the molecule. This assumption can be supported by observations made on the molecule OsO_4 [28] which gives a similar spectrum on ^{18}O enrichment to that obtained in the terminal P=O region for P_4O_{10}. Considering the stretching region only, OsO_4 (Td) has νA_1 at 963.0 cm^{-1} and νF_2 at 956.0 cm^{-1} (argon matrix). This proximity of frequencies leads to perturbation of the pattern produced by the F_2 mode on isotopic substitution, owing to the generation of A_1 modes from the F_2 mode in partially substituted molecules. This leads to frequency perturbation and intensity borrowing. The resulting IR spectrum is essentially a doublet with fine structure on the high frequency side of the prominent $Os^{16}O_4$ band, Figure 5.8(a). Frequency calculations show that (unresolved) fine structure is also expected on the high frequency side of the $Os^{18}O_4$ band. This comparison with OsO_4 has recently been used to explain the observed spectrum of ^{18}O substituted V_4O_{10} [27] and this spectrum appears in Figure 5.8(b). It is evident that this spectrum shows a marked similarity to that of OsO_4.

Table 5.5 Vibrational frequencies of isotopically substituted P_4O_6 for the highest F_2 mode

Molecule	Pt Grp	Vib modes	Frequencies
$P_4[O^{16}]_6$	Td	F_2	954.8 954.8 954.8
$P_4[O^{16}]_5[O^{18}]$	C_{2v}	A_1,B_1,B_2	954.8 954.6 937.9
$P_4[O^{16}]_4[O^{18}]_2$ (cis)	C_s	2A',A''	954.8 946.8 927.1
$P_4[O^{16}]_4[O^{18}]_2$ (trans)	D_{2d}	B_2,E	937.9 937.9 954.7
$P_4[O^{16}]_3[O^{18}]_3$ [A]	C_{3v}	A_1,E	912.5 946.8 946.8
$P_4[O^{16}]_3[O^{18}]_3$ (mer)	C_2	A_1,B_1,B_2	937.8 950.1 921.8
$P_4[O^{16}]_3[O^{18}]_3$ (fac)	C_{3v}	A_1,E	927.1 927.1 954.7
$P_4[O^{16}]_2[O^{18}]_4$ (trans)	D_{2d}	B_2,E	937.7 937.7 912.5
$P_4[O^{16}]_2[O^{18}]_4$ (cis)	C_s	2A',A''	946.7 912.5 927.1
$P_4[O^{16}][O^{18}]_5$	C_{2v}	A_1,B_1,B_2	912.5 912.4 937.7
$P_4[O^{18}]_6$	Td	F_2	954.8 954.8 954.8

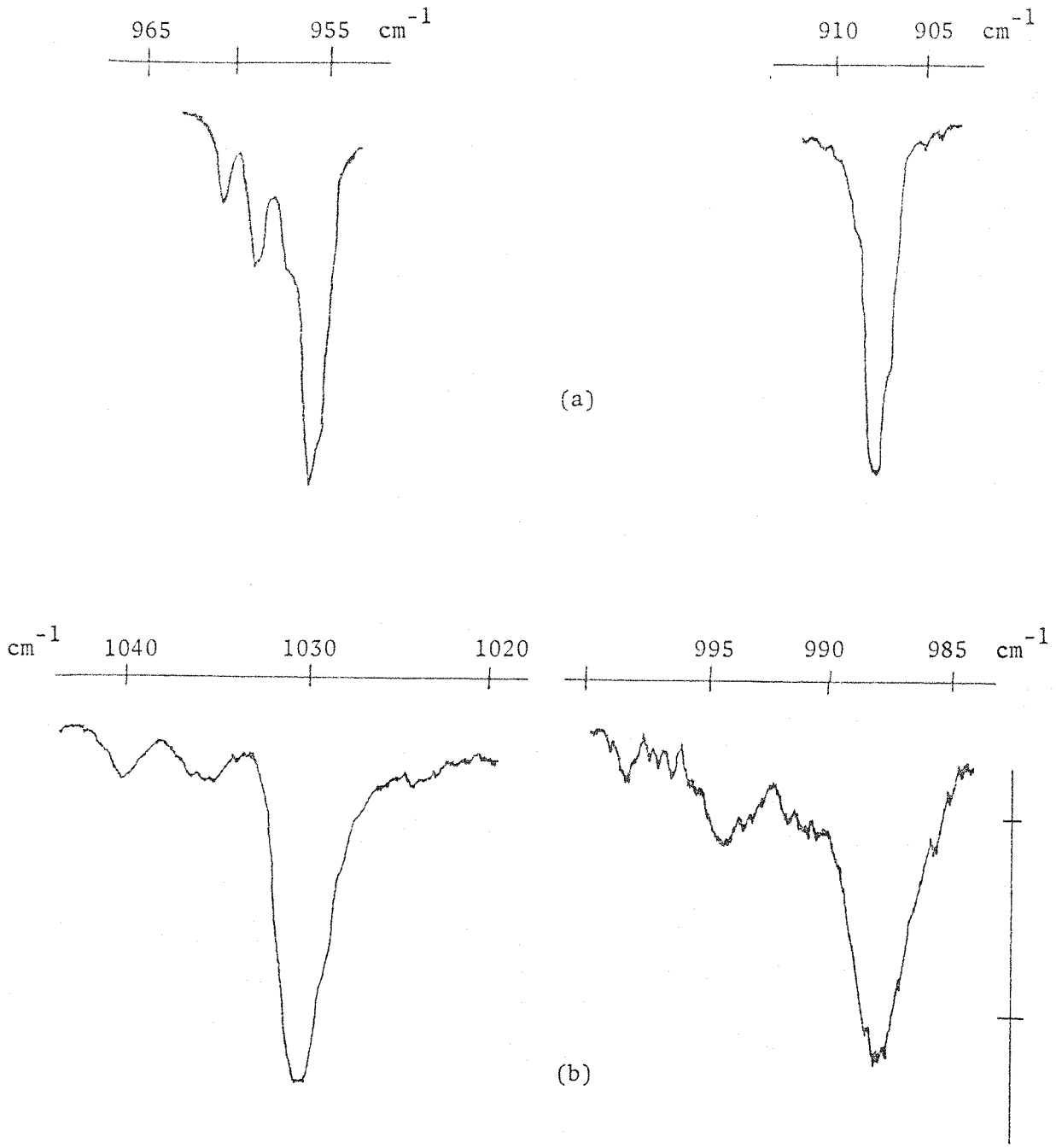

Figure 5.8 (a) Infrared spectrum of matrix isolated $Os^{16/18}O_4$ (argon matrix) from Reference 28.

(b) Infrared spectrum of matrix isolated $V_4^{16/18}O_{10}$ (nitrogen matrix) from Reference 27.

The spectrum of P_4O_{10}, in the terminal P=O region is again similar to that observed for OsO_4 (and V_4O_{10}) although no high frequency fine structure was observed on the $P_4{}^{16}O_{10}$ band. This may however be due to lack of resolution on the observed spectrum. Considerable fine structure was observed however on the low frequency side of this band and on the high frequency side of the $P_4{}^{18}O_{10}$ band. The assumption that the terminal modes can be effectively decoupled from the cage modes, and that the cage acts essentially as a heavy central atom may not be as rigorous for P_4O_{10} as it is for V_4O_{10}, when the relative masses of vanadium and phosphorus are taken into account. Isotopic frequency calculations carried out on P_4O_{10}, considering the whole molecule, and using two additional force constants to those used for the M_4O_6 species (see section 5.4) produced the following results for selected isotopomers:

Molecule		Terminal P=O cm^{-1}	Cage P-O cm^{-1}
Cage	Terminal		
$P_4{}^{16}O_6$	$^{16}O_4$	1403.0	1024.0
$P_4{}^{16}O_6$	$^{18}O_4$	1362.3	1019.6
$P_4{}^{18}O_6$	$^{16}O_4$	1400.6	986.4
$P_4{}^{18}O_6$	$^{18}O_4$	1359.2	982.8

Although these calculations reproduced the observed overall frequency shift within 1 cm^{-1} ($\Delta\nu$ = 42 cm^{-1}) the introduction of a cage/terminal interaction constant results in limited cage/terminal coupling and a consequent small frequency perturbation (of the order of <1%) in the calculated isotope patterns. This could explain the significant fine structure observed on the terminal P=O doublet of P_4O_{10} although it is not possible to tell from the observed spectra whether this occurs also for the 1024 cm^{-1} cage mode.

At worst the above procedure would appear to be a useful approximation for describing vibrational spectra of molecules of the type M_4O_{10} especially where the mass of M is greater than that of O.

5.6 THE INFRARED SPECTRA OF MATRIX ISOLATED P_4O_7, P_4O_8 and P_4O_9

(i) P_4O_7

A sample of oxidised white phosphorus prepared according to the methods of section 5.2(ii) and subsequently subjected to a mass spectroscopic study as described in section 5.2(i) showed an intense ion peak at 236 amu as well as peaks at 220 amu ($P_4O_6^+$), 173 amu ($P_3O_5^+$), 157 amu ($P_3O_4^+$), 124 amu (P_4^+), 62 amu (P_2^+) and 47 amu (PO^+). The fragmentation patterns obtained from P_4O_6 and P_4O_{10} would indicate initial loss of a 'PO_2' unit from the parent ion on ionisation. This results in the formation of $P_3O_4^+$ from P_4O_6 and $P_3O_5^+$ from P_4O_7 etc. Thus, the observation of an ion peak for $P_3O_4^+$ would indicate that the P_4O_6 observed in the mass spectrum was not a product of fragmentation of P_4O_7, but was present in the vapour phase prior to ionisation. This observation is supported by subsequent matrix isolation infrared studies. Clearly then, the two parent ion peaks are those of P_4O_6 and P_4O_7 (mw 236), the rest being products of fragmentation reactions. Previous mass spectroscopic experiments carried out on samples of P_4O_{10} indicated that the peak due to P_4O_7 was not the result of P_4O_{10} fragmentation, since the parent ion ($P_4O_{10}^+$) was always observed in these experiments, and fragmentation of P_4O_{10} proceeded by initial loss of a 'PO_2' unit to form $P_3O_8^+$, not observed in the above spectrum.

Further mass spectroscopic experiments carried out on partially oxidised samples of white phosphorus indicated that P_4O_7 was a major product of these reactions, and moreover, prolonged vaporisation of these samples resulted in the appearance of ion peaks at 252 amu ($P_4O_8^+$) and 268 amu ($P_4O_9^+$). These results were reproducible over a number of experiments, and were interpreted on the basis that partial oxidation of white phosphorus produced a mixture of P_4O_6, P_4O_7, P_4O_8 and P_4O_9. Moreover, the apparent differential volatility of these molecules presented the opportunity of simplification of the spectra obtained from subsequent matrix isolation experiments, and the mass spectroscopic facility enabled vapour composition to be monitored both before and after the matrix isolation experiments.

An attempt was made to prepare a sample of partially oxidised white phosphorus, monitor the vapour composition using mass spectroscopy,

run an infrared spectrum of the matrix isolated vapour, and subsequently re-check the vapour composition using mass spectroscopy. Figure 5.9 shows the infrared spectrum obtained from a deposit of vapour from such a sample (argon matrix) whose mass spectrum exhibited intense ion peaks at 236 amu ($P_4O_7^+$) and 220 amu ($P_4O_6^+$) both before and after the matrix study. The deposit was obtained by warming the sample to about 323K and the deposition time was approximately 20 minutes. Apart from absorptions readily assignable to P_4O_6 at 954 cm^{-1}, 640.7 cm^{-1} and 406.2 cm^{-1} strong absorptions were noted at 1380 cm^{-1} 988/976/966 cm^{-1} (triplet), 708 cm^{-1}, 653/649 cm^{-1} (doublet), 636 cm^{-1} and 428 cm^{-1}. Comparison of this spectrum with that obtained for P_4O_{10} clearly rules out interpretation on the basis of this molecule and the observed spectrum was assigned to matrix isolated P_4O_7. This experiment was found to be reproducible and at no time were relative intensity variations observed for the absorptions assigned to P_4O_7. Of course, the molecule P_4O_7 no longer possesses the Td symmetry associated with P_4O_6 and P_4O_{10}, and in fact belongs to the point group C_{3v}. This results in removal of the degeneracy of the F_2 vibrations, these now becoming A_1 + E. This will not directly affect the expected nature of the terminal P=O absorbtion however, and only one band would be expected and was observed. For the highest cage F_2 mode however, three absorptions were observed where only two are expected. This observation may be due to removal of degeneracy of the E mode by matrix cage perturbations, but no further evidence in support of this explanation was obtained. The formally inactive F_1 modes of the parent Td molecule become significant for P_4O_7 where C_{3v} symmetry is attained. On reduction of symmetry to C_{3v} these now become A_2 + E of which the E mode is both infrared and Raman active. This is suggested as a likely explanation of the absorptions observed at 708 cm^{-1} for P_4O_7; i.e. that it is the derivative of the parent F_1 mode (866 cm^{-1} calculated for P_4O_6). This may also account for the lowest component of the cage mode triplet (966 cm^{-1}). This would result in the observation of the correct number of bands derived from the parent F_2 for this mode and this explanation of the observation of the triplet is an attractive alternative to that mentioned above.

As a further test of the assignment of the observed spectrum to

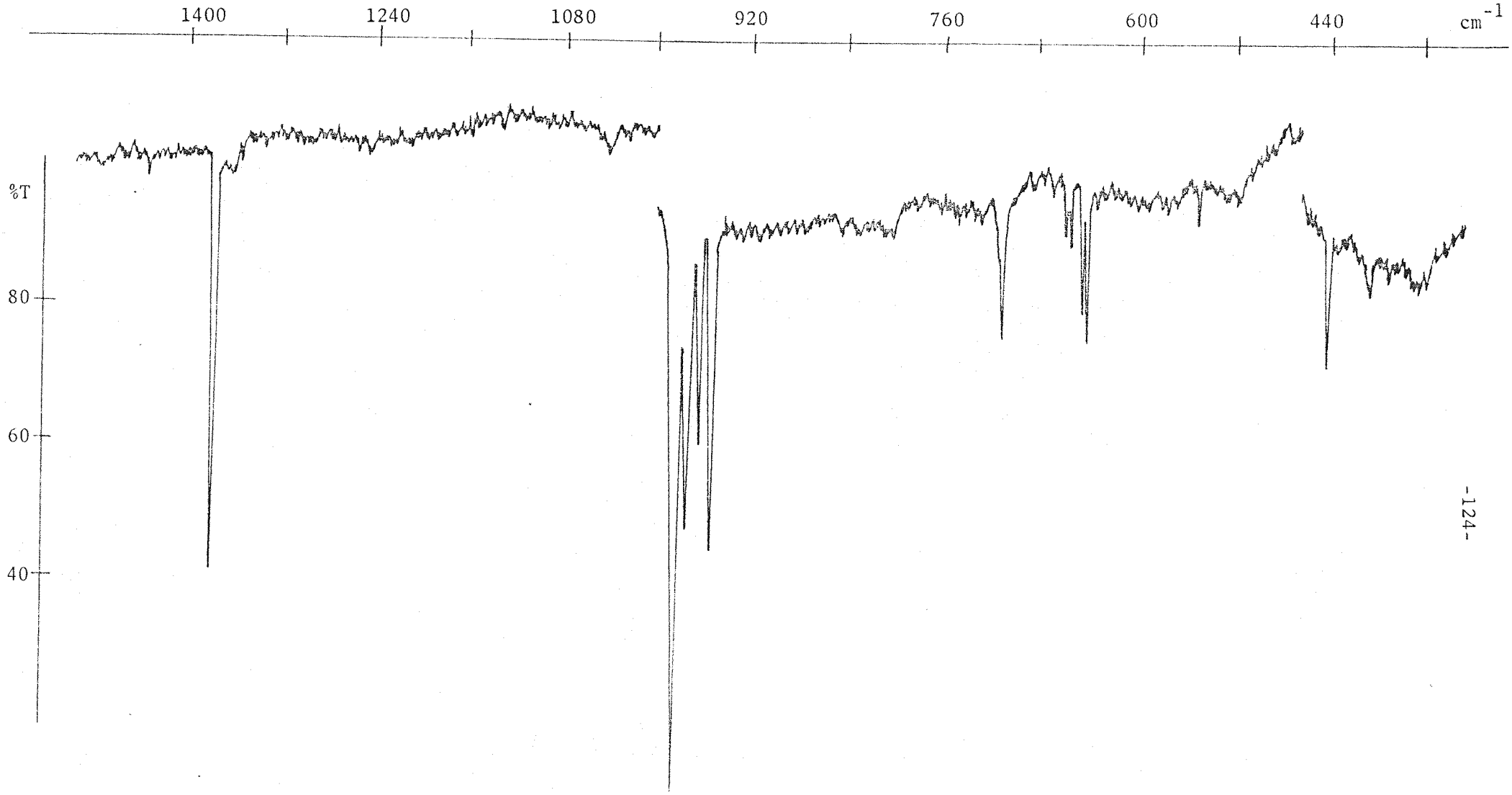

Figure 5.9 Infrared spectrum of $P_4{}^{16}O_7$ and $P_4{}^{16}O_6$ (argon matrix)

molecular P_4O_7, an attempt was made to prepare an ^{18}O substituted sample. Again, the vapour composition was checked both before and after the matrix isolation experiment using mass spectroscopy, which confirmed the presence of randomly substituted P_4O_7. Figure 5.10 shows the infrared spectrum obtained from a deposit of this sample, produced under conditions similar to above. It is clear from this spectrum that the terminal band now appears as a doublet, and the highest cage F_2 as a complex multiplet, further complicated by the presence of P_4O_6 (isotopically substituted). Figure 5.11 shows high resolution spectra obtained of the terminal and highest cage mode regions of Figure 5.10. These observations are consistent with the previous assignment to P_4O_7, although the poor quality of the spectrum of the highest cage mode renders this region unassignable.

It would appear then, from the above results that matrix isolated molecular P_4O_7 has been produced and its major infrared absorptions identified. All frequencies assigned to P_4O_7 are tabulated in Table 5.6.

(ii) $\underline{P_4O_8}$

Prolonged vaporisation of samples similar to those used above resulted in the appearance of ion peaks at 252 amu ($P_4O_8^+$) and 268 amu ($P_4O_9^+$), as well as P_4O_6 and P_4O_7, in the mass spectrum. Having identified the major infrared absorptions of P_4O_7 an attempt was now made to achieve the same for P_4O_8 and P_4O_9.

Figure 5.12 shows the infrared spectrum of a deposit (argon matrix) obtained from a sample of partially oxidised white phosphorus, the vapour from which was shown both before and after the matrix experiment to consist of P_4O_6, P_4O_7 and P_4O_8. Here after subtracting absorptions due to P_4O_6 and P_4O_7, new absorptions were observed at 1396 cm^{-1}, 1384 cm^{-1}, 1004/995 cm^{-1} (doublet), 702.5 cm^{-1}, 683.3 cm^{-1} and 439.5 cm^{-1}. As expected, if this spectrum is in fact due to matrix isolated molecular P_4O_8, then the terminal region should exhibit two P=O stretching frequencies as a result of a totally symmetric vibration and an antisymmetric vibration. P_4O_8 belongs to the point group C_{2v}, and the F_2 mode of a Td molecule becomes $A_1 + B_2 + B_1$ on reduction of symmetry to C_{2v}. As all these bands are formally both infrared and Raman active the observed doublet in the

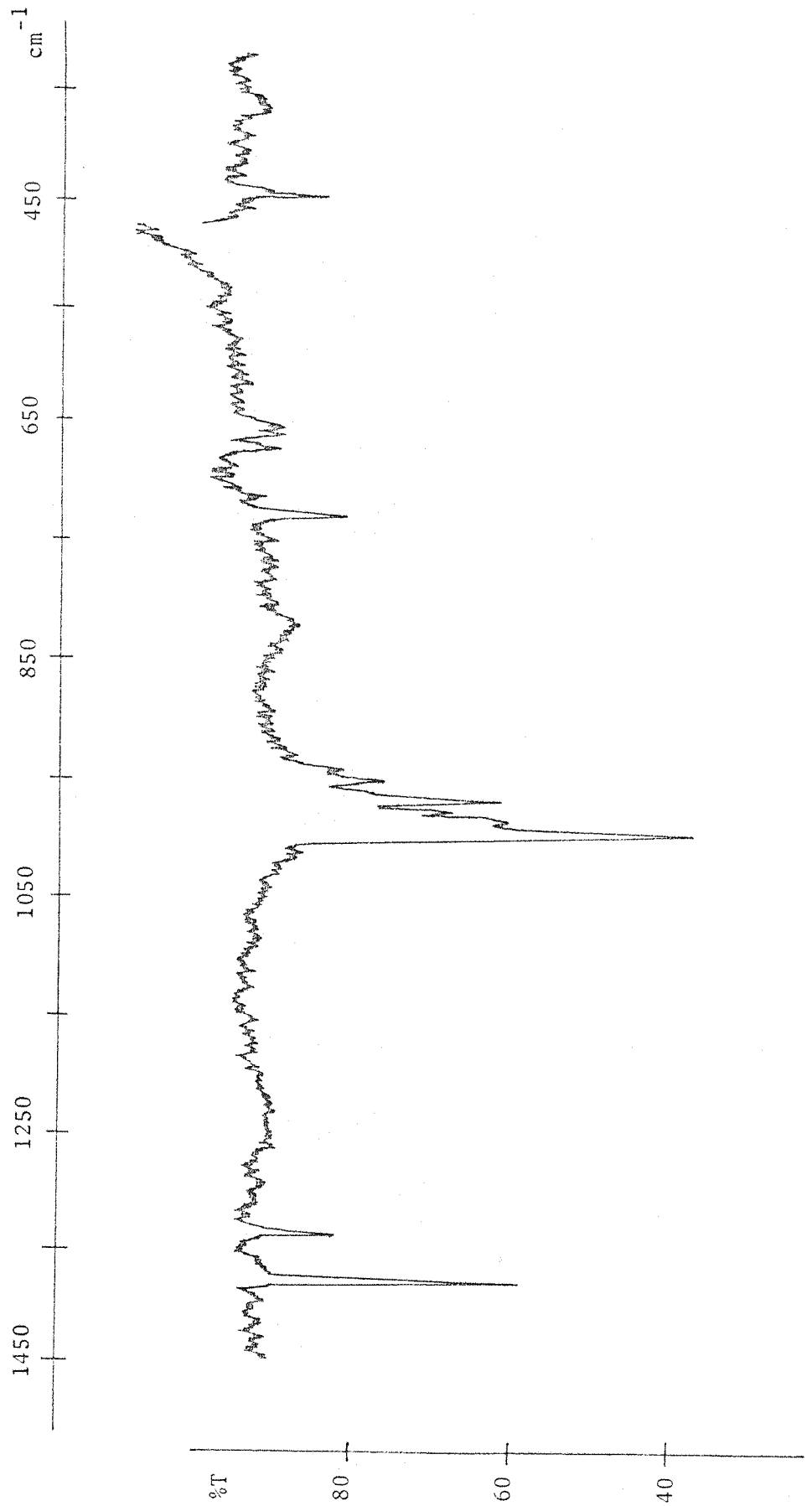

Figure 5.10 Infrared spectrum of matrix isolated $P_4^{16/18}O_7$ (with some $P_4^{16/18}O_6$) (argon matrix)

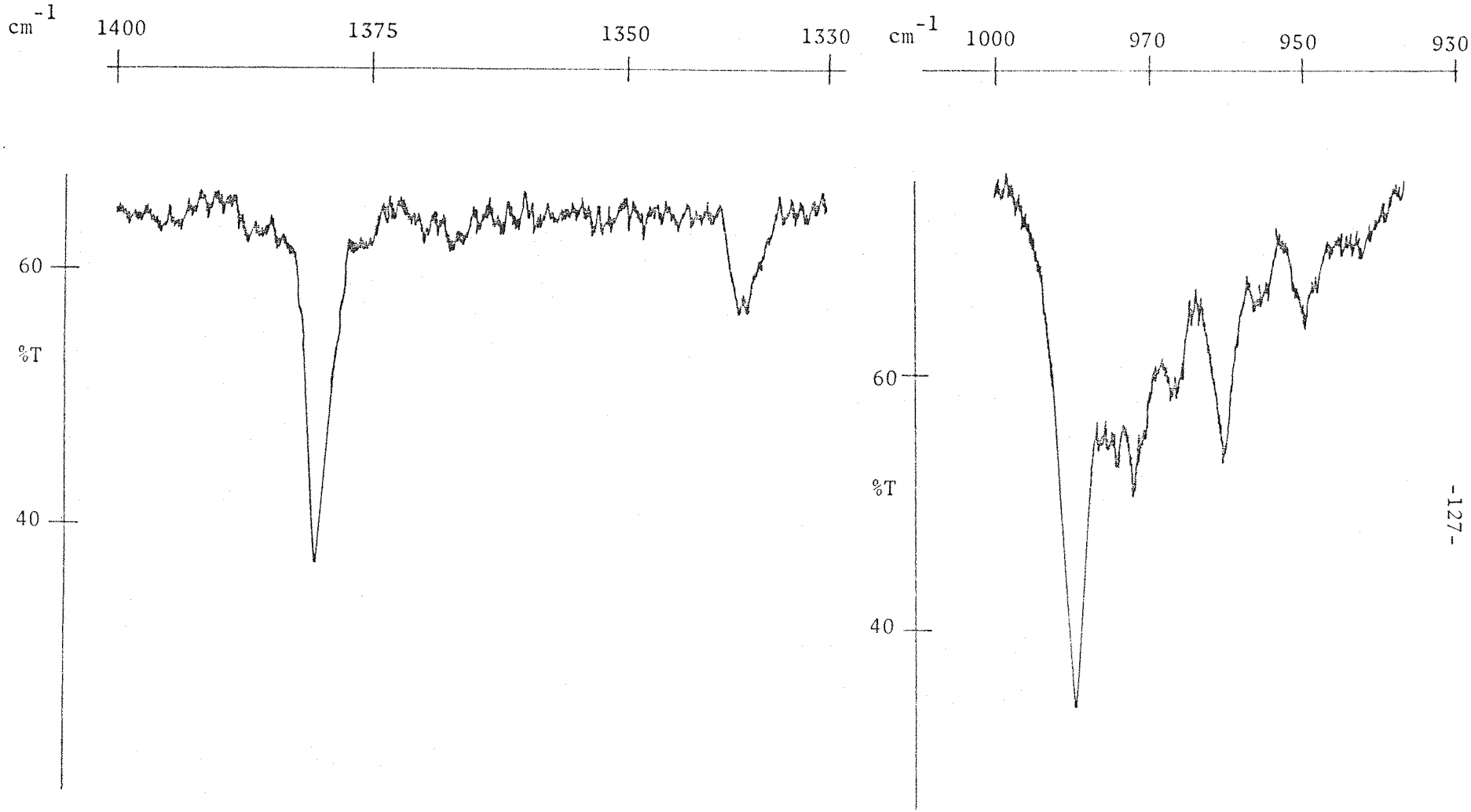

Figure 5.11 High resolution spectrum of parts of Figure 5.10

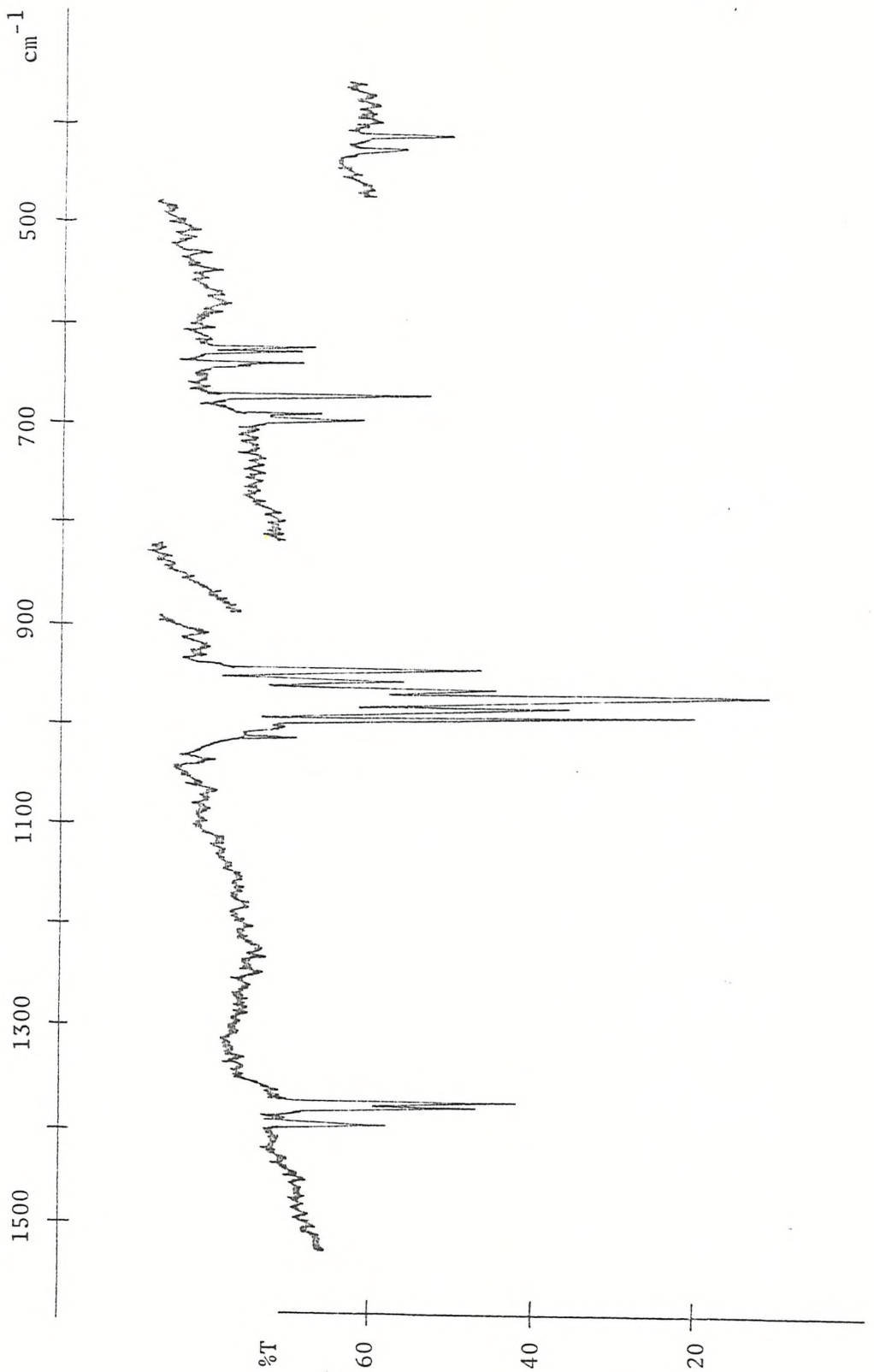

Figure 5.12 Infrared spectrum of matrix isolated $P_4{}^{16}O_7$ and $P_4{}^{16}O_8$ (with some $P_4{}^{16}O_6$) (argon matrix)

Table 5.6 Observed infrared frequencies for P_4O_6, P_4O_7, P_4O_8 and P_4O_9 and correlation diagram

P_4O_6 cm^{-1}	P_4O_7 cm^{-1}	P_4O_8 cm^{-1}	P_4O_9 cm^{-1}
	1380	1396 1384	1396?
F_2 9548	988 976 966	1004 995	1012?
F_1 866*	708	702.5 ?	
F_2 640.7	653 649	683.3	
	636		
F_2 406.2	428	439.5	
F_2 301.3			

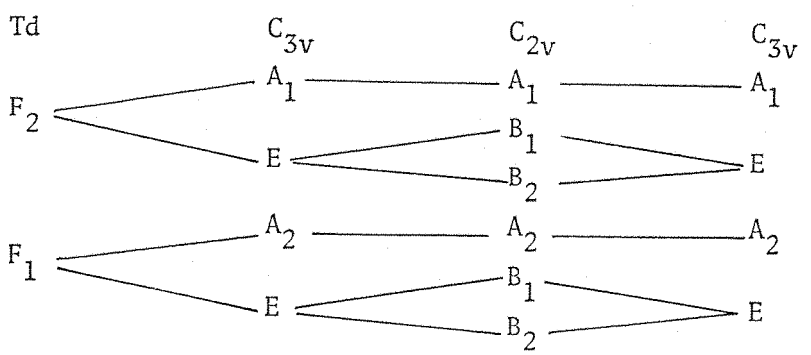

(frequency accuracy ± 0.4 cm^{-1})

* = calculated value only

terminal region is consistent with the presence of P_4O_8 in the matrix. Only two new frequencies were observed in the highest cage vibration region, and although three absorptions would be expected the possibility of coincidences cannot be ruled out. The absorption observed at 702.5 cm^{-1} is assigned as the derivative of the inactive parent F_1 mode, as was the case for P_4O_7, although for C_2 symmetry this is expected to appear as $A_2 + B_1 + B_2$, and the observation of only a single band remains unexplained.

The observed spectrum would then appear to confirm the presence of matrix isolated P_4O_8, and the frequencies assigned to this molecule appear in Table 5.6.

(iii) P_4O_9

Finally, an attempt was made using similar procedures to those used above to obtain the corresponding infrared spectrum of matrix isolated P_4O_9. Figure 5.13 shows the matrix isolation infrared spectrum obtained from a sample which exhibited ion peaks at 268 amu ($P_4O_9^+$), 252 amu ($P_4O_8^+$), 236 amu ($P_4O_7^+$) and 220 amu ($P_4O_6^+$) in its mass spectrum. Subtraction of the bands previous assigned to P_4O_6, P_4O_7 and P_4O_8 would indicate the presence of only one new band (1012 cm^{-1}). However, the relative intensities of the terminal bands has changed and comparison with the spectrum of P_4O_7 and P_4O_8 (Figure 5.12) would indicate that the highest frequency component of the P_4O_8 doublet is enhanced in intensity. This may be due to a coincidence between the terminal modes of P_4O_8 and P_4O_9, although this explanation is only tentative. In all experiments carried out, however, where P_4O_9 was present in the vapour, the appearance of the absorption at 1012 cm^{-1} was always accompanied by this relative intensity variation in the terminal region. It is not clear why, if indeed P_4O_9 is present in the matrix, only one band should be observed in the terminal region for this molecule. Of course, as the oxides P_4O_6, P_4O_7 and P_4O_8 were always present during attempts to locate the fundamentals of P_4O_9, the possibility of coincidences must be considerable. Until spectra of P_4O_9 alone can be obtained, the assignments made here and in Table 5.6 for P_4O_9 must remain tentative.

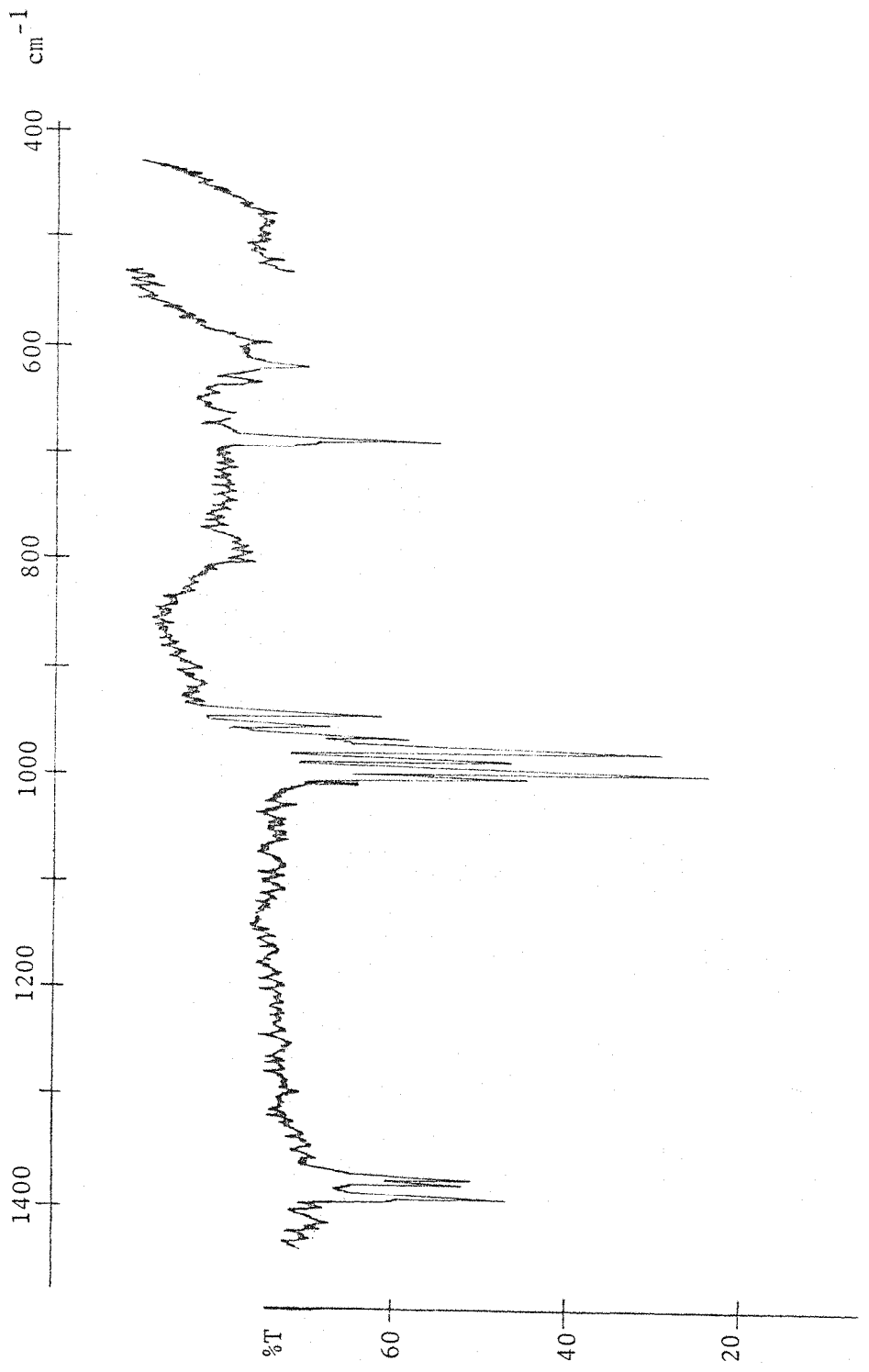

Figure 5.13 Infrared spectrum of matrix isolated $P_4{}^{16}O_7$, $P_4{}^{16}O_8$ and possibly $P_4{}^{16}O_9$ (with some $P_4{}^{16}O_6$) (argon matrix)

5.7 CONCLUSIONS

The infrared and Raman spectra of matrix isolated P_4O_6 and P_4O_{10} have been obtained and the force field developed for As_4O_6 and Sb_4O_6 has been successfully used to describe these spectra. Infrared spectra of ^{18}O substituted samples of P_4O_6 and P_4O_{10}, have been shown to be consistent with the known structures, and for P_4O_6 calculated isotopic splitting patterns were in good agreement with observed spectra, confirming the validity of the force field used. An approach via isotopic substitution to the identification of molecules of the type M_4O_{10}, containing the M_4O_6 unit by considering the terminal vibrations to be decoupled from the cage has been evaluated and shown to be a useful approximation.

By means of parallel mass spectroscopic/matrix isolation experiments, the molecules P_4O_7, P_4O_8 and P_4O_9 have been shown to exist in the vapours above heated samples of partially oxidised white phosphorus. The major infrared absorptions of matrix isolated P_4O_7 and P_4O_8 have been identified and a tentative assignment of frequencies was made for P_4O_9. The infrared spectrum of ^{18}O substituted P_4O_7 has been obtained and is shown to be consistent with the existence of a P_4O_6 cage with one terminal P=O bond.

It is interesting to compare the relative frequencies for the molecules P_4O_x (x = 6-10) in the terminal and highest cage mode regions. Figure 5.14 shows these frequencies represented by a line diagram. The fact that the frequencies of both regions increases according to $P_4O_6 < P_4O_7 < P_4O_8 \lesssim P_4O_9 < P_4O_{10}$ is consistent with an increase in π character and decrease in σ character in the unique O-P-O cage bonds and P=O terminal bonds on going from P_4O_6 to P_4O_{10}, and would imply that $d\pi$ $p\pi$ bonding becomes more important.

Finally, although the results obtained for the intermediate oxides P_4O_7, P_4O_8 and P_4O_9 are only qualitative they do represent the most complete vibrational information on these molecules so far produced, and indicate that the production of these intermediate oxides is an important feature in the oxidation of elemental phosphorus.

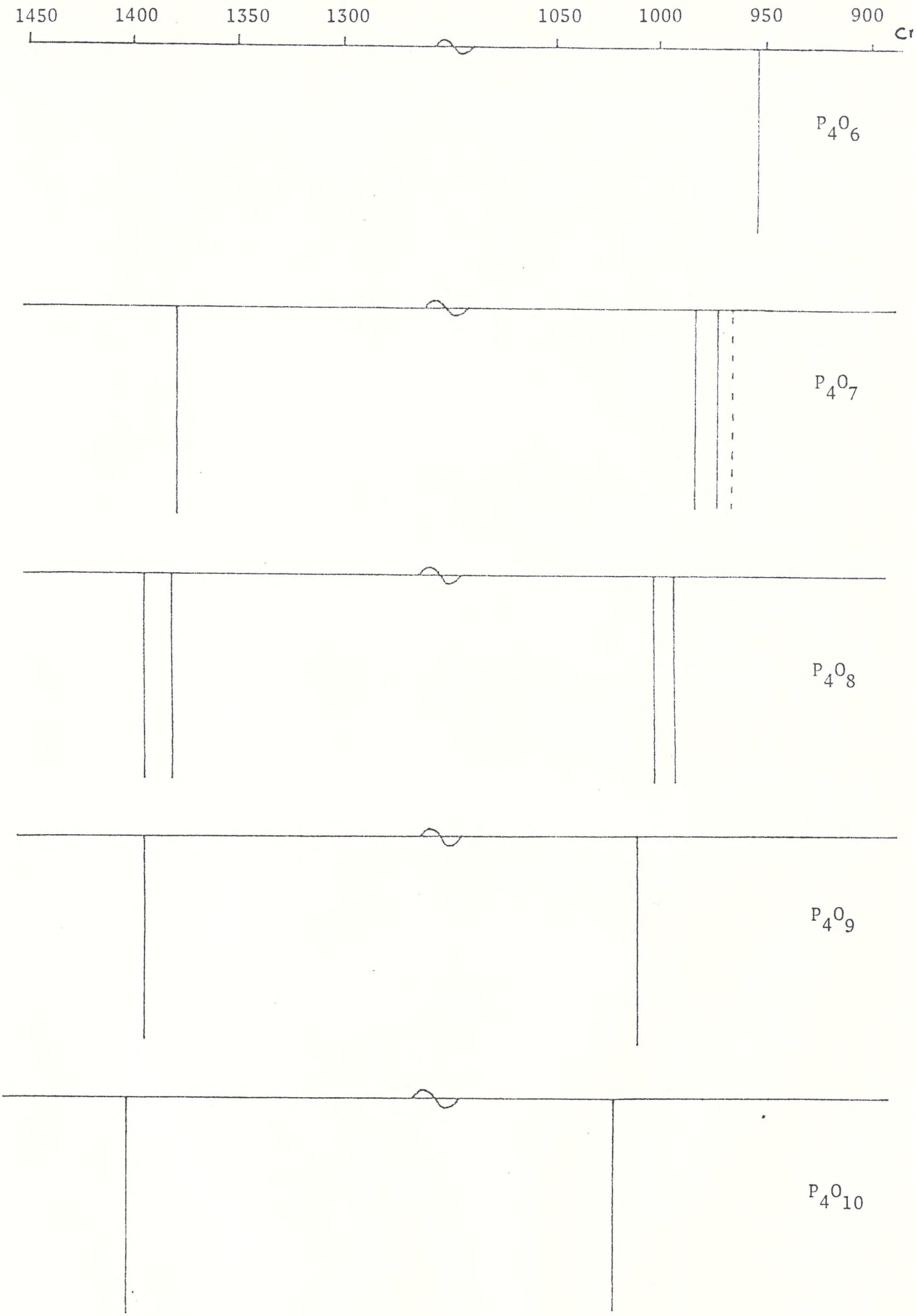

Figure 5.14 Vibrational frequencies for P_4O_x (x = 6-10) for the terminal and highest frequency cage mode regions represented by line diagrams

REFERENCES

1. B Beagley, D W J Cruickshank, T G Hewitt, K H Johst, Trans Faraday Soc, (1969), 65, 1219.

2. B Beagley, D W J Cruickshank, T G Hewitt, A Haaland, Trans Faraday Soc, (1967), 63, 836.

3. P A Akishin, N G Rambidi, E Z Zasorin, Kristallografiya (USSR), (1959), 4, 360.

4. N G Rambidi, E Z Zasorin, Zh Strukt Khim (USSR), (1966), 7, 483.

5. N G Rambidi, Yu S Ezhou, Zh Strukt Khim USSR, (1967), 8, 12.

6. L R Maxwell, S B Hendricks, L S Deming, J Chem Phys, (1937), 5, 626.

7. G C Hampson, A J Stosick, J Amer Chem Soc, (1938), 60, 1814.

8. A C Chapman, Spectrochim Acta, (1968), 24A, 1687.

9. A C Chapman, L E Thirlwell, Spectrochim Acta, (1964), 20, 937.

10. A C Chapman, D A Long, D T L Jones, Spectrochim Acta, (1965), 21, 633.

11. H Gerding, H V Brederode, H C J De Decker, Rec Trav Chim, (1942), 61, 549.

12. T A Siderov, N N Sobelov, Opt Spektroskopiya (USSR), (1957), 2, 710.

13. D H Zijp, Adv Mol Specty, (1962), 1, 345.

14. C S Venkateswaran, Proc Indian Accad, (1936), 4A, 345.

15. H Gerding, H C J De Decker, Rec Trav Chim, (1945), 64, 191.

16. T A Siderov, N N Sobelov, Opt Spektroskopiya (USSR), (1957), 2, 717.

17. I R Beattie, K M S Livingstone, G A Ozin, D J Reynolds, J Chem Soc A, 1970, 449.

18. S J Cyvin, B N Cyvin, Zeits Naturforsche, (1971), 26A, 901.

19. C Sourisseau, R Mercier, Spectrochim Acta, (1978), 34A, 173.

20. V D Heinz, Z Anorg Allgem Chem, (1965), 336, 137.

21. K H Johst, Acta Cryst, (1964), 17, 1593.

22. V D Heinz, Z Anorg Allgem Chem, (1972), 383, 12.

23. K H Johst, Acta Cryst, (1966), 21, 34.

24. M L Walker, J L Mills, Syn React Inorg Metal-Org Chem, (1975), 5(1), 29.

25. M L Walker, D E Peckenpaugh, J L Mills, Inorg Chem, (1979), 18, 10, 2792.

26. K H Johst, M Schneider, Acta Cryst, (1981), B37, 222.

27. I R Beattie, J S Ogden, D D Price, Inorg Chem, (1978), 17, 11, 3296.

28. R A Crocombe, Ph.D. Thesis, (1978), Southampton University.

APPENDIX 1

THE CALCULATION OF ISOTOPIC FREQUENCIES FOR THE OUT OF PLANE BENDING MODE FOR MOLECULES OF THE TYPE AXYZ

The general equation describing the out-of-plane bending mode of AXYZ type molecules which appears in Chapter 3 can be derived as follows.

Consider a molecule of the type:

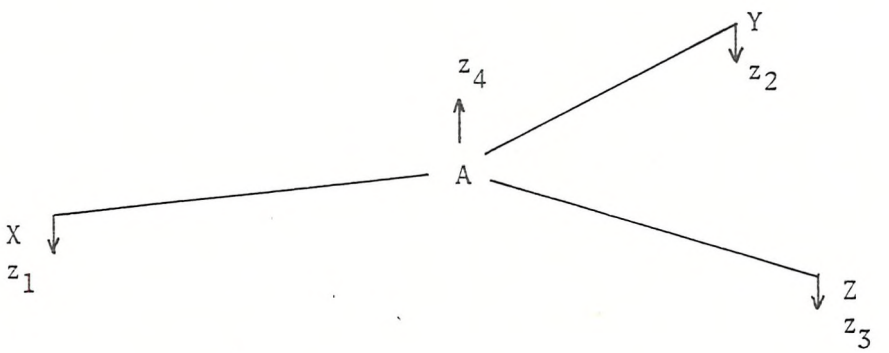

where z_1, z_2 and z_3 represent a small displacement of the atoms XY and Z below the plane XYZ and z_4 represents a displacement of A above the plane. A small displacement of X moves the plane XYZ downwards so that A now lies above this plane by an amount h_1. A set of internal coordinates may be defined as follows:

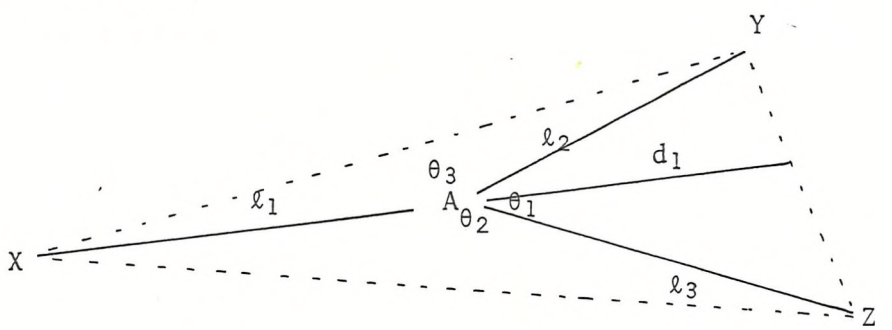

Now considering z_1 in terms of ℓ_1 and d_1 and h_1 gives:

$$\frac{z_1}{\ell_1 + d_1} = \frac{h_1}{d_1}$$

$$\therefore \quad h_1 = \frac{z_1 d_1}{\ell_1 + d_1}$$

The area of triangle XTZ α $\ell_1 + d_1$ and the area of triangle YAZ α d_1 so:

$$h_1 = \frac{z_1 \Delta_1}{\Delta_T}$$

where Δ_1 = area of triangle YAZ and

Δ_T = area of triangle XYZ

A similar treatment for z_2 and z_3 gives for the total symmetry coordinate:

$$S_{B_1} = \frac{z_1 \Delta_1}{\Delta_T} + \frac{z_2 \Delta_2}{\Delta_T} + \frac{z_3 \Delta_3}{\Delta_T} + z_4 \qquad (1)$$

Equation (1) may be rewritten as:

$$S_{B_1} = \frac{1}{\Delta_T} (z_1 \Delta_1 + z_2 \Delta_2 + z_3 \Delta_3 + z_4 \Delta_T) \qquad (2)$$

If $R_1 = \frac{\Delta_1}{\Delta_T}$, $R_2 = \frac{\Delta_2}{\Delta_T}$, and $R_3 = \frac{\Delta_3}{\Delta_T}$

then the appropriate G matrix element for this vibration will be:

$$G = \frac{1}{M_A} + \frac{R_1^2}{M_x} + \frac{R_2^2}{M_y} + \frac{R_3^2}{M_z} \qquad (3)$$

The frequency of the vibration will be given by:

$$\lambda = F\left(\frac{1}{M_A} + \frac{R_1^2}{M_x} + \frac{R_2^2}{M_y} + \frac{R_3^2}{M_z}\right) \qquad (4)$$

where $\lambda = 4\pi^2 c^2 \nu^2$ and F is the force constant associated with the out-of-

plane bend. For the D_{3h} case where $\Delta_1 = \Delta_2 = \Delta_3 = \frac{1}{3}\Delta_T$ then the frequency will be given by:

$$\lambda = F\left(\frac{9}{M_m} + \frac{1}{M_x} + \frac{1}{M_y} + \frac{1}{M_z}\right),$$

the equation used to calculate the isotopic frequencies for the β_1 mode of $NaPO_3$ (see Chapter 3) . Rearrangement of Equation (4) gives:

$$\lambda = \frac{F}{\Delta_T}\left(\frac{\Delta_T^2}{M_m} + \frac{\Delta_1^2}{M_x} + \frac{\Delta_2^2}{M_y} + \frac{\Delta_3^2}{M_z}\right) \qquad (5)$$

If $\Delta_1 = \frac{1}{2}\ell_2\ell_3\sin\theta_1 = \dfrac{\ell_1\ell_2\ell_3\sin\theta_1}{2\ell_1}$

$\Delta_2 = \frac{1}{2}\ell_1\ell_3\sin\theta_2 = \dfrac{\ell_1\ell_2\ell_3\sin\theta_2}{2\ell_2}$

$\Delta_3 = \frac{1}{2}\ell_1\ell_2\sin\theta_3 = \dfrac{\ell_1\ell_2\ell_3\sin\theta_3}{2\ell_3}$

then substitution into Equation (5) will give:

$$\lambda = \frac{F \cdot}{\frac{\ell_1\ell_2\ell_3\sin\theta_1}{2\ell_1} + \frac{\ell_1\ell_2\ell_3\sin\theta_2}{2\ell_2} + \frac{\ell_1\ell_2\ell_3\sin\theta_3}{2\ell_3}}^2 \left(\frac{1}{M_m}\left(\frac{\ell_1\ell_2\ell_3\sin\theta_1}{2\ell_1} + \frac{\ell_1\ell_2\ell_3\sin\theta_2}{2\ell_2} + \frac{\ell_1\ell_2\ell_3\sin\theta_3}{2\ell_3}\right)^2 + \frac{1}{M_x}\left(\frac{\ell_1\ell_2\ell_3\sin\theta_1}{2\ell_1}\right)^2 + \frac{1}{M_y}\left(\frac{\ell_1\ell_2\ell_3\sin\theta_2}{2\ell_2}\right)^2 + \frac{1}{M_z}\left(\frac{\ell_1\ell_2\ell_3\sin\theta_3}{2\ell_3}\right)^2\right) \qquad (6)$$

Cancellation of the factor $\left(\dfrac{\ell_1\ell_2\ell_3}{2}\right)^2$ in Equation (6) will give:

$$\lambda = \frac{F}{\frac{\sin\theta_1}{\ell_1} + \frac{\sin\theta_2}{\ell_2} + \frac{\sin\theta_3}{\ell_3}} 2\left(\frac{1}{M_m}\left(\frac{\sin\theta_1}{\ell_1} + \frac{\sin\theta_2}{\ell_2} + \frac{\sin\theta_3}{\ell_3}\right)^2 + \right.$$

$$\left. \frac{1}{M_x}\left(\frac{\sin\theta_1}{\ell_1}\right)^2 + \frac{1}{M_y}\left(\frac{\sin\theta_2}{\ell_2}\right)^2 + \frac{1}{M_z}\left(\frac{\sin\theta_3}{\ell_3}\right)^2 \right) \qquad (7)$$

Now if $R = \left(\frac{\sin\theta_1}{\ell_1} + \frac{\sin\theta_2}{\ell_2} + \frac{\sin\theta_3}{\ell_3}\right)$

then Equation (7) can be rewritten as:

$$\lambda = \frac{F}{R^2}\left(\frac{R^2}{M_m} + \frac{\sin^2\theta_1}{\ell_1^2 M_x} + \frac{\sin^2\theta_2}{\ell_2^2 M_y} + \frac{\sin^2\theta_3}{\ell_3^2 M_z}\right)$$

This equation is then generatly applicable to molecules of the type AXYZ or coordinated $[MX_3]^-$ ions, and using this expression, an idealised D_{3h} structure need not be assumed.

Appendix 2

FG MATRIX ANALYSIS OF THE BIDENTATE PHOSPHATE ION

This appendix deals only with the stretching and in plane bending modes of $[PO_3]^-$, the out of plane mode being dealt with in Appendix 1.

Consider the following model for the $[PO_3]^-$ ion:

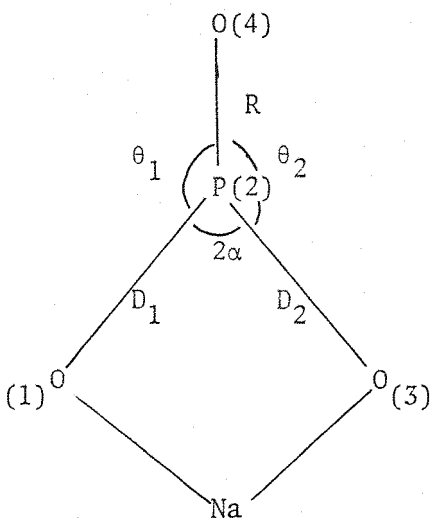

The stretching modes and in plane bending modes are $3A_1 + 2B_2$ modes. The choice of internal coordinates as above leads to the following symmetry coordinates;[1]

$$S_1 = \Delta R$$
$$S_2 = 1/\sqrt{2}(\Delta D_1 + \Delta D_2)$$
$$S_3 = 1/\sqrt{2}(\Delta \theta_1 + \Delta \theta_2)$$
$$S_4 = 1/\sqrt{2}(\Delta D_1 - \Delta D_2)$$
$$S_5 = 1/\sqrt{2}(\Delta \theta_1 - \Delta \theta_1)$$

It is not possible for all angles θ_1, θ_2 and 2α to vary independently. This results in a redundancy among these internal coordinates, and therefore the above symmetry coordinates omit 2α.

These symmetry coordinates, S, can be expressed in terms of cartesian displacements of the individual atoms:

$$S_1 = \Delta R = -z_2 + z_4$$
$$S_2 = 1/\sqrt{2}(-y_1 s - z_1 c + 2z_2 c + y_3 s + z_3 c)$$
$$S_3 = 1/\sqrt{2}(y_1{}^c/D - z_1{}^s/D + 2z_2{}^s/D - y_3{}^c/D - z_3{}^s/D)$$
$$S_4 = 1/\sqrt{2}(-y_1 s - z_1 c + 2y_2 s - y_3 s + z_3 c)$$
$$S_5 = 1/\sqrt{2}(y_1{}^c/D - 2y_2{}^c/D - 2y_2/R + y_3{}^c/D + 2y_4/R - z_1{}^s/D + z_3{}^s/D)$$

where $c = \cos\alpha$ and $s = \sin\alpha$.

The B elements can then be obtained from[2]

$$S_t = \sum_{i=1}^{3N} B_{ti} P_i$$

For example, considering S_4, the following B elements are obtained:

$$B_{41} = 0 \qquad B_{42} = -s/\sqrt{2} \qquad B_{43} = -c/\sqrt{2} \qquad B_{44} = 0$$
$$B_{45} = 2s/\sqrt{2} \qquad B_{46} = 0 \qquad B_{47} = 0 \qquad B_{48} = -s/\sqrt{2}$$
$$B_{49} = c/\sqrt{2} \qquad B_{410} = B_{411} = B_{412} = 0$$

The G matrix elements are given by:[2]

$$G_{tt'} = \sum_{i=1}^{3N} \mu_i B_{ti} B_{t'i}$$

(where μ_i is the reciprocal mass of atom i), which results in the following:

$$G_{11} = \frac{1}{M_2} + \frac{1}{M_4} \qquad G_{12} = \frac{-c\sqrt{2}}{M_2} \qquad G_{13} = \frac{-s\sqrt{2}}{M_2 D}$$

$$G_{14} = G_{15} = 0 \qquad G_{22} = \frac{1}{2M_1} + \frac{1}{2M_3} + \frac{2c^2}{M_2} \qquad G_{23} = \frac{2sc}{M_2 D}$$

$$G_{24} = \frac{1}{2M_1} - \frac{1}{2M_3} \qquad G_{25} = 0 \qquad G_{33} = \frac{1}{2M_1 D^2} + \frac{1}{2M_3 D^2} + \frac{2s^2}{M_2 D^2}$$

$$G_{34} = 0 \qquad G_{35} = \frac{1}{2D^2 M_1} - \frac{1}{2D^2 M_3} \qquad G_{44} = \frac{1}{2M_1} + \frac{1}{2M_3} + \frac{2s^2}{M_2}$$

$$G_{45} = \frac{2}{M_2(sc/D - s/R)}$$

$$G_{55} = \frac{1}{2M_1 D^2} + \frac{1}{2M_3 D^2} + \frac{2}{R^2 M_4} + \frac{2(rc + D)^2}{M_2 R^2 D^2}$$

The F matrix is given by:

$$F = U f \tilde{U}$$

where $U = SI$

$$= \begin{pmatrix} 1 & 0 & 0 & 0 & 0 \\ 0 & 1/\sqrt{2} & 1/\sqrt{2} & 0 & 0 \\ 0 & 0 & 0 & 1/\sqrt{2} & 1/\sqrt{2} \\ 0 & 1/\sqrt{2} & -1/\sqrt{2} & 0 & 0 \\ 0 & 0 & 0 & 1/\sqrt{2} & -1/\sqrt{2} \end{pmatrix} \begin{pmatrix} \Delta R \\ \Delta D_1 \\ \Delta D_2 \\ \Delta\theta_1 \\ \Delta\theta_2 \end{pmatrix}$$

$$f = \begin{pmatrix} f_{11} & f_{12} & f_{13} & \cdots & f_{15} \\ f_{12} & \vdots & & & \vdots \\ \vdots & \vdots & & & \vdots \\ f_{15} & f_{25} & \cdots & & f_{55} \end{pmatrix}$$

Because the molecule possesses C_{2v} symmetry, in practice the F matrix can be simplified owing to the fact that, for example $f_{12} = f_{13}$ (or $f_{RD_1} = f_{RD_2}$).

Therefore the following F matrix elements are obtained:

$$F_{11} = f_R \qquad F_{12} = \sqrt{2} f_{RD} \qquad F_{13} = \sqrt{2} f_{R\theta} \qquad F_{14} = F_{15} = 0$$

$$F_{22} = (f_D + f_{DD}) \qquad F_{23} = f_{D\theta(\text{trans})} \qquad F_{24} = F_{25} = 0$$

$$F_{33} = (f_\theta - f_{\theta\theta}) \qquad F_{34} = F_{35} = 0$$

$$F_{44} = (f_D - f_{DD}) \qquad F_{45} = (f_{D\theta(\text{cis})} - f_{D\theta(\text{trans})})$$

$$F_{55} = (f_\theta - f_{\theta\theta})$$

where $f_{D_1\theta_1} = f_{D_2\theta_2} = f_{D\theta}\text{cis}$

and $f_{D_1\theta_2} = f_{D_2\theta_1} = f_{D\theta}\text{trans}$

REFERENCES

1. 'Chemical Applications of Group Theory', F A Cotton, Wiley-Interscience, NY, (1971).

2. 'Molecular Vibrations', E B Wilson, J C Decius, P C Cross, McGraw-Hill, NY, (1955).